2012

# Endoplasmic Reticulum Calcium-Independent Phospholipase A2 gamma (ER-iPLA2γ): Role in Oxidative Stress-Induced Lipid Peroxidation, Ca2+ Release, Phospholipid Homeostasis and Cell Death in the Kidney

Andre Chioke Eaddy
*Medical University of South Carolina*

# Endoplasmic Reticulum Calcium-Independent Phospholipase $A_2$ gamma (ER-iPLA$_2\gamma$): Role in Oxidative Stress-Induced Lipid Peroxidation, $Ca^{2+}$ Release, Phospholipid Homeostasis, and Cell Death in the Kidney

By

Andre Chioke Eaddy

A dissertation submitted to the faculty of the Medical University of South Carolina in partial fulfillment of the requirements for the degree of Doctor of Philosophy in the College of Graduate Studies.

Program in Biomedical and Pharmaceutical Sciences

2012

Approved by:

Chairman, Advisory Committee

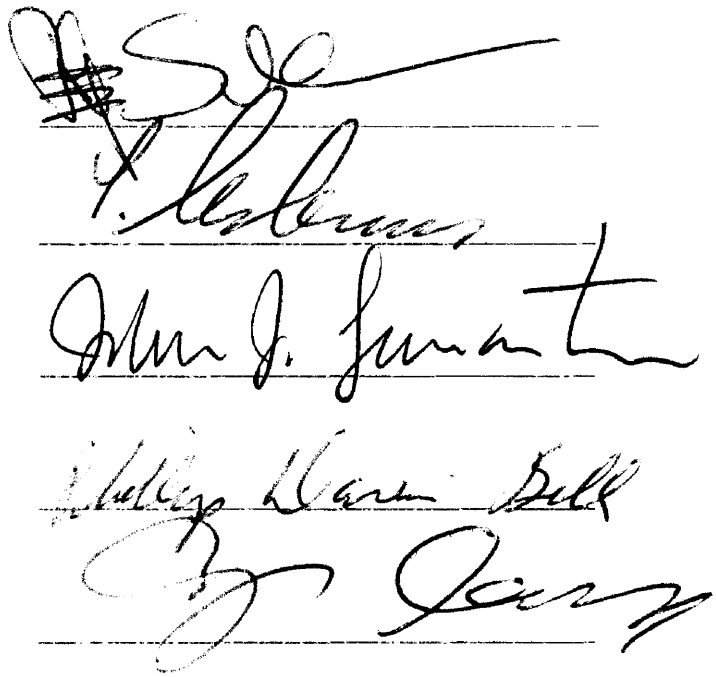

## DEDICATION

This Dissertation is dedicated to my father, Joseph Daniel Eaddy, mother, Robin Anderson Eaddy, brother, Michael T. Eaddy, and my son Deontae J. Eaddy.

## ACKNOWLEDGEMENTS

I gratefully acknowledge the guidance, support and mentorship of Dr. Rick G. Schnellmann, which enabled the completion of this project. I am also grateful to Dr. Gilbert R. Kinsey, who taught me an incredible amount about this project and science in general. I am thankful to Dr. Brian S. Cummings and the members of his laboratory for the assistant and guidance with the mass spectrometry studies needed for the completion of this project. In addition, I am thankful to the other members of my committee: Drs. Craig Beeson, P. Darwin Bell, John J. Lemasters, and Yefim Manevich for their scientific contributions and guidance. I would like to acknowledge several members of the laboratory for generously providing their time to assist in the completion of this project; they are (in alphabetical order): David Arrington, Jennifer Blakely, Jason Blum, Marisa Covington, Jason Funk, Chris Giguere, Mark Hallman, Jenn Hanger, Vijay Kale, Matthew Smith, Ryan Whitaker, and Lauren Wills. I especially thank The Center of Academic Excellence (Tom Waldrep) and Dr. Perry Halushka, Amy Connolly, and members of the MSTP Program for their support.

# TABLE OF CONTENTS

ANDRE CHIOKE EADDY. Endoplasmic Reticulum Calcium-Independent Phospholipase $A_2$ gamma (ER-iPLA$_2\gamma$): Role in Oxidative Stress-Induced Lipid Peroxidation, $Ca^{2+}$ Release, Phospholipid Homeostasis, and Cell Death in the Kidney (Under the direction of RICK G. SCHNELLMANN)

## ABSTRACT

Acute kidney injury and chronic kidney disease are becoming more prevalent and have high morbidity and mortality, and despite several therapies targeted towards treating or preventing kidney injury, outcomes have been unchanged for many years. Calcium-independent phospholipase A$_2\gamma$ (iPLA$_2\gamma$) is one of seven $Ca^{2+}$-independent PLA$_2$ enzymes and represents a potential therapeutic target in kidney disease because of its unique subcellular localization and its potential as the putative membrane remodeling/repair enzyme. Studies in our laboratory suggest iPLA$_2\gamma$ is cytoprotective during oxidant injury by preventing and/or repairing oxidant-induced lipid peroxidation and pointed to ER- iPLA$_2\gamma$ as the major component of membrane repair and remodeling. The goals of these studies are to understand the role of ER- iPLA$_2\gamma$ in oxidant-induced ER lipid peroxidation, $Ca^{2+}$ release, loss of lipid homeostasis, and renal cell death. Our studies in isolated microsomes (ER) provide evidence that inhibition of ER-iPLA$_2\gamma$ results in the potentiation of oxidant-induced lipid peroxidation. Studies in renal proximal tubule cells confirmed that iPLA$_2\gamma$ is protective of oxidant-induced lipid peroxidation and genetic ablation of iPLA$_2\gamma$ in mice resulted in oxidant injury (lipid peroxidation and mitochondrial DNA damage). To determine the role of ER- iPLA$_2\gamma$ in oxidant-induced $Ca^{2+}$ release we developed assays to measure ER $Ca^{2+}$ release from

isolated microsomes and in RPTC using $Ca^{2+}$-sensitive fluorophores. These studies showed ER- iPLA$_2\gamma$ prevented oxidant-induced ER $Ca^{2+}$ release.

To determine the role of iPLA$_2\gamma$ in oxidant-induced loss of lipid homeostasis, we employed electron spray ionization-mass spectrometry (ESI-MS) to measure lipid changes (phospholipids and fatty acids) in isolated microsomes, RPTC, and iPLA$_2\gamma$ KO mouse urine. These studies provide evidence that ER- iPLA$_2\gamma$ mediates oxidant-induced fatty acid release (oxidized and/or unsaturated) in isolated microsomes; iPLA$_2\gamma$ inhibition results in the build-up several phospholipids within renal cell membranes; and genetic ablation of iPLA$_2\gamma$ in mice results in decreased phosphatidylcholine containing phospholipids and increased fatty acids with methyl or keto additions (likely lipid hydroperoxides) in mouse urine.

Our studies in RPTC demonstrated ER- iPLA$_2\gamma$ protects renal cell from oxidant-induced necrotic cell death by preventing ER membrane disruption and subsequent $Ca^{2+}$ release. We report the first *in vivo* studies suggesting that genetic ablation of iPLA$_2\gamma$ results in kidney oxidant injury, induces compensatory mitochondrial changes and upregulation of antioxidant stress pathways, however does not result measurable loss of kidney function. Together these data support our previous findings that iPLA$_2\gamma$ is cytoprotective in renal cells and provide evidence that iPLA$_2\gamma$ is critical for the prevention and/or repair of lipid peroxidation in oxidative kidney injury.

# Chapter 1

## Review of Acute Renal Failure and Phospholipase $A_2$ Biology

**Kidney Function and Dysfunction.** The kidneys are involved many functions including water and electrolyte balance, regulation of arterial blood pressure, regulation of blood cell synthesis, vitamin D production and fasting-induced gluconeogenesis [1]. The kidneys are also responsible for the removal of water soluble waste products, such as blood urea nitrogen (BUN) and creatinine, and xenobiotics, such as cisplatin and aminoglycosides. Impaired kidney function, resulting in loss of electrolyte and water balance and the build up of these compounds, results in neurological disturbances (ie delirium, coma, and seizure), cardiac arrhythmias, fatigue, edema, and hypertension. Complications from loss of kidney function result in significant morbidity and mortality.

**Acute Kidney Injury.** Acute kidney injury (AKI), in the clinical setting, is generally diagnosed based upon an abrupt increase in serum creatinine ($S_{Cr}$) within the setting of clinical symptoms such as nausea, vomiting, fatigue, and/or edema. This syndrome was once termed acute renal failure until a more strict and accurate definition was adopted. AKI requires a greater than 0.3 mg/dl (425 mmol/l) rise or a > 50% increase in serum creatinine, oliguria (a reduction in urine output <0.5 ml/kg/h for greater than 6 h, or an acute palliative need for dialysis [2]. The most recent criteria for defining the severity of AKI stratifies the stages of injury from a minor insult causing minimal damage to significant injury resulting in End-Stage Renal Disease (ESRD) [3]. These criteria are termed RIFLE (Risk, Injury, Failure, Loss, and ESRD) and were developed because the

progression of AKI correlates well, clinically, with morbidity and mortality (Figure 1-1) [4].

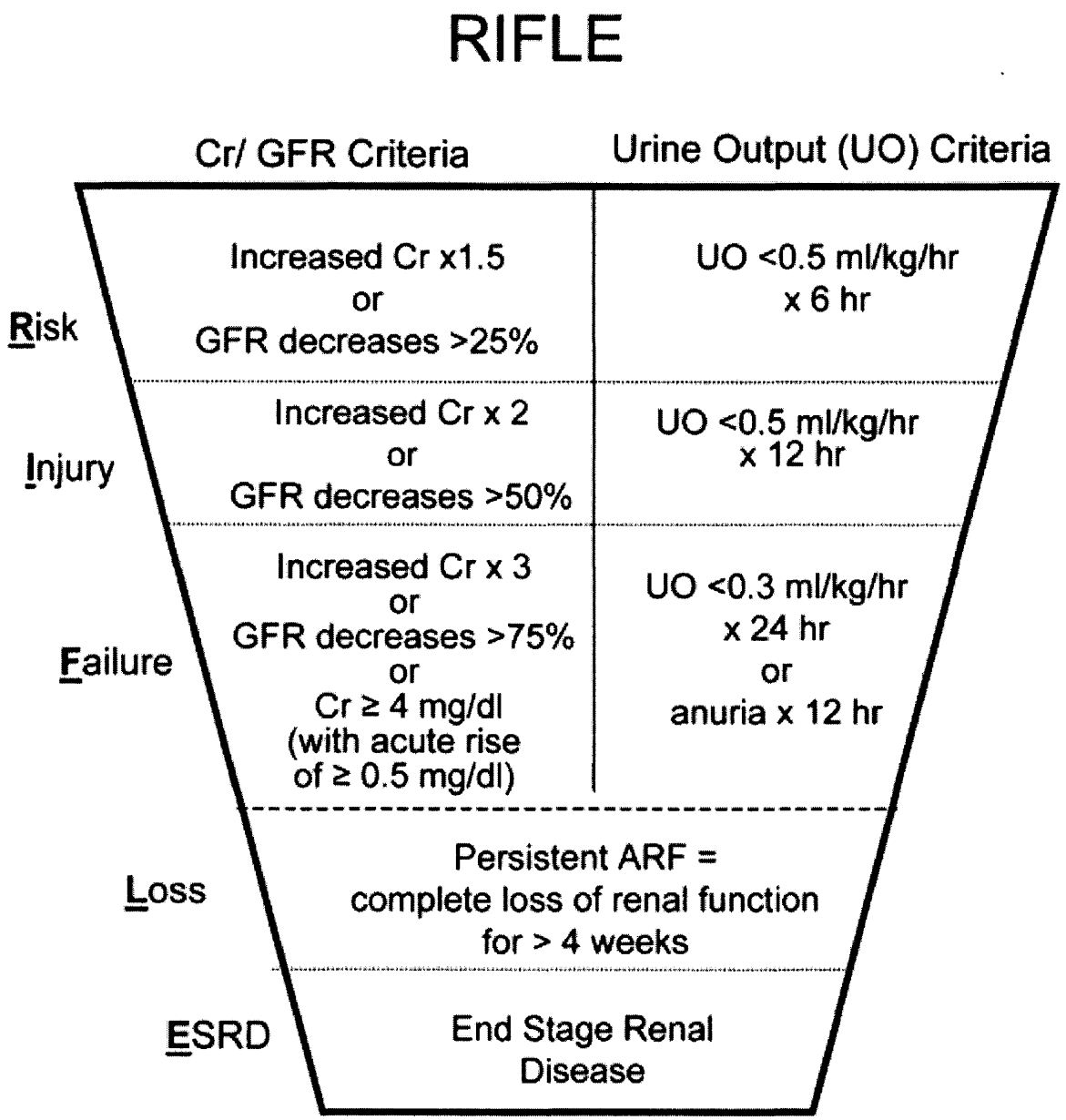


**Figure 1-1. The RIFLE classification.** The RIFLE criteria stratifies the stage of insult from minor to major resulting in ESRD. The shape of the figure reflects the incidence of patients within each stage. Importantly, more patients will be included in the mild category while the bottom criteria are more strict and therefore more specific. GFR, glomerular filtration rate; ARF, acute renal failure, ESRD, end stage renal disease. From Bellomo *et al* [3].

**AKI Morbidity and Mortality.** AKI is associated with significant morbidity and mortality. Epidemiological studies revealed that most AKI cases occur in hospitalized patients and more specifically, patients in intensive care unit (ICU) [5]. ICU patients with AKI are associated with as high as 90% mortality rates, presumably due to the presence co-morbidities, including liver/heart failure and sepsis [6]. Although AKI is associated with co-morbidities and the presence of other diseases may influence mortality rates, AKI is independently associated with increased mortality in epidemiological studies that adjust for the contribution of co-mobidities [7]. The mortality rate in uncomplicated AKI is estimated to be as high as 23%. Mortality rates range from 10-80% depending on the population studied (from uncomplicated AKI to those patients requiring renal replacement therapy) [8-9].

Reliable statistics on incidence, cost, and mortality associated with AKI are hard to assess because the numbers are inherently dependent on the population studied and incidence is often tied with other disease states. However, retrospective studies from in-patient hospital records estimate the incidence rate to be approximately 5-7% (approximately 1% community-acquired), and this number increases to approximately 20% in critically-ill patients [10] A more useful and likely more appropriate assessment of the contribution of AKI to poor health outcomes would be to quantify the added mortality, length of stay and cost attributed to hospital-acquired AKI. One study examining the data by incremental changes in serum creatinine, found that even a moderate change in serum creatinine (0.3 – 0.4 mg/dl) resulted in a 70% increase in risk of death, a 3.5 day increase in length of stay, and a $9000 increase in health care associated costs [11]. These

numbers were greatly increased when considering more robust changes in serum creatinine (0.5 – 2.0 mg/dl increases).

**AKI and Chronic Kidney Disease.** Recent studies suggest AKI contributes to incident and prevalence of chronic kidney disease (CKD) and end-stage renal disease (ESRD). Approximately 10-40 million adults have CKD and over one half million were treated for ESRD via dialysis or kidney transplantation in the US in 2007 [12]. The number of patient with ESRD is projected to increase to 0.8 million by 2020. Additionally, there has been a considerable increase in the incidence of AKI, which appears to be related to the increased number of invasive medical and surgical procedures in the management of critically ill elderly patients. In summary, AKI is responsible for significant increases in morbidity, mortality, health care costs, and length of stay of both hospitalized/critically-ill patients and in patients presenting with AKI as a primary diagnosis.

**Treatments for AKI.** Clinical treatment options for AKI are limited to supportive measures including maintenance of intravascular volume, blood pressure regulation, immediate discontinuation of suspected nephrotoxic drugs and correction of electrolyte abnormalities [2]. Hyperkalemia is a common consequence of AKI, which can lead to life threatening arrhythmias. Potassium binding resins, fluid maintenance, and dietary restriction are first line treatments for hyperkalemia associated with AKI [2]. Unfortunately, dialysis and kidney transplant have remained the gold standard of care for the treatment of AKI for over 40 years and there has been no improvement in health outcomes. Continuous renal replacement therapy (CRRT) and intermittent hemodialysis

cost approximately $4000/week and $1000/week, respectively while kidney transplant carries with it it's own risks and co-morbidities such as the necessary immunosuppression and related complications [13]. Several new agents have been proposed for the treatment of AKI and target the many components contributing to kidney injury. Unfortunately, while these treatment approaches seem promising in the laboratory setting, none have contributed significantly to outcomes in clinical trials (Figure 1-2) [14].

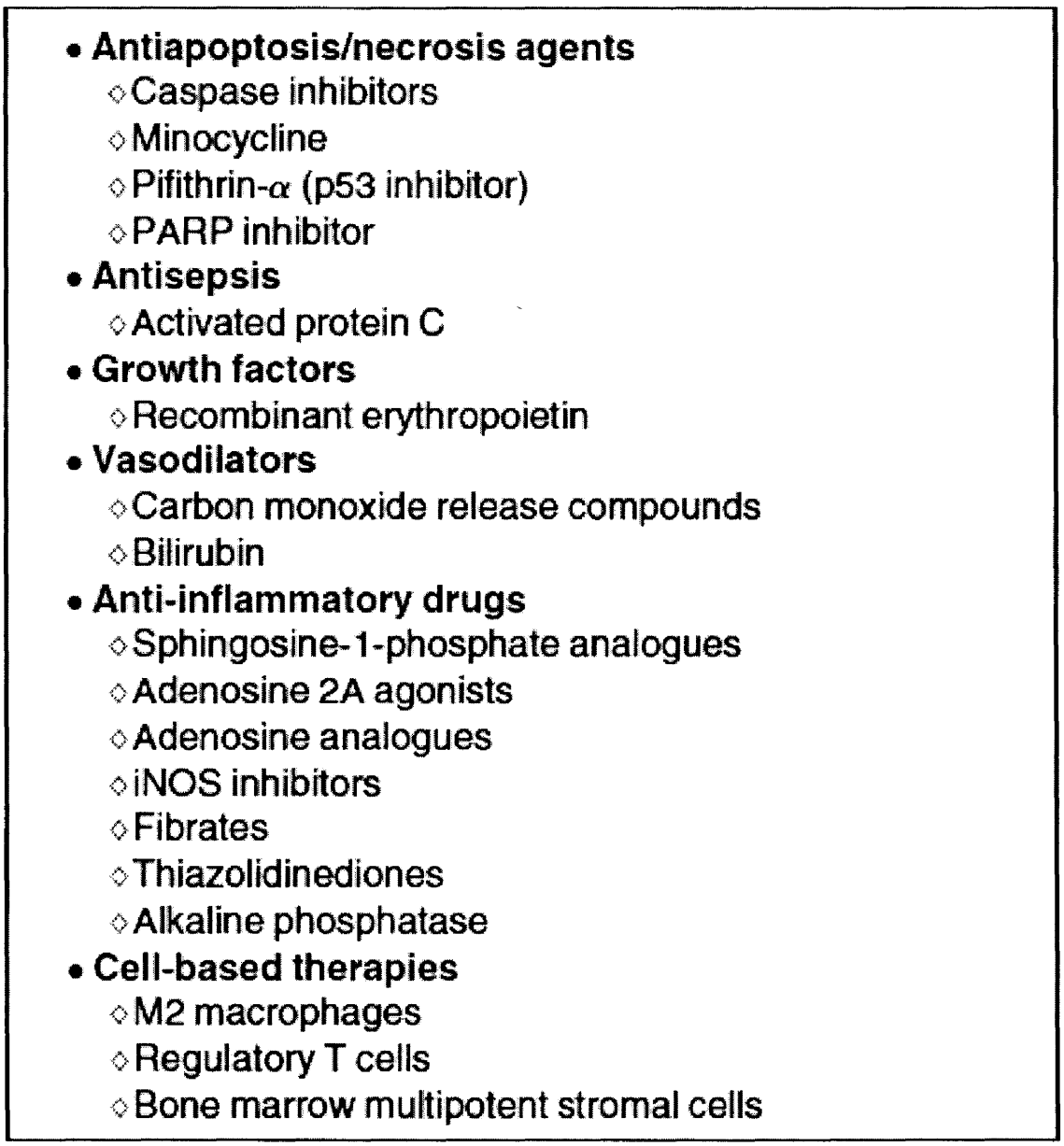


**Figure 1-2 Proposed Treatment Strategies for AKI.** Many therapeutics have been developed but none have resulted in significant improvement in clinical outcomes. Adapted from Kinsey and Okusa, 2011 [14].

**Causes of AKI** There are three major causes of AKI or ARF, classified as prerenal, intrarenal and postrenal. Prerenal ARF is characterized by decreased blood flow to the kidney secondary to decreased intravascular volume (ie. dehydration from excessive diuresis, vomiting, and/or diarrhea) or decreased blood flow (ie. renal artery stenosis, liver and heart failure, and shock associated loss of intravascular pressure) [2]. The widely used medications, non-steroidal anti-inflammatory drugs (NSAIDs) and angiotensin-converting enzyme inhibitors (ACEIs) can cause prerenal ARF by decreasing the pressure in Bowman's capsule. NSAIDs block the production of vasodilatory prostaglandins and drive the production of thromboxane $A_2$ causing the vasoconstriction of afferent arterioles resulting in decreased blood flow into the capsule in the absence of compensatory changes within the efferent arterioles leading to decreasing glomerular pressure and glomerular filtration rate (GFR). ACEIs decrease levels of angiotensin II resulting in dilation of efferent arterioles in the absence of increased blood flow into the glomerulus through the afferent arterioles resulting in a similar drop in glomerular pressure and GFR [15]. Pre-renal failure accounts for 40-70% of all renal failure and is primarily observed in the community setting and upon admission into the hospital [16]. Clinically, pre-renal failure may be diagnosed by measuring urine and serum electrolytes and creatinine and calculating the Fractional Excretion of Sodium (FENA). A FENA value of less that 1% is suggestive of a pre-renal component of kidney dysfunction.

Post-renal ARF can be identified by an obstruction of urine outflow from the kidneys. Obstruction may be caused by anatomical obstruction (developmental abnormalities,

strictures, benign prostatic hypertrophy, abdominal aortic aneurysms, or tumors) or physical obstruction (ie. kidney stones, cellular debris or catheters) [17]. The extent of damage to the kidney and therefore risk of end stage renal disease is proportional to the extent of obstruction and the length of time the obstruction is present [2]. Anatomical malformations, hyperkalemia, and other metabolic disturbances are common sequelae of post-renal obstruction and should be monitored closely and treated promptly.

Intra-renal ARF is a result of dysfunction within the kidney and is divided into 4 groups characterized by the anatomical region most significantly affected (glomerular, interstitial, vascular and tubular). Intrarenal ARF is sometimes used interchangeably with acute tubular necrosis (ATN), although necrosis does not seem to be the only underlying mechanism of cell death. Intrarenal ARF is the most common cause of kidney failure in the hospital setting [2].

Glomerular causes of ARF are relatively uncommon and are often associated with immunological disorders such as systemic lupus erythematosus, Goodpasture's disease, and other nephritic/nephrotic disorders. Systemic findings such as fever, arthritis and rash are commonly present in patients with glomerular ARF [2]. Interstitial ARF is less well understood, but is often caused by infection, autoimmune diseases or allergic reaction to several drugs (ie. allopurinol; cephalosporins; ciprofloxacin; NSAIDs; penicillins; sulfonamides and thiazide diuretics) [2]. Vascular ARF results from renal artery stenosis or occlusion of smaller vessels inside the kidney. Because of the apparent overlap in the causes of ARF and their classification, grouping is becoming less relevant,

but the mechanism of injury has become more important to understanding the etiology of the disease.

**Acute Tubular Necrosis.** Although ATN is often used interchangeably with intra-renal failure, necrosis is often not the only and sometimes not the major mechanism of cell death. However, ATN is characterized by injury to and death of tubular epithelial cells. Histological findings associated with ATN include: loss of brush border, thinning of the tubular epithelial cell layer, interstitial edema, sloughing of cells into the lumen of the tubule and tubular dilation (Figure 1-3) [18] . ATN is most commonly caused by ischemia, ischemia/reperfusion, anoxia, or drug and toxicant injury.

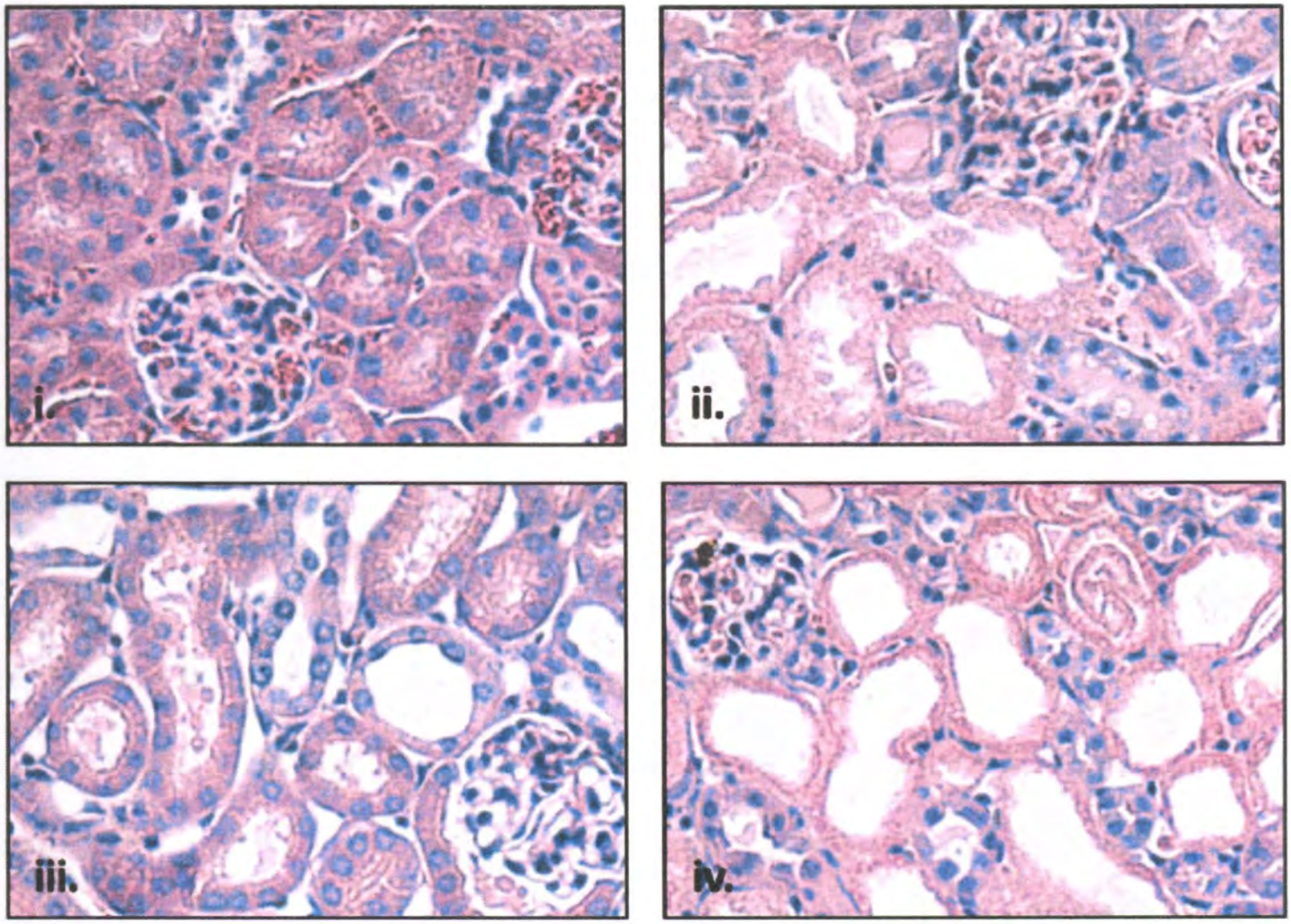


**Figure 1-3. Representative histology (hematoxin and eosin stain) of a normal kidney and of a kidney exhibiting acute tubular necrosis.** i. Normal kidney cortex morphology. Ischemia/reperfusion-induced acute tubular necrosis at 24 h (ii), 72 h (iii), or 144 h (iv) after ischemia-reperfusion injury at 40X magnification. Morphology consistent with acute tubular necrosis including tubular dilation, loss of brush border and increased space between tubules. From Funk and Schnellmann, 2011 [19].

nephrotoxic drugs or chemicals [20-21]. Proximal tubule cells are especially sensitive to insult because of their high energy demand secondary to their extensive ATP-dependent transport capacity. Renal proximal tubule cells lack the capability of producing glycolytic ATP during periods of ischemia [22]. Several drugs selectively target RPTC

because, in the process of transporting nephrotoxic drugs into and out of the urine, intracellular concentrations of these drugs reach high levels. Aminoglycoside antibiotics and anticancer drugs such as cisplatin are examples of agents that are directly toxic to RPTC and induce ARF. Mercury and cadmium are examples of environmental toxins that can induce cell death of RPTC and precipitate ARF [23].

There are 3 stages of ATN termed: initiation, maintenance and recovery. Initiation is the time immediately following toxicant exposure or ischemia and GFR is severely reduced. The maintenance phase can last up to 2 weeks and is associated with a continued reduction in GFR, decreased urine output and increased BUN and $S_{Cr}$. The kidney has restorative and regenerative capacities very similar to the liver that enable them to restore function following ATN if the initiating insult is not overwhelming. The recovery phase is characterized by increased urine output, increased GFR, and a decline in $S_{Cr}$ and BUN. Interestingly, most patients who survive ATN recover full renal function with little evidence of dead tubular tissue, demonstrating the regenerative capacity of the kidney [21].

**RPTC Cell Death in ATN.** Epithelial cell death can occur via necrosis and/or apoptosis and both are involved in the pathophysiology of ATN [24]. ATP levels during and following injury is a major determinant of the type of cell death that ensues [25]. Sufficient ATP levels are required to initiate and execute apoptosis and apoptosis is generally considered an ATP dependent process. For example, an insult that depletes

ATP levels acutely in a cell to 15% or less will induce necrotic cell death, while cell injury with less ATP depletion usually results in apoptosis [25]. Apoptosis and necrosis have significant different effects on surrounding cells and tissues and these differences may be very important in the progression of many disease processes. Apoptosis, the more organized form of cell death, is thought to protect surrounding tissues from non-specific proteolytic degradation while signaling to neighboring injured cells to carry out the same process. It is also important to note that some types of cell death display combinations of necrotic and apoptotic characteristics [26].

**Necrosis.** Necrosis is characterized by loss of plasma membrane integrity and release of intracellular contents. The intracellular contents themselves contain activated proteolytic enzymes which damage neighboring cells while resulting in the robust activation of immune cells which can lead to inflammation and further disruption of neighboring tissues [27]. Rapid ATP depletion is a major trigger of necrotic cell death in the kidney. ATP depletion impairs ion transporters, especially the $Na^+/K^+$-ATPase and $Ca^{2+}$-ATPase, leading to increased cytosolic concentrations of $Na^+$ and $Ca^{2+}$ [28]. The increased cytosolic $Na^+$ has two major impacts that facilitate the progression of necrotic cell death. Initially, the $Na^+$ drives the osmotic movement of water into the cell causing swelling. Additionally, the intracellular $Na^+$ inhibits the $Na^+/Ca^{2+}$ exchanger leading to further increased cytosolic $Ca^{2+}$, which has several deleterious effects on the cell. $Ca^{2+}$ activates cytosolic calpains, mediating the loss of cell membrane integrity by cleaving cytoskeletal proteins which support the plasma membrane [29]. Increased cytosolic $Ca^{2+}$ is also buffered by active mitochondria. $Ca^{2+}$ sequestration promotes the opening of a

proteinaceous pore called the mitochondrial permeability transition (MPT) pore, leading to further ATP depletion [30]. Late in necrotic cell death, $Cl^-$ and water influx facilitate opening of a glycine-sensitive plasma membrane pore, the "death channel", which is porous to macromolecules up to 145 kDa, leads to membrane rupture [31-32].

**Apoptosis.** Apoptosis is a major contributor to cell death following ischemic and toxic insults [20, 24]. Apoptosis is an ATP-dependent process that is highly regulated and involves several signaling pathways that results in the organized cell death. During apoptosis, cells maintain plasma membrane integrity and results in cell shrinkage rather than swelling (swelling is a characteristic finding of necrotic cell death). Externalization of phosphatidylserine in the setting of preserved plasma membrane integrity signals phagocytic cells such as macrophages to migrate towards and engulf injured cells undergoing apoptotic cell death. The apoptosis may be initiated by both extracellular stimuli and intracellular signals. Interestingly, while rapid and severe ATP depletion is a hallmark of necrotic cell death, GTP (guanosine triphosphate) depletion is a major trigger for apoptotic cell death in the kidney [33].

Extracellular-mediated (extrinsic) apoptosis is initiated by the binding of signaling ligands to receptors on the plasma membrane, which results in the activation of very organized signaling cascades. For example, tumor necrosis factor (TNF)-related apoptosis-inducing ligand (TRAIL), Fas, and TNF receptor 1 (TNFR1) ligand binding results in receptor aggregation on the plasma membrane, initiating the formation of the death-inducing signaling complex (DISC) The DISC is comprised of activated and

aggregated receptors, the Fas-associated death domain (FADD), and procaspase 8 and its formation results in procaspase 8 cleavage to caspase 8. Caspases are a family of cysteine proteases that play a role in the initation and execution of apoptotic cell death. Caspase 8 directly cleaves and activates procaspses 3, 6, and 7 (executioner caspases). In the proximal tubule, death receptors are expressed and up-regulated after injury [34] representing one mechanism of RPTC apoptosis during ARF. Additionally, mice lacking TNFR1 exhibit less apoptotic cell death and decreased kidney dysfunction following a toxic insult.

Opening of the mitochondrial permeability transition (MPT) pore [30] or permeablization of the outer mitochondrial membrane by members of the BCL-2 family or other mechanisms [35] releases cytochrome c and other factors that facilitate apoptosis. When cytochrome c is released from the mitochondria it interacts with Apaf-1 and procaspase-9 to form the apoptosome. The apoptosome, if ATP is present, activates caspase-9 which cleaves and activates procaspase-3. Permeablization of the outer mitochondrial membrane also releases Smac/Diablo, Endonuclease G and apoptosis inducing factor (AIF). Smac/Diablo releases causes apoptosis by inhibiting inhibitor of apoptosis proteins (IAPs). IAPs prevent caspase cleavage and activation [36]. Endonuclease G and AIF participate in DNA degradation associated with apoptosis [36]. Interestingly, the kidneys of mice lacking cyclophillin D, a critical component of the MPT pore, are protected from ischemia-reperfusion injury. Additionally, proapoptotic members of the BCL-2 family including BID and BAX translocate to mitochondria and form pores leading to release of apoptotic mediators in models of AKI, while

overexpression of antiapototic members such as BCL-xL prevents the release of these mediators, prevents apoptosis, and preserves kidney function following kidney injury.

**ROS.** Reactive oxygen species are a major component of many disease processes and mediate injury and response to injury during ATN [20-21]. ROS is the byproduct of several cellular processes (ie. the incomplete reduction of $O_2$ in mitochondria, inflammatory cell activation, and drug and toxicant metabolism) [20]. Superoxide and hydrogen peroxide ($H_2O_2$) are important oxidant molecules that are produced by mitochondria under normal conditions and in greater quantities upon reperfusion or in mitochondria damaged by toxicants [37]. Increased cytosolic $Ca^{2+}$ also leads to superoxide production by activation of proteases which cleave xanthine dehydrogenase to yield xanthine oxidase [38]. Superoxide dismutase is a major intracellular antioxidant enzyme that metabolizes superoxide to $H_2O_2$. $H_2O_2$ can then be reduced to water by catalase or it can be converted to the damaging HO· radical in the presence of ferrous iron ($Fe^{2+}$) or cuprous ions. HO· radicals are produced in the kidney shortly after reperfusion in experimental models of ARF [39-40]. Finally, peroxynitrite, produced from the reaction of superoxide with nitrous oxide, is also reported to contribute to the pathology associated with ischemic ARF [41].

ROS damage cellular proteins, DNA and lipids. Protein oxidation is elevated after ischemia and reperfusion in the rat kidney and the increase is blocked by the antioxidant n-acetylcysteine [38]. ROS, especially $H_2O_2$ are implicated in DNA strand breaks which can induce cells to undergo apoptosis [20]. Lipid peroxidation describes the chain

reaction initiated when a free radical abstracts hydrogen from an unsaturated fatty acid linked to a phospholipid inside a cellular membrane. If it is not stopped, lipid peroxidation can potentially destroy an organelle or cell membrane. Lipid peroxidation of cell and organelle membranes increases membrane rigidity and permeability to ions [20-21]. Furthermore, ROS-mediated lipid oxidation in the mitochondrial inner membrane inhibits the function of the electron transport chain [42]. End products of lipid peroxidation such as 4-hydroxy-2,3-nonenal have biological actions including increasing passive $Ca^{2+}$ permeability in biological membranes [43]. In summary, ROS damage various intracellular targets and lipid peroxidation inhibits membrane structure and function, impairs mitochondrial function and leads to $Ca^{2+}$ influx.

**$Ca^{2+}$ Regulation**. $Ca^{2+}$ acts as a universal second messenger and regulates numerous cellular functions including metabolism, motility, and transport[44]. Loss of $Ca^{2+}$ homeostasis is critical to many disease processes and is a major component of cell death pathways including necrosis, apoptosis, and autophagy [45-51] (Figure 1-4). Sarcoplasmic/endoplasmic reticulum (ER) $Ca^{2+}$ is the most abundant store of intracellular $Ca^{2+}$and its disruption often initiates the deleterious cascade of events leading to cell death and dysfunction [48-54]. Release of the ER $Ca^{2+}$ stores is a key trigger for necrotic cell death in renal cells [53]. Thapsigargin inhibits the ER $Ca^{2+}$-ATPase (SERCA) causing release of ER $Ca^{2+}$ and in the presence of ATP the cell can pump out the excess cytosolic $Ca^{2+}$, effectively depleting the ER $Ca^{2+}$ store. Harriman et al. (2002) showed that thapsigargin exposure prior to ATP depletion blocked calpain activation and necrotic

cell death, establishing the importance of this intracellular pool of $Ca^{2+}$ in the death of renal epithelial cells [53].

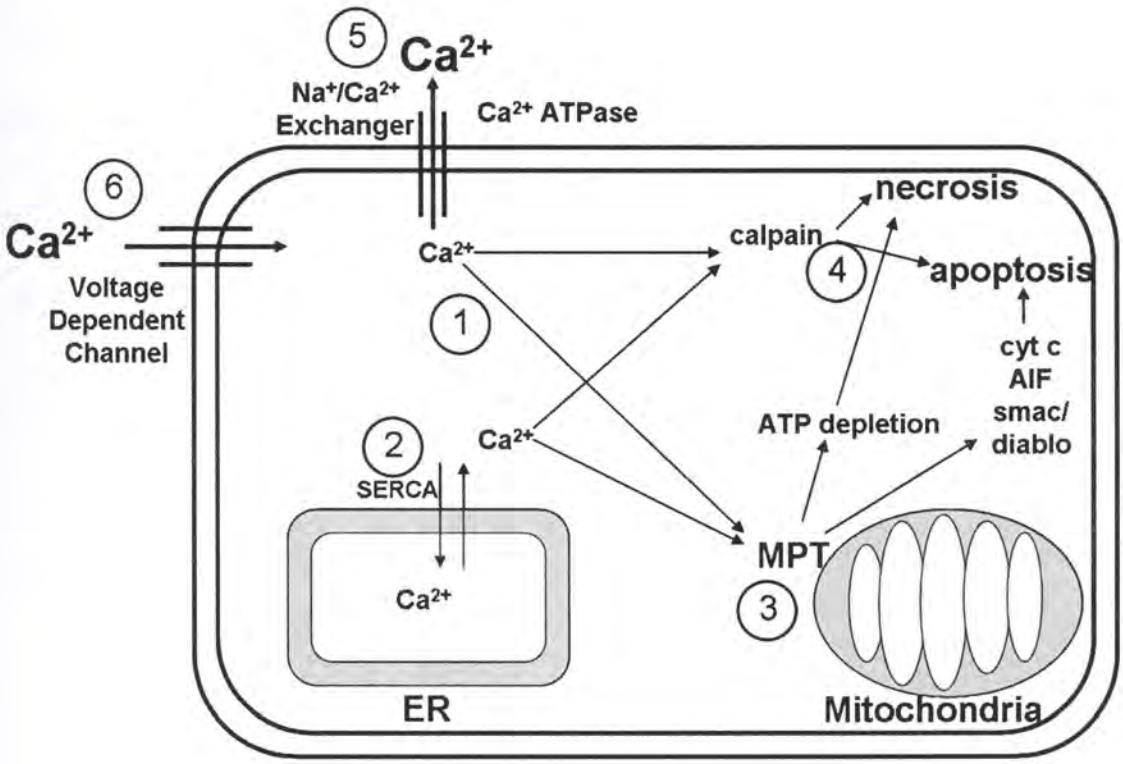


**Figure 1-4. Schematic of the role of $Ca^{2+}$ in renal cell death.** **1.** Cytosolic $Ca^{2+}$ is regulated by numerous mechanisms and organelles inside renal cells. **2.** Endoplasmic reticulum $Ca^{2+}$-ATPase (SERCA) pumps on the ER membrane pump $Ca^{2+}$ into the lumen of the ER to buffer cytosolic levels participate in signaling. **3.** During injury cytosolic $Ca^{2+}$ concentrations exceed 400-500 nM and mitochondria begin to actively sequester $Ca^{2+}$. This causes opening of the mitochondrial permeability transition (MPT) pore leading to mitochondrial swelling and inhibition of ATP synthesis. Mitochondrial swelling facilitates the release of cytochrome c (cyt c), apoptosis inducing factor (AIF), smac/diablo from the intermembrane space of mitochondria which in the presence of ATP cause the cell to undergo apoptosis. If MPT has spread to a sufficient proportion of mitochondria and cellular ATP becomes depleted the cell will undergo necrosis. **4.** A rise in cytosolic $Ca^{2+}$ also activates cytosolic calpain, a protease which mediates apoptosis and necrosis. **5.** Membrane bound $Ca^{2+}$ efflux pumps use the $Na^{+}$ gradient and ATP to remove $Ca^{2+}$ from the cytosol. **6.** $Ca^{2+}$ enters from the extracellular space through a voltage gated channel. Adopted with permission from Kinsey GR 2007.

Mitochondria have a large capacity for $Ca^{2+}$, which is shuttled into the matrix by a ruthenium red (RR)-sensitive channel called the $Ca^{2+}$ uniporter [55]. In the kidney, substantial mitochondrial $Ca^{2+}$ uptake occurs after cytosolic concentrations reach 400 nM or greater which is usually only seen during cell injury [56]. There is a negative correlation between the matrix $Ca^{2+}$ concentration and oxidative phosphorylation and ATP production [21]. Furthermore, mitochondrial $Ca^{2+}$ accumulation favors the opening of the MPT pore, which depolarizes the inner membrane and compounds the injury with futile ATP hydrolysis by F(1)F(0)-ATP synthase in reverse mode in an attempt to restore mitochondrial membrane potential [57]. In summary, $Ca^{2+}$ is an important signal from the ER and to the mitochondria during renal cell death.

**Role of Phospholipase $A_2$ in AKI.** Phospholipase $A_2$ ($PLA_2$) activity has been implicated in the progression of ischemia/reperfusion-induced failure of the heart, brain, and kidney. Ischemia has been shown to activate $PLA_2$ leading to membrane degradation and lysophospholipid accumulation, which impair membrane function and integrity and lead to cell death [58-61]. Additionally, secretory and $Ca^{2+}$-dependent phospholipase $A_2$ inhibitors prevented cell death *in vivo* after heart [62] and brain [63] ischemia/reperfusion (I/R). The addition of purified bee or snake venom secretory $PLA_2$ to hypoxic rat renal proximal tubules caused degradation of phospholipids which increased as ATP levels declined and was mitigated by addition of ATP [64]. While cell death was not measured, $PLA_2$ addition inhibited uncoupled respiration and decreased intracellular $K^+$ content during hypoxia [64]. Cytosolic $Ca^{2+}$-independent $PLA_2$ ($iPLA_2$)

is reportedly activated by hypoxia in rabbit renal proximal tubule sections, while no change was observed in membrane-bound $iPLA_2$ activity in this model during hypoxia [65]. Inhibition of cytosolic $iPLA_2$ activity inhibited hypoxia-induced arachidonic acid generation and lactate dehydrogenase release [65]. In summary, many studies have implicated $PLA_2$-mediated membrane degradation in the cell injury induced by I/R in several organs including the kidney.

However, in different studies, addition of pancreatic $PLA_2$ or venom $PLA_2$ to hypoxic rat renal proximal tubule segments prevented cell death even in the presence of ATP depletion [66-67]. The protective effect of $PLA_2$ in these studies is hypothesized to be due to a negative feedback effect of unsaturated free fatty acids on endogenous $PLA_2$ [21]. Additionally, studies from our laboratory have shown that membrane-associated $iPLA_2$ inhibition in primary cultures of rabbit RPTC potentiates oxidant-induced lipid peroxidation and necrosis [68]. In summary, the different isoforms of $PLA_2$ may have different roles in ARF and the role of $iPLA_2$ in ARF may depend on its intracellular localization.

**Phospholipids.** The major structural components of cell and organelle membranes are phospholipids (PLs). There are hundreds of different types of phospholipids in mammalian membranes which can vary in the fatty acids linked at the *sn*-1 and *sn*-2 positions, the type of linkage between the glycerol backbone and the *sn*-1 fatty acid, and the polar head group [69] (Figure 1-5). In addition to providing a barrier between the extra- and intracellular space, PLs play a vital role in cell signaling. For example, stimulation of G-protein coupled receptors (GPCRs) activates phospholipase C (PLC)

which cleaves the PL phosphatidylinositol-4,5-bisphosphate in the cell membrane, generating inositol-triphosphate and diacylglycerol (DAG). These two molecules play key roles in the intracellular signaling of GPCR activation by triggering the release of ER $Ca^{2+}$ and activating PKC, respectively. PLs are precursors of platelet activating factor (PAF) that interacts with a GPCR to regulate cardiac function and renal blood flow and may mediate atherogenesis [70-71]. In summary, phospholipids are a class of molecules with an extremely large number of members, are required as a major structural component of cell and organelle membranes and are used to transmit signals inside the cell and from one cell to another.

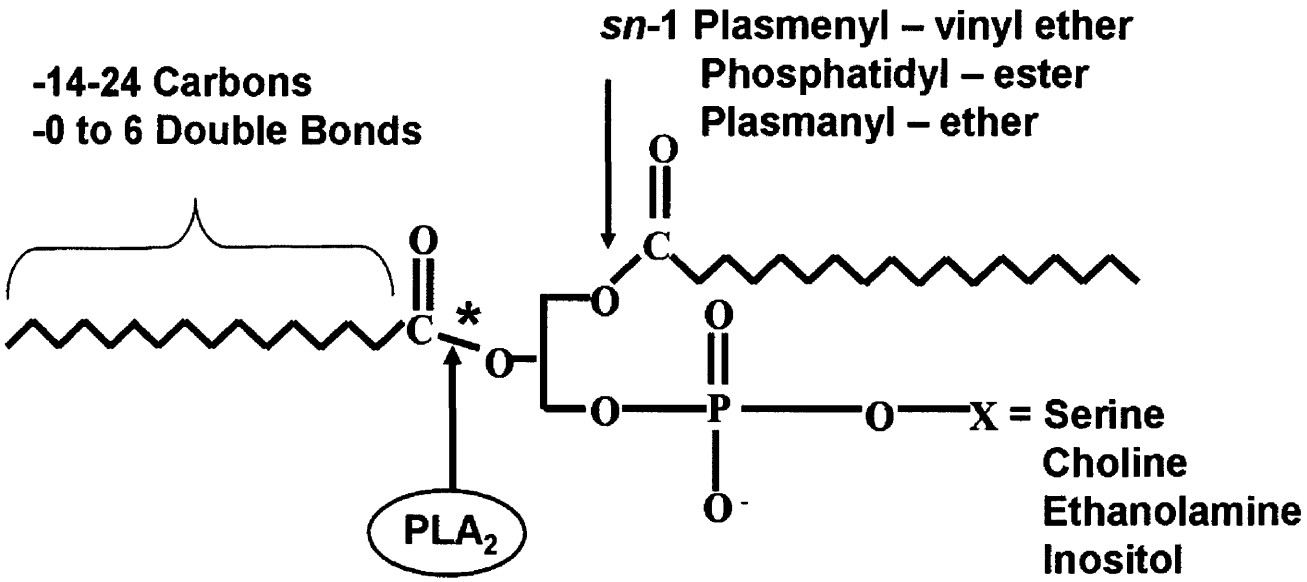


**Figure 1-5. Glycerophospholipids and site of $PLA_2$ hydrolysis.** $PLA_2$ enzymes catalyze the cleavage of the *sn*-2 ester bond of glycerophospholipids (*). Fatty acids of 14 to 24 carbons in length, containing 0 to 6 double bonds are esterified to the glycerol backbone at the *sn*-2 position. At the *sn*-1 position, fatty acids can be linked to the glycerol backbone by an ester bond (shown) and referred to as a phosphatidyl- or diacyl-phospholipid or by a vinyl ether bond and referred to as a plasmenyl- phospholipid. Phospholipids with an ether linkage at the *sn*-1 are termed plasmanyl- phospholipids.

**Fatty acids.** Phospholipids are a reservoir of fatty acids, the structural building blocks of phospholipids and another very important component of cell signaling. Arachidonic acid (AA, a fatty acid with 20 carbons and 4 double bonds, denoted 20:4) is the most well known and extensively studied fatty acid although many other fatty acids have biological activity. AA is metabolized by: cyclooxygenases to prostaglandins and thromboxane $A_2$; lipoxygenases to leukotrienes and cytochrome p450 enzymes to several other oxidized signaling molecules [72]. Other fatty acids, such as linoleic, oleic, and palmitic acids are

in high abundance in the kidney and are thought to play a major role in phospholipid structure and function and cell signaling (Figure 1-6) [73].

| # of Carbons: Double Bonds | Trivial Name | Systematic Name | Weight Percentage in Kidney* |
|---|---|---|---|
| 14:0 | Myristic | tetradecanoic | <1 |
| 15:0 | n.a. | pentadecanoic | <1 |
| **16:0** | **Palmitic** | **hexadecanoic** | **19.2** |
| 16:1 | Palmitoleic | hexadecenoic | 2.4 |
| 17:0 | Margaric | heptadecanoic | <1 |
| **18:0** | **Stearic** | **octadecanoic** | **13.4** |
| **18:1** | **Oleic** | **octadecaenoic** | **21.9** |
| **18:2** | **Linoleic** | **octadecadienoic** | **24.4** |
| 18:3 | Linolenic | octadecatrienoic | <1 |
| 20:1 | Gondoic | eicosenoic | <1 |
| **20:4** | **Arachidonic** | **eicosatetraenoic** | **12.1** |
| 20:5 | n.a. | eicosapentaenoic | <1 |
| 22:5 | n.a. | docosapentaenoic | 1.7 |
| 22:6 | n.a. | docosahexaenoic | <1 |

**Figure 1-6. Common fatty acid components of mammalian kidney phospholipids.** *Mean weight percentage of each fatty acid in lipids of kidney from D. C. Rule et al., 1994 [73]. Most abundant fatty acids are in bold. n.a. – fatty acids without established trivial names.

**Lipid Peroxidation.** ROS generation is a major component of ischemia/reperfusion and drug and toxicant injury. Major targets of ROS are cell and organelle membrane phospholipids [74]. The initiation step of lipid peroxidation involves the abstraction of a

hydrogen atom from the methylene carbon of a fatty acid and therefore fatty acids with more double bonds are more vulnerable to the initiation of lipid peroxidation [75]. These fatty acid species are usually polyunsaturated fatty acids (PUFAs). Abstraction of the hydrogen atom from PUFAs forms a pentadienyl radical, which in aerobic conditions reacts with oxygen to form a peroxyl radical. The resulting peroxyl radical is capable of abstracting a hydrogen atom from adjacent fatty acids, thus propagating the lipid peroxidation and potentially producing several lipid hydroperoxides [76]. This chain of events can be terminated by the removal of the reactive lipid from the site of reaction or a chain-breaking antioxidant (Figure 1-7) [75-77].

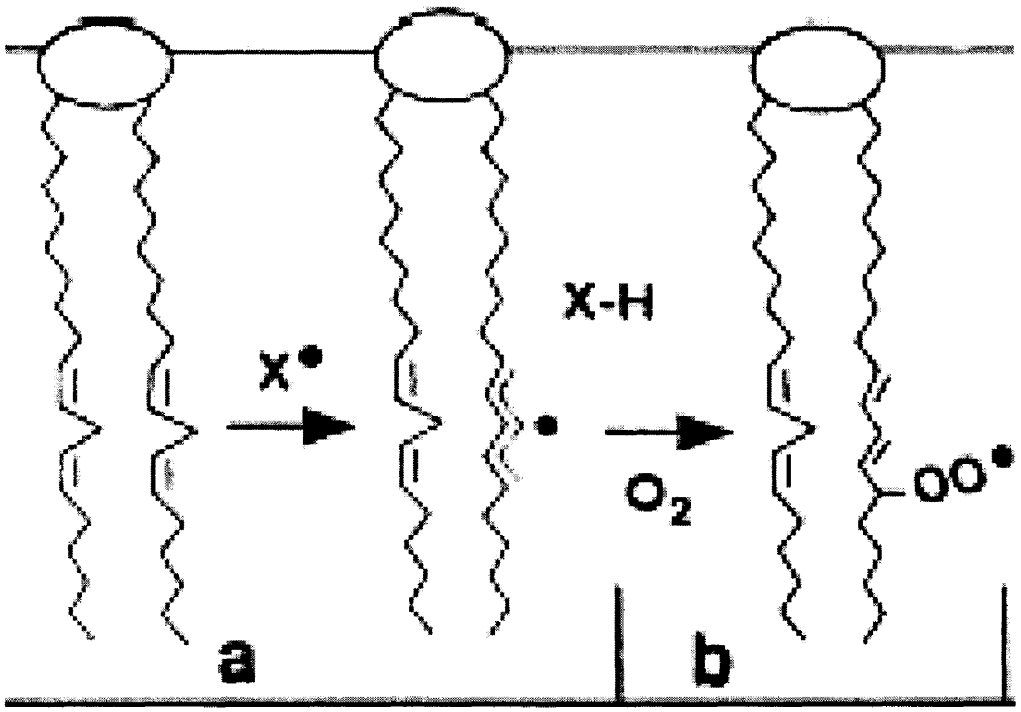


A.

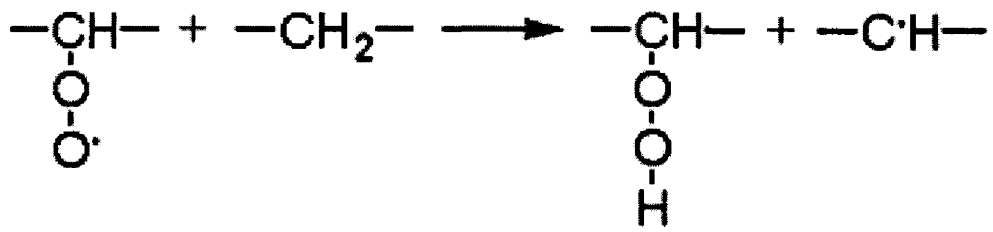


B.

**Figure 1-7. Schematic representation of free radical attack on membrane phospholipids.** (A) Initiation of lipid peroxidation. The free radical (X·, normally a hydroxyl radical) abstracts a proton from an *sn*-2 unsaturated fatty acid linked to the glycerol backbone of a membrane phospholipid, forming a pentadienyl radical (a). Oxygenation forms a peroxyl radical and a conjugated diene (b). (B) Propagation of lipid peroxidation. The peroxyl radical abstracts a proton from a methylene of a neighboring polyunsaturated fatty acid forming a new pentadienyl radical that react with oxygen to form another peroxyl radical and this pattern continues until the oxidized fatty acids are removed from the membrane or react with a chain terminating molecule such as α-tocpherol. Adapted from [78-79]

In mammalian tissues, PUFAs are predominantly esterified at the *sn*-2 position of PLs [80]. It has been proposed that phospholipases play a role in membrane remodeling and repair during oxidant stress by cleaving oxidized and/or unsaturated fatty acids from the membrane, preventing the initiation and propagation of lipid peroxidation, and allowing for the incorporation of unoxidized fatty acids [74]. ER and mitochondria are the major sites of reactive oxygen species (ROS) production and the presence of $iPLA_2\gamma$ in mitochondria and ER of rabbit RPTC makes it a likely candidate for a role in membrane repair and remodeling. The most probable mechanism by which these enzymes prevent or repair lipid peroxidation is through the cleavage and removal of oxidized fatty acids from the membrane [81] The liberated oxidized free fatty acid can then be reduced by cytosolic glutathione peroxidase (GPx) and the lysophospholipid reacylated by a CoA-dependent acyltransferase to reform a non-oxidized phospholipid and preserve membrane integrity [82]. *In vitro* analyses in non-cell based systems have demonstrated that, in concert with GPx, $PLA_2$ enzymes are capable of performing this protective repair function [83-85]. Thus far, the $PLA_2$ isoform(s) involved in this important cell survival function has not been determined *in vivo* or in an intact cell model. However, recent studies from our laboratory have demonstrated that inhibition of membrane-associated $iPLA_2$ activity in RPTC potentiated oxidant-induced lipid peroxidation [68], but thus far the tools necessary to identify this isoform have not been available. Furthermore, the role of this lipid peroxidation repair pathway in prevention of or hastening recovery from ARF has not been addressed.

## Review of Phospholipase $A_2$ Biology

**$PLA_2$ Overview.** Phospholipase $A_2$ ($PLA_2$) enzymes catalyze the hydrolysis of fatty acids at the *sn*-2 position of glycerophospholipids resulting in the production of a free fatty acid and a lysophospholipid [86]. Free fatty acids and their metabolites are biologically active in such processes as inflammation, cell signaling, and cell death. Interestingly, Polyunsaturaed fatty acids (PUFAs) are predominately esterified at the *sn*-2 position of phospholipids [80]. Arachidonic acid, for example, is metabolized to prostaglandins, prostacyclins, thromboxanes and leukotrienes, all of which play a role in inflammatory responses and cell signaling [87]. The resulting lysophospholipids serve as substrates for the re-esterification of free fatty acids by CoA-dependent acyltransferases and are also cell signaling molecules [82]. The deacylation and reacylation of phospholipids is termed "The Lands Cycle" and may be involved in membrane remodeling and the maintenance of membrane homeostasis under physiological and pathological conditions. However, there are limited studies investigating this phenomenon in cellular systems [88].

$PLA_2$ enzymes are classified according to the homology of their nucleotide sequences into 14 groups designated groups I-XIV [86] or according to a historical classification based on functional characteristics into 4 groups: secretory $PLA_2$ ($sPLA_2$), cytosolic $PLA_2$ ($cPLA_2$), lipoprotein associated PLA2s platelet-activating factor acetylhydrolases, and $Ca^{2+}$-independent $PLA_2$ ($iPLA_2$) [89].

Calcium-independent phospholipase $A_2\gamma$ ($iPLA_2\gamma$) is one of seven $Ca^{2+}$-independent $PLA_2$ enzymes [81] (Figure 1-8). $iPLA_2$ enzymes do not require $Ca^{2+}$ for activity or translocation, range in size from 29 to 85 kDa, have an ATP-binding motif and lipase sites, and, with the exception of certain splice variants of $iPLA_2\beta$, are membrane-associated [90]. The first mammalian $iPLA_2$ described was $iPLA_2\beta$ [91] (Group VIA $PLA_2$) and much is now known about this enzyme including regulation of activity [92] and its physiological and pathological roles (see below). $iPLA_2\delta$ (Group VIC $PLA_2$) is also called the neuropathy target esterase and is found predominately in neurons [93]. Three newer members, $iPLA_2\varepsilon$, $\zeta$ and $\eta$ (Groups VID, VIE and VIF) possess modest classical $PLA_2$ activity (*sn*-2 hydrolysis of phospholipids) and are efficient triglyceride lipases and acylglycerol transacylases [94]. Mancuso et al. and Tanaka et al. identified $iPLA_2\gamma$ in non-mammalian Sf-9 (insect) and COS-7 (bacterial) cells, respectively in 2000 [95-96]. In 2002, our laboratory reported the expression of an 85-kDa mammalian $iPLA_2$ selective for plasmalogen phospholipids and with an inhibitor profile not consistent with $iPLA_2\beta$ in the ER of rabbit RPTC [68]. We identified the ER $iPLA_2$ as $iPLA_2\gamma$; showed its presence in different species including humans; confirmed its activity in various tissues including the brain, heart, and kidney; and excluded the presence of $iPLA_2\beta$ [97]. More recent studies identified $iPLA_2\gamma$ in the mitochondria of rabbit renal cortex and RPTC [98].

| Calcium-Independent $PLA_2$ Isoforms | | | |
|---|---|---|---|
| **Historical Classification** | **Group Number** | **PNPLA Number** | **Other Names** |
| **$iPLA_2\alpha$ (alpha)** | **n.a.** | **n.a.** | **patatin** |
| **$iPLA_2\beta$ (beta)** | **VIA** | **9** | **PLA2G6** |
| **$iPLA_2\gamma$ (gamma)** | **VIB** | **8** | **$iPLA_2$-2** |
| **$iPLA_2\delta$ (delta)** | **VIC** | **6** | **neuropathy target esterase** |
| **$iPLA_2\varepsilon$ (epsilon)** | **VID** | **3** | **adiponutrin** |
| **$iPLA_2\zeta$ (zeta)** | **VIE** | **2** | **TTS-2.2** |
| **$iPLA_2\eta$ (eta)** | **VIF** | **4** | **GS2** |

**Figure 1-8 Different naming systems for $iPLA_2$.** Commonly used names for the members of the $iPLA_2$ family. Historical classifications and group numbers have been reviewed [81]. Human $iPLA_2$ genes were named patatin-like $PLA_2$ (PNPLA) by Wilson et al. (2006) and each assigned a number. Other names used in the literature to identify each $iPLA_2$ isoform are also listed. n.a. – not assigned.

**$iPLA_2\beta$.** $iPLA_2\beta$ is predominately expressed as a cytosolic protein and is regulated by several different mechanisms. The peptide sequence encodes ankyrin repeats [99] which participate in protein-protein oligomerization interactions of different $iPLA_2\beta$ splice variants that regulate catalytic activity [100]. The stability and activity of purified $iPLA_2\beta$ are increased in the presence of ATP [101] and activity is inhibited by calmodulin binding [102]. Caspase-mediated $iPLA_2\beta$ activation results in increased free fatty acid release and generates lysophosphatidylcholine, a novel chemotactic signal to attract phagocytes toward apoptotic cells [103].

$iPLA_2\beta$ is reported to mediate pancreatic insulin secretion [104], phospholipid remodeling [105], store operated $Ca^{2+}$ entry [106], and ischemia induced

arrythmyogenesis [107]. Ramanadham et al. (2003) demonstrated that overexpression of iPLA$_2$β in pancreatic insulinoma cells amplifies glucose-stimulated insulin secretion and this effect is inhibited by the irreversible mechanism based iPLA$_2$ inhibitor bromoenol lactone (BEL) [104]. In a human lymphoma cell line (U937), BEL blocked the production of lysophospholipid acceptors for AA, and the incorporation of AA into membrane phospholipids [105]. In a follow-up study, overexpression of iPLA$_2$β accelerated AA incorporation into U937 cell membrane PLs, confirming the role of iPLA$_2$β in phospholipid remodeling [108]. In summary, iPLA$_2$β activity is associated with many physiological functions.

Taking advantage of the fact that mice express very little iPLA$_2$β activity in the heart, Mancuso et al. (2003) generated an iPLA$_2$β transgenic mouse and utilized isolated perfused hearts from wild type and transgenic animals to investigate the role of iPLA$_2$β during I/R. Transgenic mice were no different than wild type mice in terms of body weight, heart weight or cardiac function as measured by echocardiograph, prior to ischemia [107]. After I/R, transgenic hearts had greatly increased amounts of FFAs and lysophospholipids (products of PLA$_2$ activity known to cause electrical abnormalities in excitable cells) and arrhythmias occurred in the transgenic hearts but not wild type [107]. Pretreatment with BEL completely blocked FFA and lysoPL accumulation and arrhythmias in the transgenic mice [107] suggesting that iPLA$_2$β inhibition may lead to clinical benefit after myocardial infarction. In summary, iPLA$_2$β has been studied extensively and demonstrated to play important roles in physiology and pathology.

**iPLA$_2\gamma$.** In 2000, two independent laboratories identified a novel iPLA$_2$, iPLA$_2\gamma$ (Group VIB PLA$_2$), which appeared to be constitutively membrane bound and possesses a C-terminal SKL peroxisomal targeting sequence [95-96]. Since then, several studies have revealed that iPLA$_2\gamma$ is subject to transcriptional and translational regulation, is targeted to various intracellular organelles and is implicated in physiology and pathophysiology of different organs [95, 109-110]. Importantly, rabbit iPLA$_2\gamma$ shares approximately 88% amino acid sequence homology with human iPLA$_2\gamma$ and the sequence of its catalytic domain shares 100% homology, suggesting similar lipase activities [97-98].

**Expression of iPLA$_2\gamma$.** Based on segments of homology, between a predicted protein encoded on the long arm of chromosome 7 discovered during the Human Genome Project, and the previously identified members of the iPLA$_2$ family, Mancuso et al. (2000) determined the full-length mRNA sequence of iPLA$_2\gamma$. In a separate laboratory, the C-terminal DNA sequence of iPLA$_2\beta$ was compared to EST databases in an effort to discover a novel iPLA$_2$ (termed iPLA$_2$-2) [96]. Both iPLA$_2$ enzymes had identical 782 amino acid sequences and are homologous to iPLA$_2\alpha$ and iPLA$_2\beta$ only through the ATP binding and GXSTG lipase motifs. Whether expressed in insect or mammalian cells, iPLA$_2\gamma$ localized to crude membrane fractions and was not detected in cytosol [95-96]. In COS-7 cells (kidney fibroblast cell line), transfection with full-length iPLA$_2\gamma$ cDNA resulted in the expression of the expected 88 kDa protein [96]. In contrast, the full-length

cDNA in a rabbit reticulocyte lysate protein expression system or in Sf9 insect cells produced 77 and 63 kDa protein products [95]. These protein products correspond to translation initiation at downstream in-frame methionine residues on iPLA$_2\gamma$ mRNA [95, 110].

Mancuso et al. (2004) performed extensive experiments designed to determine how the expression of different sized iPLA$_2\gamma$ isoforms is regulated at the transcriptional and post-transcriptional levels. They discovered that iPLA$_2\gamma$ expression is repressed by transcriptional regulatory elements in the coding regions of iPLA$_2\gamma$ between the 88 kDa and 63 kDa start sites [110]. Using electrophoretic mobility shift analyses, the binding of unidentified nuclear proteins to iPLA$_2\gamma$ DNA was demonstrated which may also regulate transcription [110]. Initiation of translation at in-frame methionines of different splice variants potentially results in the expression of 92, 88, 77, 74 and 63 kDa isoforms and an inactive 33 kDa isoform of iPLA$_2\gamma$ [110]. In summary, multiple forms of iPLA$_2\gamma$ exist and the expression of iPLA$_2\gamma$ is subject to rigorous control at many levels and is still not completely understood.

**Regulation of iPLA$_2\gamma$ Activity.** Little is known about the regulation of iPLA$_2\gamma$ activity. Initial analysis of the protein revealed numerous potential phosphorylation sites including protein kinase A, PKC and mitogen-activated protein kinase consensus sequences [96]. Phosphorylation of iPLA$_2\gamma$ at specific amino acids has not been unambiguously

demonstrated, but several experiments from different laboratories support the hypothesis that iPLA$_2\gamma$ activity is regulated by phosphorylation. First, separation of heart proteins from a heart-specific iPLA$_2\gamma$ transgenic mouse, by two dimensional gel electrophoresis, revealed that each molecular weight isoform of iPLA$_2\gamma$ separated into multiple distinct spots with different isoelectric points (potentially representing different patterns of phosphorylation) [109]. Furthermore, isolated microsomes from rabbit heart and kidney cortex, treated with phorbol 12-myristate 13-acetate (PMA, an activator of PKC), demonstrated increased iPLA$_2$ activity [111-112]. Further studies revealed renal cortex mitochondrial iPLA$_2\gamma$ activity is enhanced in the presence of ATP and blocked by PKC inhibitor (PKC$\varepsilon$ inhibitor V1-2) [98, 113].

Extensive oxidative stress negatively regulates iPLA$_2$ activity in rabbit kidney cortex [114] and rat myocyte microsomes [115]. tert-Butyl hydroperoxide (TBHP)-induced inactivation of kidney microsomal iPLA$_2$ was reversible by adding the reducing agent dithiothreitol (DTT) suggesting that oxidants target protein thiols on iPLA$_2$ [114]. However, non-lethal oxidant stress increased iPLA$_2\gamma$ expression and activity [116].

A calcium ionophore, A23187, was shown to activate iPLA$_2\gamma$ when overexpressed in HEK293 cells [117] suggesting that iPLA$_2\gamma$ activity may be indirectly regulated by increased intracellular $Ca^{2+}$ concentrations. ER-iPLA$_2$ in rat ventricular myocytes is activated by the inflammatory cytokine IL-1$\beta$ in a BEL-sensitive manner, which may indicate that iPLA$_2\gamma$ plays a role in stimulus-induced AA generation and inflammation

[118]. Murakami et al. (2005) also reported that AA and oleic acid release was greatly increased in $iPLA_2\gamma$ overexpressing cells when exposed to fetal calf serum and IL-1β. Thrombin receptor activation, by thrombin or analogs thereof, also activates microsomal $iPLA_2$ in the heart leading to the production of arrhythmogenic lyso-phosphatidylcholine and FFAs [119]. The activation of $iPLA_2\gamma$ by cytosolic $Ca^{2+}$, inflammatory cytokines and thrombin demonstrate that $iPLA_2\gamma$ is regulated by diverse mechanisms and establish $iPLA_2\gamma$ as a potential drug target for treatment of inflammatory diseases as well as prevention of post-ischemic arrhythmia in the heart. The regulation of $iPLA_2\gamma$ in the kidney has not been elucidated.

**$iPLA_2\gamma$ Pharmacological Inhibition**. Predominate $iPLA_2$ isoforms may be distinguished by their activity profiles in response to pharmacological inhibitors. These differential inhibitor profiles have been used to identify the presence of the enzymes in subcellular fractions and are used to investigate the roles of phospholipases in both physiological and pathological processes. Methyl arachidonyl fluorophosphonate (MAFP) inhibits $cPLA_2\gamma$ and cytosolic $iPLA_2\beta$, but not $iPLA_2\gamma$ [68, 112]. Racemic BEL inhibits both $iPLA_2\beta$ and $iPLA_2\gamma$, but the enantiomers of BEL are differentially selective for the two enzymes . $iPLA_2\gamma$ is more sensitive to R-BEL than S-BEL, whereas $iPLA_2\beta$ is more sensitive to S-BEL than R-BEL [68, 97, 112-113].

$iPLA_2\gamma$ is sensitive to the pharmacological inhibitor racemic BEL at low micromolar concentrations [95], similar to $iPLA_2\beta$ [120]. However, other pharmacological inhibitors, arachidonyl trifluoromethylketone ($AACOCF_3$) and methylarachidonyl

fluorophosphonate (MAFP), which inhibit $iPLA_2\beta$ at low micromolar concentrations [121-122] do not inhibit microsomal $iPLA_2$ [68, 123]. Furthermore, Jenkins et al. (2002) demonstrated that separation of racemic BEL into the R- and S-enantiomers provides a mechanism to discriminate between $iPLA_2\gamma$ and $iPLA_2\beta$ activity (i.e. $iPLA_2\gamma$ is 10-fold more sensitive to R-BEL than S-BEL and $iPLA_2\beta$ is 10-fold more sensitive to S-BEL than R-BEL) (Figure 1-9). The use of different $iPLA_2$ inhibitors to confirm the participation of $iPLA_2\gamma$ in various biological processes has recently been used by several investigators [124-125].

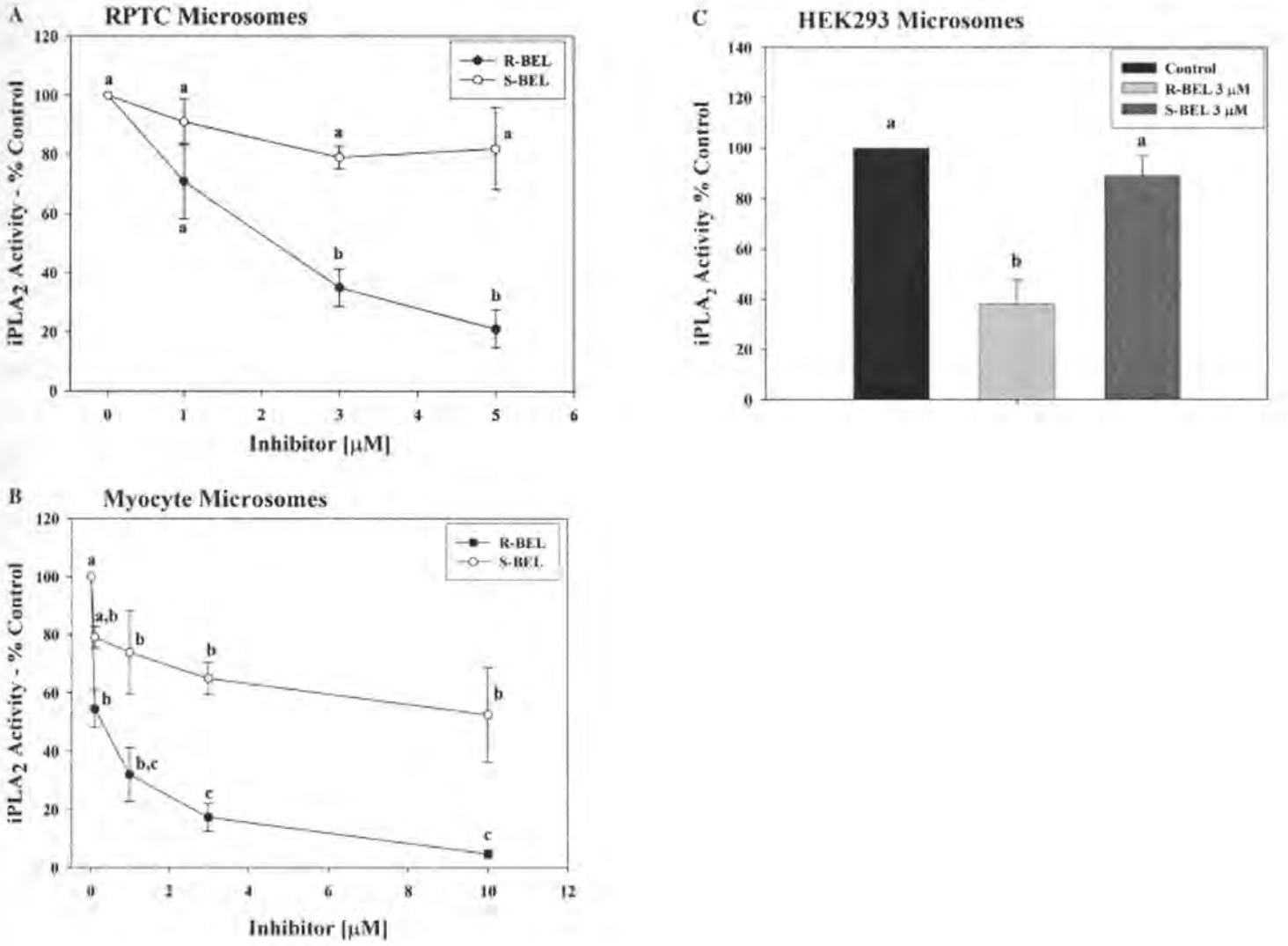


**Figure 1-9. Differential effect of R and S enantiomers of BEL on microsomal $iPLA_2$ activity in RPTC, ventricular myocyte microsomes or in microsomes isolated from HEK293 cells.** RPTC (**A**) were treated for 30 minutes with either (acetonitrile), R-BEL or S-BEL. Rabbit cardiomyocyte (**B**) and HEK293 (**C**) microsomes were isolated and incubated with solvent control (acetonitrile), R-BEL or S-BEL for 10 minutes prior to activity assays. $iPLA_2$ activity was measured using plasmenylcholine (16:0, [$^3$H]18:1) or substrates in the presence of 4mM EGTA. Values are means + SEM of at least 3 separate experiments. Means with different subscripts are significantly different from each other, $P<0.05$. Adopted from Kinsey et. al 2007.

**$iPLA_2\gamma$ Substrate Specificity.** The initial characterization of $iPLA_2\gamma$ substrate specificity demonstrated that membrane fractions from Sf9 insect cells expressing $iPLA_2\gamma$

cleaved phosphatidylcholine (PC) with unsaturated fatty acids at the *sn*-2 position but did not cleave palmitic acid (16:0) from the *sn*-2 position [95]. Of the unsaturated fatty acids at the *sn*-2 position tested, iPLA$_2\gamma$ activity was highest against AA containing PC. iPLA$_2\gamma$ was also slightly more active against plasmenylcholine (PlasC) with *sn*-2 oleic acid compared to oleic acid containing PC [95]. The authors of this study cautioned that differences observed in the activity of a membrane bound enzyme measured using exogenous substrates may only reflect the rate of membrane incorporation of different types of PLs [95]. Several subsequent studies have further examined the activity of iPLA$_2\gamma$ against different PL species using different methodologies.

The same group later overexpressed a His-tagged iPLA$_2\gamma$ and was able to purify a soluble 63 kDa isoform from Sf9 cytosol [126]. Interestingly, the soluble iPLA$_2\gamma$ cleaved *sn*-2 oleic acid more rapidly than *sn*-2 AA from PC with palmitic acid at the *sn*-1 position. Using electrospray ionization/mass spectrometry (ESI/MS) and tandem MS it was determined that soluble iPLA$_2\gamma$ would preferentially cleave the *sn*-1 palmitic acid from PC, generating 2-arachidonyl lysoPC [126]. This finding was unexpected, but potentially significant, since 2-arachidonyl lysoPC is a key signaling molecule with the potential to be metabolized to prostaglandins, leukotrienes or 2-arachidonylglycerol (an endocannabinoid). Soluble iPLA$_2\gamma$ also displayed significant lysophospholipase activity against 1-palmitoyl lysoPC [126]. While these studies attempt to identify the activity of soluble iPLA$_2\gamma$, the substrate specificity of soluble iPLA$_2\gamma$ may be very different than the isoforms of iPLA$_2\gamma$ that are constitutively membrane bound. In intact renal cortex mitochondria, our laboratory showed iPLA$_2\gamma$ displays preferential activity against

plasmenylcholine with AA in the sn-2 position over oleic acid [98] and further studies revealed a preference for AA in both stressed and basal conditions in renal cortical mitochondria [127].

The activity of microsomal $iPLA_2$ in the heart using different radiolabeled PL substrates and reverse-phase HPLC quantitation of PL abundances has also been studied. Rabbit ventricular myocyte $iPLA_2$ preferred PlasC 16:0;18:1 over PC 16:0;18:1 and liberated significantly more *sn*-2 AA than oleic acid from synthetic PC, PlasC and plasmanylcholine PLs [123]. Furthermore, thrombin stimulation of rabbit ventricular myocytes caused a BEL-sensitive decrease in abundance of *sn*-2 AA containing PlasC and PlasE and no change in PC or PE containing *sn*-2 AA [128]. In the kidney, microsomal $iPLA_2$ also prefers PlasC over PC PLs with oleic acid at the *sn*-2 position, but the AA and polar head group selectivity has not been determined [68].

In summary, different substrate specificities of $iPLA_2\gamma$ have been reported which may reflect differences in techniques used for measurement (e.g. radiolabeled synthetic substrates vs. ESI/MS of changes in cellular phospholipid abundances), differences in the isoform responsible for activity (e.g. cytosolic His-tagged vs. overexpressed membrane-bound vs. native microsomal $iPLA_2\gamma$) or differences in the regulatory mechanisms in place in the different cellular extracts used for measurement (e.g. phosphorylation state of $iPLA_2\gamma$, presence of $Ca^{2+}$ or ROS). Overall, when acting as a classical $PLA_2$, $iPLA_2\gamma$ preferentially cleaves AA from the *sn*-2 position of vinyl ether containing PLs (plasmalogens).

**Intracellular Localization of iPLA$_2\gamma$.** The localization of iPLA$_2\gamma$ to crude membrane fractions when overexpressed in Sf9 and COS-7 cells and the presence of a C-terminal SKL peptide sequence led to speculation that this enzyme was targeted to peroxisomes [95]. In fact, the first demonstration of native iPLA$_2\gamma$ expression was the 63 kDa isoform in purified rat liver peroxisomes [129]. Subsequently, Mancuso et al. (2004) reported that higher molecular weight isoforms were found in rat heart mitochondria and nuclear fractions. The mechanism for mitochondrial targeting was determined to be an N-terminal amino acid sequence present in the 88, 77 and 74 kDa isoforms but absent in the 63 kDa iPLA$_2\gamma$ [110]. Additionally, cytosolic iPLA$_2\gamma$ was observed following overexpression in a transgenic mouse [109] Our laboratory demonstrated the expression of an iPLA$_2$ activity in the microsomal (ER) fraction of rabbit RPTC that is sensitive to BEL [68] and Beckett et al. (2006) reported that the majority of human platelet iPLA$_2$ activity is cytosolic and is inhibited by R-BEL, an iPLA$_2\gamma$ selective pharmacological inhibitor. A strongly immunoreactive protein of approximately 50 kDa in platelet cytosol was detected with an anti-iPLA$_2\gamma$ antibody [130]. Later, we demonstrated the presence of iPLA$_2\gamma$ in renal mitochondria and excluded the presence of iPLA$_2\beta$ activity [68, 97-98]. In summary, iPLA$_2\gamma$ protein and/or activity has been identified in peroxisomes, mitochondria, nuclei, microsomes and cytosol and its presence in other subcellular compartments has not been ruled out.

**Mitochondrial iPLA$_2$.** $Ca^{2+}$-independent PLA$_2$ activity has been demonstrated in rat liver mitochondria [131] and in rabbit ventricular myocyte mitochondria [132]. The

isoform identity of each $iPLA_2$ was hypothesized to be $iPLA_2\beta$, based on positive immunoblot analyses with a commercially available $iPLA_2\beta$ antibody and sensitivity of the activity to racemic BEL [131-132]. In rat liver mitochondria the $iPLA_2$ is supposedly activated by dissipation of the mitochondrial membrane potential and is hypothesized to facilitate removal of poorly functioning mitochondria by destruction of mitochondrial phospholipids [131]. Prevention of I/R-induced cardiac infarct in isolated perfused hearts by BEL was attributed solely to mitochondrial $iPLA_2$ inhibition and the contribution of the well-described microsomal $iPLA_2$ in rabbit ventricular myocytes was not taken into account [132]. Both mitochondrial $iPLA_2$ are localized to membrane fraction of mitochondria and the rabbit heart $iPLA_2$ was specifically localized to the inner mitochondrial membrane [132]. Gross and colleagues have demonstrated the presence of $iPLA_2\gamma$ protein in mitochondria from rat heart with an $iPLA_2\gamma$ antibody, but mitochondrial $iPLA_2\gamma$ activity was not measured [110]. It is possible that both $iPLA_2$ activities described previously in rabbit heart and rat liver are the result of $iPLA_2\gamma$ and not $iPLA_2\beta$, based on the inhibition profile of these mitochondrial enzymes. These studies report that $AACOCF_3$ either does not inhibit mitochondrial $iPLA_2$ activity [131] or has no effect on ischemia-induced infarct size [132], while racemic BEL potently inhibits both endpoints in these studies. The inhibitor sensitivity profile (BEL-sensitive and $AACOCF_3$-insensitive) matches $iPLA_2\gamma$ and not $iPLA_2\beta$. In 2007, Kinsey et. al. identified $iPLA_2\gamma$ in rabbit renal proximal tubules by immunoblot analysis and activity studies and excluded the presence of $iPLA_2\beta$ [98]. Interestingly, pharmacological inhibition of $iPLA_2\gamma$ with BEL potentiated oxidant-induced mitochondrial lipid

peroxidation and swelling, but prevented $Ca^{2+}$-induced mitochondrial permeability transition (MPT) by preventing arachidonic acid release in isolated mitochondria [98, 113].

**Endoplasmic Reticulum iPLA$_2\gamma$** Prior to the identification of mitochondrial iPLA$_2\gamma$ most studies did not take into account differential subcellular localization of iPLA$_2\gamma$ and activity was considered either microsomal (ER) or peroxisomal. Additionally, lack of organelle specific inhibitors of iPLA$_2\gamma$ has made identification of differential function of iPLA$_2\gamma$ within organelle difficult. Therefore studies are limited to isolated organelle to determine organelle specific activity. Interestingly, pharmacological inhibition of iPLA$_2\gamma$ with the selective inhibitor bromoenol lactone (BEL) reduced cisplatin-induced apoptotic renal proximal tubule cell (RPTC) death and in contrast, iPLA$_2\gamma$ inhibition potentiated oxidant-induced lipid peroxidation and necrotic RPTC death [68, 98]. These data provide further evidence that iPLA$_2\gamma$ may have divergent roles in cell injury and death, which may be explained by unique roles and functions within subcellular compartments [81]. These data implicate iPLA$_2\gamma$ as a mediator of apoptotic cell death and as a protectant in oxidant-induced necrotic cell death. Recent studies in our laboratory used iPLA$_2\gamma$-specific shRNA to decrease iPLA$_2\gamma$ activity and expression in RPTC [116]. While the loss of mitochondrial iPLA$_2\gamma$ was correlated with decreased mitochondrial uncoupled respiration, these studies pointed to ER- iPLA$_2\gamma$ in the lipid peroxidation repair/prevention pathway because knockdown of ER- iPLA$_2\gamma$ was correlated with

increased lipid peroxidation [116]. These studies underscore the need of further studies to elucidate the differential roles of iPLA$_2\gamma$ with respect to subcellular localization.

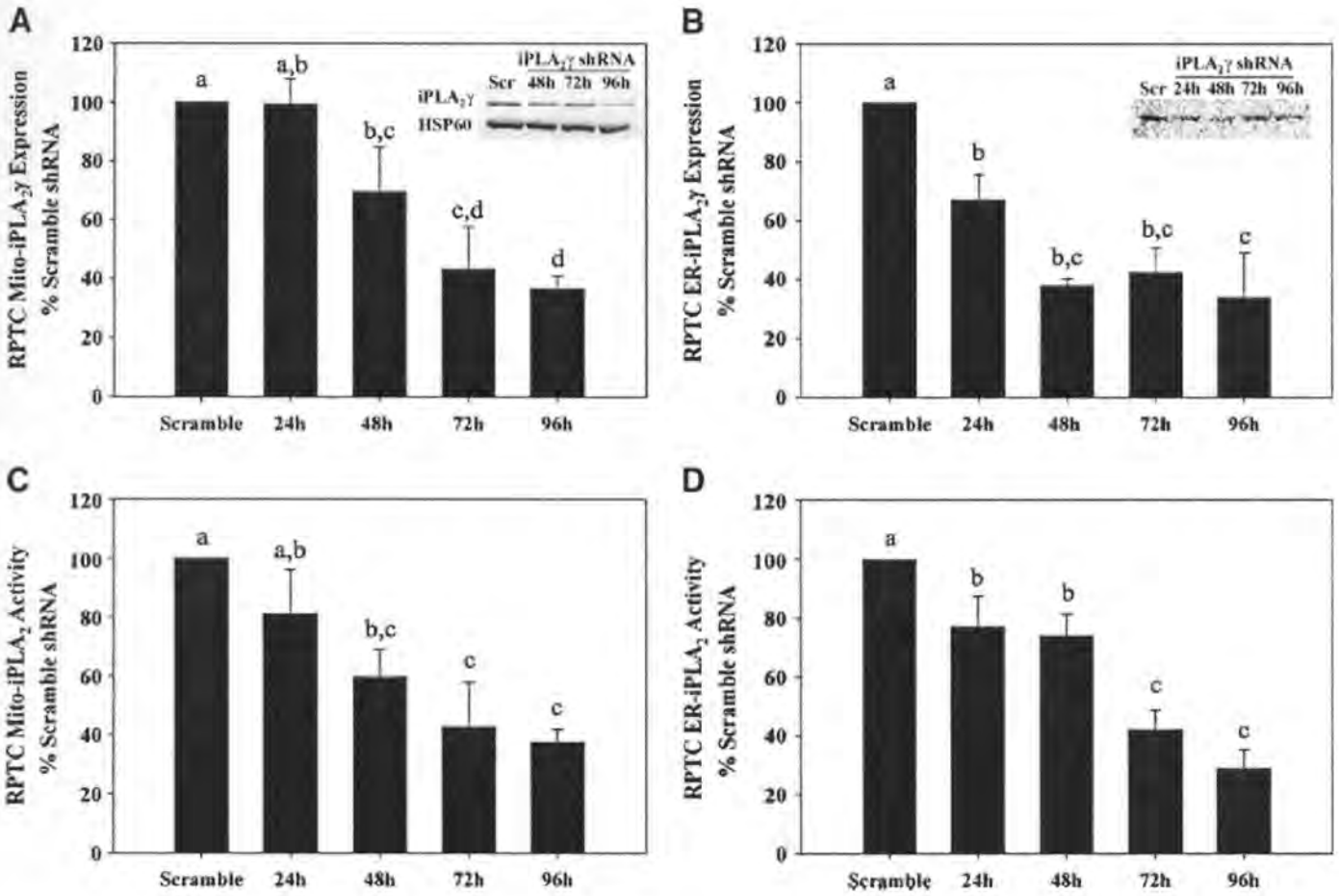


**Figure 1-10. Small hairpin ribonucleic acid (shRNA)-mediated decreases in mitochondrial and ER- iPLA$_2\gamma$ in RPTC.** Confluent RPTCs were exposed to either adenoviral iPLA$_2\gamma$ or scramble shRNA and cultured normally for 4 days. iPLA$_2\gamma$ expression was measured by immunoblot analysis (A, B) and iPLA$_2$ activity was measured (C, D) in mitochondrial (A, C) and ER (B, D) fractions at 24, 48, 72, and 96 h after exposure. The amount of iPLA$_2\gamma$ expression and activity in cells exposed to iPLA$_2\gamma$ shRNA is expressed as means +SEM, percentage of iPLA$_2\gamma$ expression and activity in cells exposed to scramble shRNA for the same amount of time. Insets show representative immunoblots. Means with different superscripts are significantly different from each other ($P < 0.05$, n = 4-5). Note: ER- iPLA$_2\gamma$ expression and activity decreases prior to decreases in mitochondrial-iPLA$_2\gamma$ expresion and activity. From Kinsey et al [116].

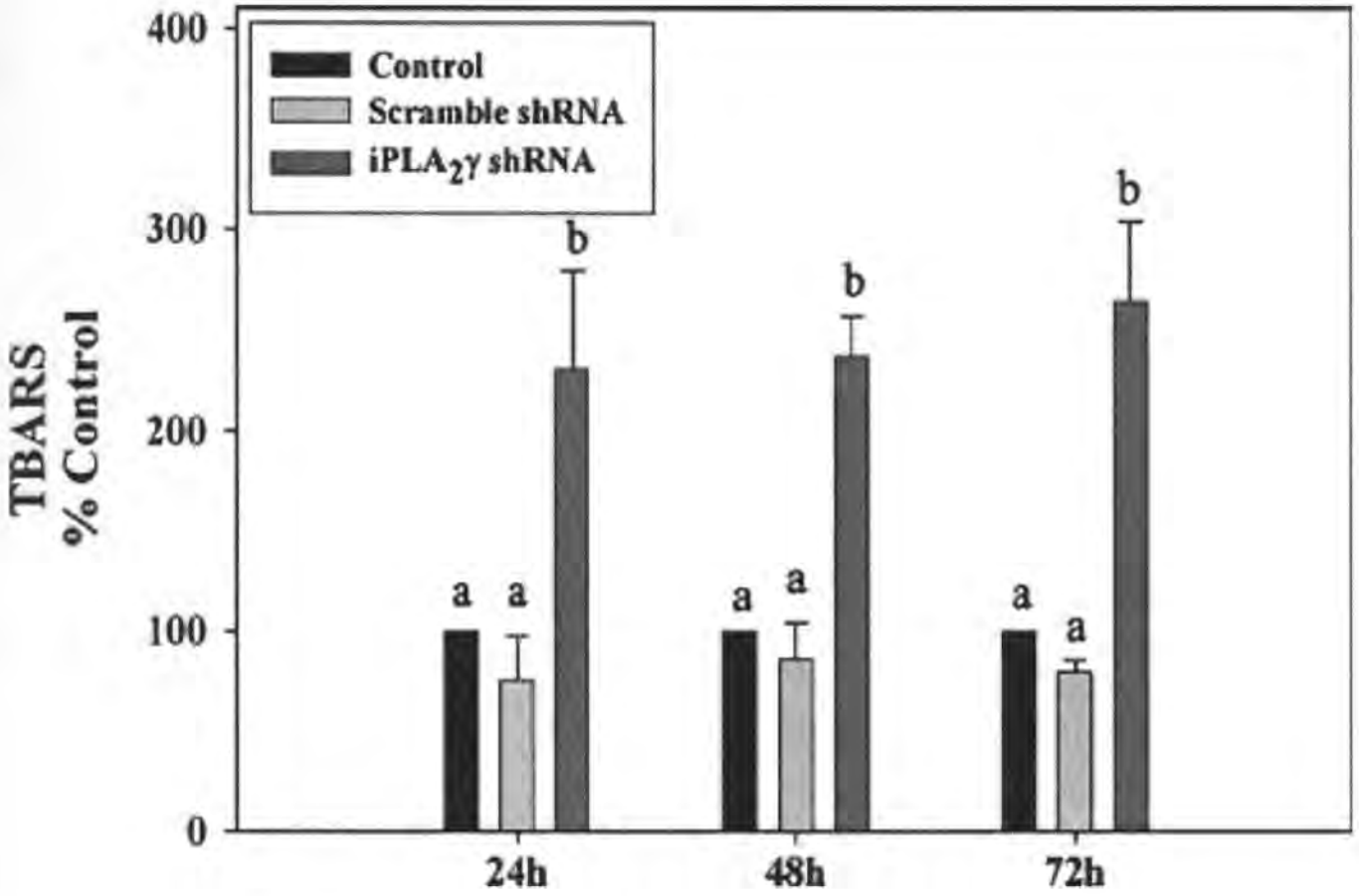


**Figure 1-11. Effects of decreased iPLA$_2\gamma$ expression on RPTC lipid peroxidation.** The thiobarbituric acid-reactive substances (TBARS) assay was performed in noninfected (control), scramble shRNA, and iPLA$_2\gamma$ shRNA adenovirus-treated RPTCs at 24, 48, and 72 h after virus exposure as a measure of cellular lipid peroxidation. Data are presented as means + SEM, percentage of control TBARS formation. Means with different superscripts are significantly different from each other ($P < 0.05$, n=4). Note: lipid peroxidation occurred at 24 h and correlated with decreases in ER- iPLA$_2\gamma$ and prior to decreases in mitochondrial- iPLA$_2\gamma$ activity and expression. From Kinsey et. al [116].

**iPLA$_2\gamma$ in the Brain.** iPLA$_2\gamma$ has been suggested to play a protective role in the brain during oxidant stress. Inhibition of iPLA$_2\gamma$ prior to oxidant treatment in astrocytes potentiated oxidant induced cell death[133]. Mice genetically ablated of iPLA$_2\gamma$ exhibited cognitive dysfunction and cortical tissues exhibited multiple inclusion bodies following immunohistochemical staining [134-136]. These consequences of genetic ablation of iPLA$_2\gamma$ were attributed to loss of cardiolipin homeostasis, resulting in mitochondrial dysfunction.

**iPLA$_2\gamma$ in the Heart.** Gross and colleagues investigated the consequences of overexpressing iPLA$_2\gamma$ in the mouse heart [109]. Compared to wild type hearts, iPLA$_2\gamma$ transgenic (TG) mice had significantly less PC and PE PLs. Fasting induced an increased abundance of triacylglycerol (TAG) and the fatty acid content of the TAG was changed to include more saturated fatty acids than TAG in wild type mice [109]. As described above, soluble iPLA$_2\gamma$ generated 2-arachidonyl lysoPC *in vitro* and analysis of the lysoPC species in wild-type vs. TG mice revealed that there was an 11-fold increase in 2-arachidonyl lysoPC in TG hearts [109]. Mitochondria from TG hearts had impaired mitochondrial state 3 (ADP-stimulated) respiration rates and isolated perfused hearts from TG mice demonstrated a metabolic shift from utilizing glucose to oxidizing palmitate [109]. The authors point out that this type of metabolic shift is a feature of obesity and diabetes. Caloric restriction-induced changes in TG mice (TAG accumulation, mitochondrial dysfunction, etc.) resulted in a decrease in the overall performance of the heart manifested by a decreased heart rate, increased ventricular internal diameter at end systole and worsening of several other endpoints [109].

Rabbit heart microsomes possess iPLA$_2$ activity which resembles iPLA$_2\gamma$ based on membrane localization and inhibitor sensitivity [123]. This iPLA$_2$ is activated by thrombin in a BEL-sensitive manner and its products, lysoPC and lysoPlasC mediate arrhythmogenesis during myocardial infarction Additionally, anthracycline-mediated cardiotoxicity is at least partially mediated by an inhibitory effect of this class of drugs, especially doxorubicin, on microsomal iPLA$_2$ [137-139]. *In vitro* and *in vivo*, doxorubicin exposure potently inhibited microsomal iPLA$_2$, but not cytosolic iPLA$_2$, in

the heart [138-139]. The toxicity of doxorubicin in the heart is related to increased ROS production, causing lipid peroxidation in cardiac membranes, and anthracyclines also prevent the repair of lipid peroxidation by inhibiting microsomal $iPLA_2$ [137]. Similar to the effects of $iPLA_2$ inhibition on oxidant-induced necrosis in the kidney, BEL pretreatment significantly potentiated lactate dehydrogenase release from cardiac myocytes exposed to doxorubicin [139]. Most recently, Mancuso et. al. reported that mice genetically ablated of $iPLA_2\gamma$ were more vulnerable to cardiac stress (transverse aortic constriction) [136].

**$iPLA_2\gamma$ in the Kidney.** Inhibition of microsomal $iPLA_2$ in RPTC with racemic BEL, potentiates lipid peroxidation and necrotic cell death induced by diverse oxidants but has no effect on non-oxidant induced necrosis [68] (Figure 1-10). Effects of BEL on glutathione, ATP, GTP and mitochondrial function were ruled out, and BEL-induced potentiation of oxidant-induced lipid peroxidation was observed well before cell death was detectable [68] (Figure 1-11). In a subsequent study, treatment of RPTC with TBHP resulted in the significant loss (presumably by oxidative damage) of 4 individual PL species (of 28 total measured), but pretreatment with BEL caused a TBHP-induced loss of 15 out of 28 PLs [114].

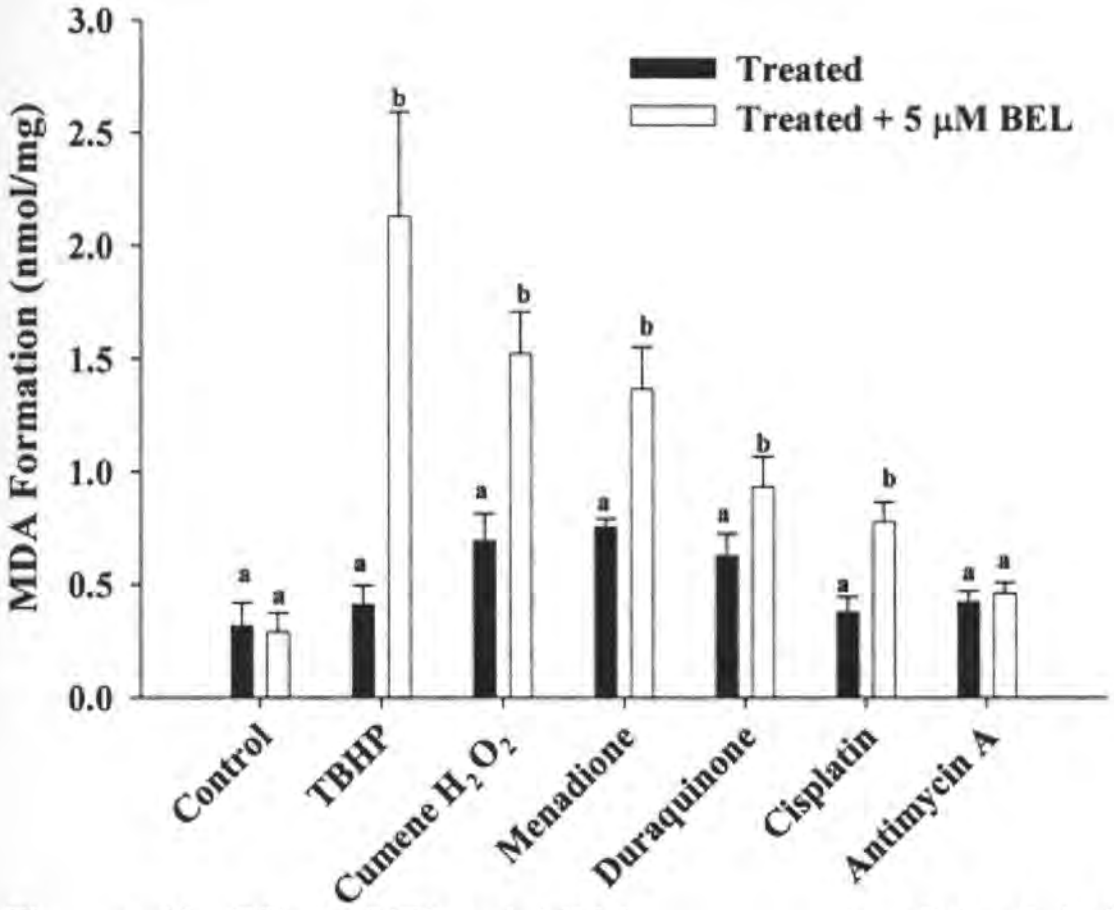


**Figure 1-12. Effect of $iPLA_2$ inhibition on necrotic cell death in RPTC.** RPTC were treated with diluent or racemic BEL (5 μM) 30 minutes prior to exposure to the oxidants: TBHP (200 μM) for 24 hr; cumene $H_2O_2$ (200 μM) for 24 hr; menadione (10 μM) for 12 hr; duraquinone (400 μM) for 24 hr and cisplatin (400 μM) for 24 hr, or the non-oxidant, antimycin A (0.3 μM) for 4 hr, and necrotic cell death measured by flow cytometry as the percent cells positively stained with propidium iodide (PI). From Cummings et. al [68].

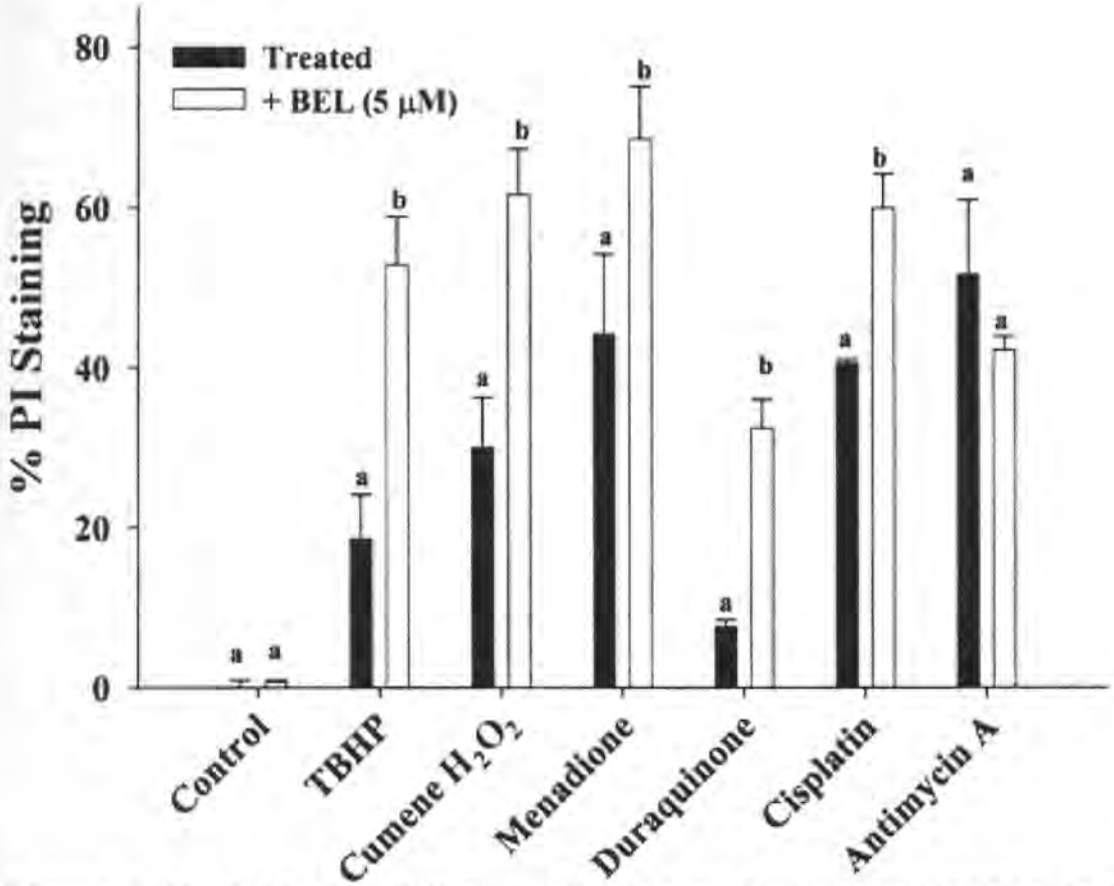


**Figure 1-13. Effect of $iPLA_2$ inhibition on lipid peroxidation in RPTC.** RPTC were treated with diluent or racemic BEL (5 μM) 30 minutes prior to exposure to TBHP (200 μM), cumene $H_2O_2$ (200 μM), menadione (10 μM), duraquinone (400 μM), cisplatin (400 μM) and antimycin A (0.3 μM) each for 2 hr, and prior to any increase in cell death, lipid peroxidation (malondialdehyde (MDA) formation) estimated using the thiobarbituric acid reactive substances assay. From Cummings et. al [68].

In the same RPTC model, inhibition of microsomal $iPLA_2$ blocks non-oxidant mediated cisplatin (50 μM)-induced apoptosis (PS externalization, chromatin condensation and caspase 3 activity) but not p53 nuclear translocation [112]. In addition, activation of microsomal $iPLA_2$ with PMA increased cisplatin-induced annexin-V staining and cell shrinkage [112]. These results suggest that, during cisplatin-induced RPTC apoptosis, $iPLA_2$ activity regulates caspase activation presumably by an AA-mediated mechanism [140]. Cisplatin is a widely used chemotherapeutic drug with a major dose-limiting side effect of renal toxicity. Similarly, Kinsey et. al showed that mitochondrial $iPLA_2\gamma$ mediates $Ca^{2+}$-induced mitochondrial swelling through a AA-dependent

mechanism [98]. Overall, the role of $iPLA_2$ in RPTC necrosis and apoptosis suggest that manipulation of this enzyme in the setting of ARF may provide novel therapeutic possibilities.

**$iPLA_2\gamma$ in Skeletal Muscle.** Mancuso et al reported skeletal muscle lacking the bioenergetic capacity of Interestingly, Yoda et al. also generated mice null of $iPLA_2\gamma$ and reported in skeletal muscle, increased lipid peroxidation, the induction of oxidative stress related proteins, and, similarly to the work of Mancuso et al., alterations in cardiolipin content and mitochondrial dysfunction[141]. Skeletal muscle ablated of $iPLA_2\gamma$ displayed atrophy of myofilaments, reduced fiber diameter, and alterations in prostanoid and phospholipids content. Mancuso et al. reported similarly mitochondrial dysfunction in $iPLA_2\gamma$ -/- mice. Skeletal muscle mitochondria exhibited reduced state 3 respiration and altered cardiolipin composition. Together, these changes seemingly resulted in mice insensitive to high fat diet induced weight gain and reduced their exercise endurance [134, 136, 141].

**$iPLA_2\gamma$ in Other Tissues.** In the first demonstration of native $iPLA_2\gamma$ expression, Yang et al. (2003) showed that hepatic peroxisomes possess a 63 kDa protein immunoreactive to an anti-$iPLA_2\gamma$ antibody. Based on the phospholipid content of peroxisomes from rat liver (exhibiting a relatively high content of *sn*-2 AA), it was hypothesized that $iPLA_2\gamma$ may play a role in cellular signaling [129].

Both iPLA$_2\gamma$ and iPLA$_2\beta$ were demonstrated to participate in hormone-induced differentiation of preadipocytes using RNA interference and R- and S-BEL [142]. Temporal patterns of iPLA$_2$ expression during differentiation were described and use of the siRNA and pharmacological inhibitors for both isoforms prevented differentiation [142]. In addition, increased expression of the 63 kDa isoform of iPLA$_2\gamma$ was demonstrated by immunoblot analysis in obese vs. lean rats [142]. These results suggest that iPLA$_2$ enzymes (including iPLA$_2\gamma$) may be involved in the progression of obesity. Most recently, Mancuso et al. showed that mice genetically ablated of iPLA$_2\gamma$ were resistant to high fat diet-induced weight gain and insulin resistance[134].

Human platelets possess a cytosolic isoform of iPLA$_2\gamma$ of approximately 50 kDa [130]. Similar to ventricular myocytes and aortic endothelial cells, platelet iPLA$_2\gamma$ is activated by thrombin and the activation is completely blocked by BEL [130]. Thrombin stimulation caused the BEL-sensitive production of AA, lysoPlasC, and thromboxane A$_2$ over the course of several minutes [130]. iPLA$_2\gamma$ mediated platelet activation may represent another potentially inhibitable function of iPLA$_2\gamma$ in multiple settings where clotting is unwanted.

**Conclusions and Rationale.** In conclusion, acute kidney injury (AKI) and chronic kidney disease (CKD) are becoming more prevalent and have high morbidity and mortality that have been unchanged for many years. Current therapeutics targeted

towards preventing or treating kidney injury and disease have been unsuccessful. Calcium-independent phospholipase $A_2\gamma$ ($iPLA_2\gamma$) is one of seven $Ca^{2+}$-independent $PLA_2$ enzymes and represents a potential thearapeutic target in kidney disease [81]. Our studies in renal cells showed that $iPLA_2\gamma$ has a unique subcellular localization in that its expression and activity were found in both the endoplasmic reticulum (ER) and the mitochondria, while $iPLA_2\beta$ activity was not present [68, 97-98]. We also determined that $iPLA_2\gamma$ has divergent roles in cell injury and death, which may be explained by unique roles and functions within subcellular compartments [81]. Recent studies in our laboratory using $iPLA_2\gamma$-specific shRNA to decrease $iPLA_2\gamma$ activity and expression in RPTC confirmed its role in preventing lipid peroxidation and preserving mitochondrial function and viability under basal conditions [116]. While the loss of mitochondrial $iPLA_2\gamma$ was correlated with decreased mitochondrial uncoupled respiration, these studies pointed to ER- $iPLA_2\gamma$ in the lipid peroxidation repair/prevention pathway because knockdown of ER- $iPLA_2\gamma$ was correlated with increased lipid peroxidation. However, no studies have elucidated the role of $iPLA_2\gamma$ in the ER nor has the mechanism by which $iPLA_2\gamma$ preserves phospholipid homeostasis been determined. The goals of these studies are to elucidate the role of ER- $iPLA_2\gamma$ in oxidant-induced ER lipid peroxidation, loss of lipid homeostasis, $Ca^{2+}$ release and renal cell death.

Recently, Mancuso et al. generated mice null of $iPLA_2\gamma$ by genetically ablating the enzyme's active site [136]. These mice were more vulnerable to cardiac stress (transverse aortic constriction), resistant to high fat diet-induced weight gain, and

exhibited cognitive dysfunction and multiple bioenergetic dysfunctional phenotypes, such as cold intolerance and reduced exercise endurance[134-136]. These consequences of genetic ablation of iPLA$_2\gamma$ were attributed to loss of cardiolipin (a lipid found primarily in mitochondria) homeostasis, resulting in mitochondrial dysfunction. Interestingly, Yoda et al. also generated mice null of iPLA$_2\gamma$ and reported in skeletal muscle, increased lipid peroxidation, the induction of oxidative stress related proteins, and, similarly to the work of Mancuso et al., alterations in cardiolipin content and mitochondrial dysfunction[141]. Additionally, these findings provide evidence that loss of iPLA$_2\gamma$-induced oxidative stress and mitochondrial dysfunction leads to organ dysfunction in brain, heart, and skeletal muscle. However, the role of ER- iPLA$_2\gamma$ in oxidant- or genetic ablation- induced lipid peroxidation has not been investigated nor has its role in organ dysfunction been elucidated.

Based on the current knowledge of the pathophysiology of AKI and CKD and the biology of PLA$_2$ enzymes, especially iPLA$_2$ in the kidney, the current project was developed. The specific aims were as follows: 1) to determine the role of ER- iPLA$_2\gamma$ in oxidant-induced lipid peroxidation, $Ca^{2+}$ release, and renal cell death, 2) to elucidate the mechanism by which ER-iPLA$_2\gamma$ maintains phospholipid homeostasis following oxidant injury and 3) determine the consequences of iPLA$_2\gamma$ ablation *in vivo* on kidney function and oxidant injury.

# Chapter 2

## Visualization and quantification of endoplasmic reticulum $Ca^{2+}$ in renal cells using confocal microscopy and Fluo5F


## ABSTRACT

Sarcoplasmic/endoplasmic reticulum (ER) $Ca^{2+}$ is the most abundant store of intracellular $Ca^{2+}$, and its release is an important trigger of physiological and cell death pathways. Previous work in our laboratory revealed the importance of ER $Ca^{2+}$ in toxicant-induced renal proximal tubular cell (RPTC) death. The purpose of this study was to evaluate the use of confocal microscopy and Fluo5F, a low affinity $Ca^{2+}$ indicator, to directly monitor changes in RPTC ER $Ca^{2+}$. Fluo5F staining reflected ER $Ca^{2+}$, resolved ER structure, and showed no colocalization with tetramethyl rhodamine methyl ester (TMRM), a marker of mitochondrial membrane potential. Thapsigargin, an ER $Ca^{2+}$ pump inhibitor, decreased ER fluorescence by 30% and 55% at 5 and 15 min, respectively, whereas A23187, a $Ca^{2+}$ ionophore caused more rapid ER $Ca^{2+}$ release (55% and 75% decrease in fluorescence at 5 and 15 min).

Carbonylcyanide-p-trifluoromethoxyphenylhydrazone (FCCP), a mitochondrial uncoupler, added at the end of the experiment, further decreased ER fluorescence after thapsigargin treatment, revealing that thapsigargin did not release all ER $Ca^{2+}$. In contrast, FCCP did not decrease ER fluorescence after A23187 treatment, suggesting complete ER $Ca^{2+}$ release. ER $Ca^{2+}$ release in response to A23187 or thapsigargin

resulted in a modest but significant decrease in mitochondrial membrane potential. These data provide evidence that confocal microscopy and Fluo5F are useful and effective tools for directly monitoring ER $Ca^{2+}$ in intact cells.

**Introduction**

$Ca^{2+}$ acts as a universal second messenger and regulates numerous cellular functions including metabolism, motility, and transport[44]. Loss of $Ca^{2+}$ homeostasis is critical to many disease processes and is a major component of cell death pathways including necrosis, apoptosis, and autophagy [45-51]. Sarcoplasmic/endoplasmic reticulum (ER) $Ca^{2+}$ is the most abundant store of intracellular $Ca^{2+}$and its disruption often initiates the deleterious cascade of events leading to cell death and dysfunction [48-54].

Traditional methods of measuring of ER $Ca^{2+}$ are indirect or require difficult probe loading techniques (i.e. membrane permeabilization, microinjection, or fused cell hybrids). For example, human embryonic kidney cells require 1 h of dye loading (2 μM Fluo-3 at room temperature) and extracellular $Ca^{2+}$ chelation using BAPTA or EGTA, just to monitor increases in cytosolic $Ca^{2+}$ as an indirect measure of ER $Ca^{2+}$ stores [143]. To monitor ER $Ca^{2+}$ directly, Montero and Robert *et al.* engineered an ER-targeted aequorin chimera, a $Ca^{2+}$-sensitive photoprotein with a lower affinity for $Ca^{2+}$. However, in HeLa and skeletal muscle cells, the aequorin chimera was rapidly saturated by the high $Ca^{2+}$ concentrations within the ER and required a non-physiological reduction of ER $Ca^{2+}$ to detect changes in $Ca^{2+}$ stores [144-145].

Primary cultures of renal proximal tubular cells (RPTC) are highly aerobic, gluconeogenic, and exhibit robust transport capacity, making them ideal for the study of

kidney tubular function and injury [146-147]. Previous work in our laboratory revealed the importance of ER $Ca^{2+}$ in toxicant-induced kidney injury; although, the mechanism by which $Ca^{2+}$ plays such a pivotal role is not completely understood [48, 50, 52-53, 68, 112].

Confocal microscopy is a useful method for the visualization and quantification of fluorophores at the subcellular level in living cells, and is compatible with most $Ca^{2+}$ indicators. Chemical fluorescent (UV and visible-wavelength excitation fluorescent indicators) and bioluminescent calcium indicators ($Ca^{2+}$ binding photoproteins and GFP-based $Ca^{2+}$ indicators) differ in their characteristics (loading requirements, excitation/emission spectrum, permeability, compartmentalization, relative brightness, and $Ca^{2+}$ affinity) and have inherent drawbacks (i.e., dye leakage, cytotoxicity, bleaching, autofluorescence, intracellular buffering, and lack of ion specificity)[148]. Fluo5F is a chemical fluorescent $Ca^{2+}$ indicator with a lower affinity for $Ca^{2+}$ ($K_d$ ~2.3 μM), limited cytoxicity and bleaching, and high $Ca^{2+}$ specificity, making it ideal for studying ER $Ca^{2+}$. The purpose of this study was to evaluate the use of confocal microscopy and Fluo5F for directly monitoring changes in ER $Ca^{2+}$ in RPTC.

## MATERIALS AND METHODS

### Materials

Female New Zealand White rabbits (1.5–2.0 kg) were purchased from Myrtle's Rabbitry (Thompson Station, TN). Tetramethyl rhodamine methyl ester (TMRM) and Fluo-5F-AM were purchased from Molecular Probes, Invitrogen (Carlsbad, CA). All other chemical and materials were obtained from Sigma Chemical (St. Louis, MO).

**Isolation of Rabbit RPTC and Culture Conditions**

Rabbit RPTC were isolated using the iron oxide perfusion method and grown to confluence in 35-mm tissue culture dishes under improved conditions as previously described [146-147]. The culture medium was a 1:1 mixture of Dulbecco's modified Eagle's medium/Ham's F-12 medium (without glucose, phenol red, or sodium pyruvate) supplemented with 15 mM HEPES buffer, 2.5 mM L-glutamine, 1 μM pyridoxine HCl, 15 mM sodium bicarbonate, and 6 mM lactate. Hydrocortisone (50 nM), selenium (5 ng/ml), human transferrin (5 μg/ml), bovine insulin (10 nM), and L-ascorbic acid-2-phosphate (50 μM) were added daily to fresh culture medium.

**RPTC Loading**

RPTC were loaded with 2 μM Fluo-5F-AM (Fluo5F) and 100 nM TMRM for 20 min at 37° C, washed twice with 37° C phosphate buffered saline, and media was replaced. Then, 1 μM Fluo5F and 40 nM TMRM were added to the media to maintain dye equilibrium and incubated for 30 min at 37° C prior to imaging. The TMRM loading protocol was modified from Lemasters and Ramshesh [149].

**Microscopic Imaging and Analysis**

RPTC were imaged on a Leica Microsystems, TCS SP2 AOBS laser scanning confocal microscope (LSCM) using standardized pinhole, gain, and black level settings. A 63X0.9 NA water-immersion objective was used in an upright microscope configuration. All images were acquired at 8-bit resolution and at 1024X1024 with a line averaging of two.

RPTC were monitored for 10 min prior to treatment to establish baseline. Then, RPTC were treated and monitored an additional 15 min prior to Carbonylcyanide-p-

trifluoromethoxyphenylhydrazone (FCCP, 1 μM) addition to depolarize mitochondria. Images were acquired in 1-min intervals during the course of experiments. To quantify data, images were analyzed using Adobe Photoshop. Mean intensities of images in the green and red channel after background subtraction were interpreted as a quantitative measure of ER $Ca^{2+}$ and mitochondrial membrane potential, respectively. Values are graphed as the percent mean intensity of each subsequent image vs. mean intensity of the image taken at time zero. Images comprise of 7–10 cells.

**Statistical Analysis**

RPTC isolated from one animal represents one experiment (N=1). Data are presented as means ± SE, and multiple means were compared using Student-Newman-Keuls test at each time point. Means with values $p<0.05$ were considered statistically significant.

## RESULTS AND DISCUSSION

To investigate the use of confocal microscopy to monitor ER $Ca^{2+}$ dynamics in RPTC, Fluo5F fluorescence was monitored as described above (Fig. 2-1a). Fluo5F fluorescence revealed a reticular pattern around nuclei void of staining. The peripheral granularity of staining and scarcity of staining at the cell margins provided evidence that the probe is not fluorescing in the cytosol. To confirm that Fluo5F was not in the mitochondria, RPTC were loaded with tetramethyl rhodamine methyl ester (TMRM), a marker of polarized mitochondria. TMRM staining (Fig. 2-1b) had a punctuate/tubular pattern unlike Fluo5F staining with no co-localization (Fig. 2-1c), confirming that Fluo5F does not reflect mitochondrial $Ca^{2+}$, the second most significant storage/buffering compartment for intracellular $Ca^{2+}$[47].

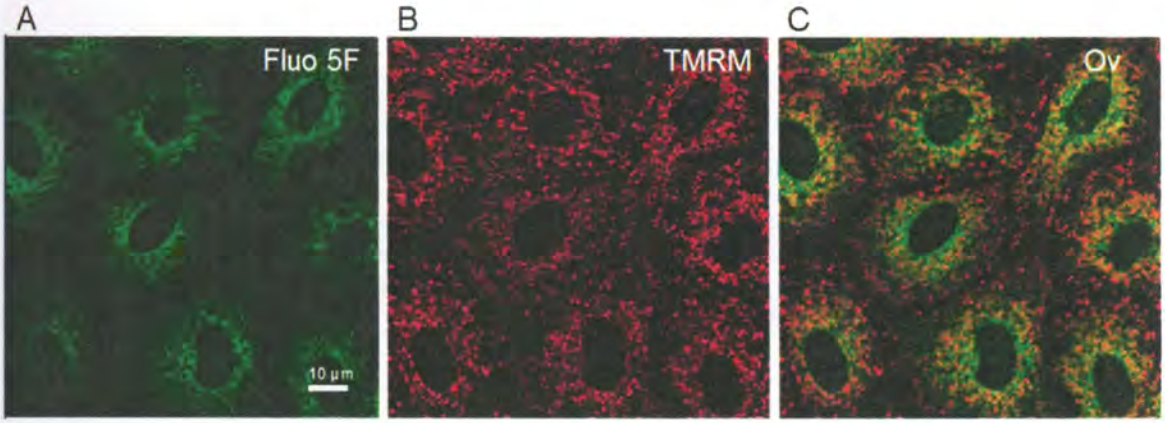


**Figure 2-1. Morphology of Renal Proximal Tubule Cells (RPTC) co-loaded with Fluo5F and TMRM using confocal microscopy.** RPTC were co-loaded with Fluo5F (2 µM) and TMRM (100 nM) as described in the materials and methods. Green fluorescence of Fluo5F and red fluorescence of TMRM were imaged by laser scanning confocal microscopy. The white bar represents 10 µm. Fluo5F fluorescence (A) represents endoplasmic reticulum (ER) $Ca^{2+}$, TMRM fluorescence (B) represents polarized mitochondria, and there was no co-localization (C).

We investigated the use of Fluo5F to monitor real-time changes in RPTC ER $Ca^{2+}$. TMRM was used to measure mitochondrial membrane potential. In control cells, both Fluo5F and TMRM fluorescence intensity, morphology, and resolution were maintained over time (Fig. 2-2). Carbonylcyanide-p-trifluoromethoxyphenylhydrazone (FCCP), a mitochondrial uncoupler, was added at the end of each experiment to cause mitochondrial depolarization and indirectly ER $Ca^{2+}$ release, due to ATP depletion and cessation of sarcoplasmic/ER $Ca^{2+}$ ATPase (SERCA) activity.

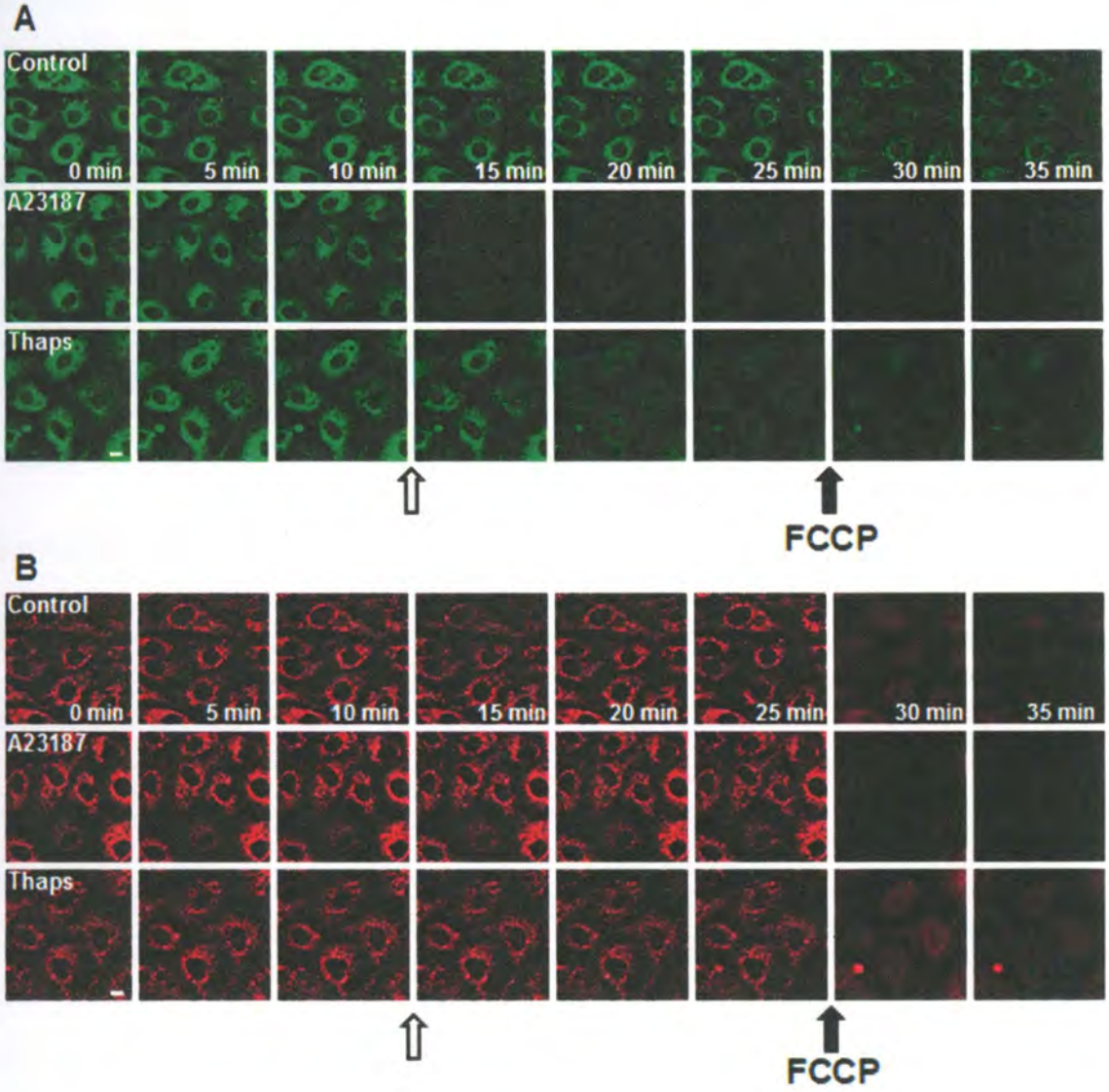


**Figure 2-2. ER $Ca^{2+}$ release RPTC exposed to A23187 and thapsigargin.** RPTC were loaded with Fluo5F and TMRM (see in Fig. 1-1), monitored for 10 min to establish baseline, exposed to diluent (DMSO, Control), A23187 (10 μM), or thapsigargin (10 μM) for 15 min, and then exposed to FCCP (1 μM), a mitochondrial uncoupler. Open arrows represent time of A23187 or thapsigargin treatment and closed arrows represent the addition of FCCP. Green fluorescence (A) and red fluorescence (B) represents ER $Ca^{2+}$ and mitochondrial polarization, respectively. Note the more rapid ER $Ca^{2+}$ release (A) in response to A23187 exposure compared to thapsigargin and the rapid loss of mitochondrial polarization (B) in response to FCCP.

We then explored the effects of two pharmacological agents known to alter ER $Ca^{2+}$. RPTC were treated with the SERCA inhibitor, thapsigargin, and the $Ca^{2+}$ ionophore, A23187. Thapsigargin decreased ER $Ca^{2+}$ over several min (Fig. 2-2A), which was more indicative of ER $Ca^{2+}$ leakage than receptor-dependent ER $Ca^{2+}$ release that is

characterized by DAG, ryanodine, and $IP_3$ receptor sensitive stores [44, 150-151]. In contrast, A23187 caused a more rapid release of ER $Ca^{2+}$, an anticipated finding due to its ionophore activity.

Temporal and incremental changes in ER $Ca^{2+}$ release and mitochondrial membrane potential were quantified (Fig. 2-3). A23187 decreased fluorescence by 50% and 70% at 5 and 15 min after treatment, respectively, and FCCP addition did not decrease fluorescence further. Thapsigargin decreased fluorescence by 25% and 55% at 5 and 15 min after treatment, respectively. In contrast to A23187, FCCP addition further decreased fluorescence after thapsigargin, providing evidence that thapsigargin did not completely release all ER $Ca^{2+}$ stores under these conditions.

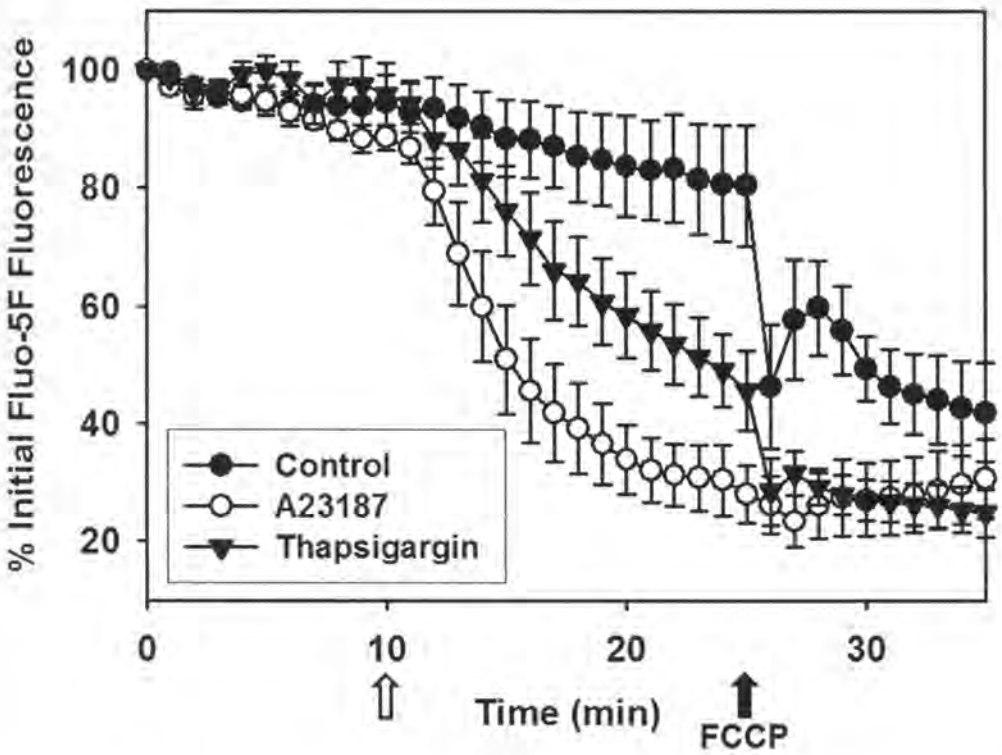


**Figure 2-3. Quantification of A23187- and thapsigargin- induced ER $Ca^{2+}$ release in RPTC.** RPTC were co-loaded with Fluo5F and TMRM, treated as described in fig. 2, and images acquired as described in Materials and Methods. Values are mean intensities of images in the green channel ± SE and loss of intensity represents ER $Ca^{2+}$ release. The open arrow represents exposure to A23187, thapsigargin, or diluent control and the

closed arrow represents the addition of FCCP. Note the more rapid ER $Ca^{2+}$ release after A23187 exposure compared to thapsigargin and an additional loss of fluorescence with FCCP following thapsigargin exposure.

The advantage of this approach is that ER $Ca^{2+}$ stores are measured directly, allowing observation of spatiotemporal differences between A23187- and thapsigargin-induced ER $Ca^{2+}$ release that would otherwise be masked by measuring cytosolic free $Ca^{2+}$. Interestingly, Jiang *et al.* reported a higher rate and magnitude of cytosolic $Ca^{2+}$ increase in response to A23187 over thasigargin using Fluo-3, but this approach required chelation of extracellular $Ca^{2+}$ prior to treatment [143].

The effect of ER $Ca^{2+}$ release on mitochondrial polarization was monitored using TMRM (Fig. 2-4). A23187- and thapsigargin-induced ER $Ca^{2+}$ release decreased TMRM fluorescence by approximately 10%. In contrast, FCCP, the mitochondrial uncoupler added at the end of each experiment, decreased TMRM fluorescence by 60%, reflecting complete mitochondrial depolarization. Together, these data reveal that ER $Ca^{2+}$ release produced by A23187 or thapsigargin partially decreases mitochondrial polarization and is consistent with previous reports [152].

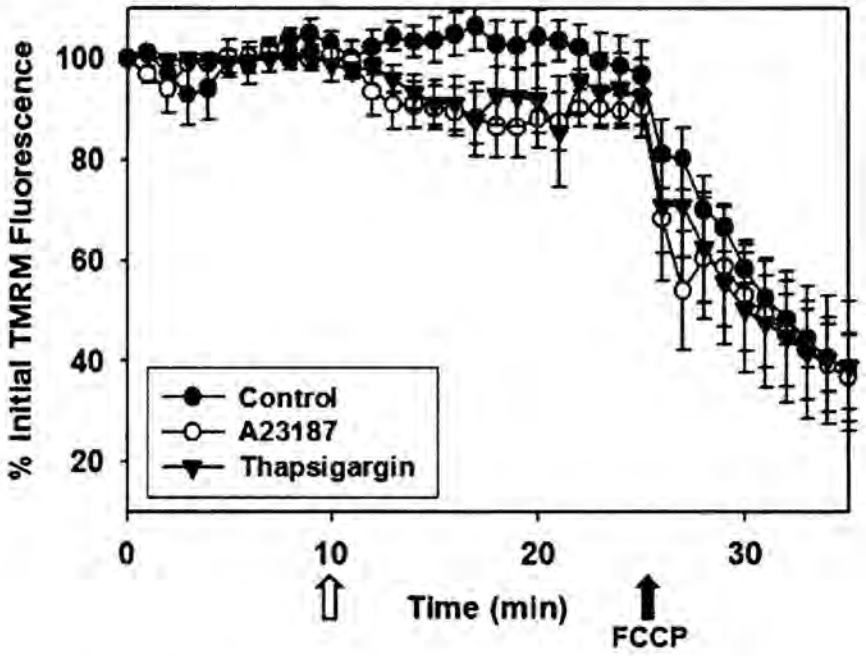


**Figure 2-4. Quantification of A23187- and thapsigargin-induced mitochondrial depolarization in RPTC.** See above for experimental details. Values are mean intensities of images in the red channel ± SE and loss of intensity represents mitochondrial depolarization. The open arrow represents exposure to A23187, thapsigargin, or diluent control and the closed arrow represents the addition of FCCP. Note the decrease in mitochondrial polarization following A23187 or thapsigargin exposure compared with control and the rapid loss of mitochondrial polarization following FCCP exposure in all groups.

In conclusion, confocal microscopy and Fluo5F are valuable tools for visualization of spatiotemporal dynamics of ER $Ca^{2+}$ release in complex cellular systems in real time and will aid in our understanding of cellular dynamics and death.

# Chapter 3

## The Role of Endoplasmic Reticulum $Ca^{2+}$–Independent Phospholipase $A_2\gamma$ in Oxidant-induced Lipid Peroxidation, $Ca^{2+}$ Release, and Renal Cell Death


### Abstract

Oxidant-induced lipid peroxidation and cell death are major components of ischemia-reperfusion and toxicant injury. Our previous studies showed that renal proximal tubular cells (RPTC) express $Ca^{2+}$-independent phospholipase $A_2\gamma$ (iPLA$_2\gamma$) in endoplasmic reticulum (ER) and mitochondria and that iPLA$_2\gamma$ is cytoprotective. Our present studies reveal the role of ER- iPLA$_2\gamma$ in oxidant-induced ER lipid peroxidation, $Ca^{2+}$ release, and cell death. Oxidant *tert*-butyl hydroperoxide (TBHP) caused ER lipid peroxidation and $Ca^{2+}$ release in isolated rabbit kidney cortex microsomes. ER- iPLA$_2\gamma$ inhibition, using bromoenol lactone (BEL), potentiated both oxidant-induced ER lipid peroxidation and $Ca^{2+}$ release. Assessment of fatty acids using electrospray ionization-mass spectrometry revealed that ER- iPLA$_2\gamma$ mediates the TBHP-induced release of arachidonic acid (20:4), linoleic acid (18:2), and their oxidized forms (18:2-OH, 18:2-OOH, 20:4-OH, 20:4-OOH, 20:4-(OH)$_3$). iPLA$_2\gamma$ inhibition also accelerated oxidant-induced ER $Ca^{2+}$ release in RPTC. Depletion of RPTC ER $Ca^{2+}$ stores with thapsigargin, an ER $Ca^{2+}$ pump inhibitor, prior to TBHP exposure reduced necrotic cell death and blocked the potentiation of TBHP-induced necrotic cell death by BEL. Together, these data provide strong evidence

that ER- iPLA$_2\gamma$ protects renal cells from oxidant-induced necrotic cell death by releasing unsaturated and/or oxidized fatty acids from ER membranes, thereby preserving ER membrane integrity and preventing ER $Ca^{2+}$ release.

## Introduction

Phospholipase $A_2$ ($PLA_2$) enzymes catalyze the hydrolysis of fatty acids at the *sn*-2 position of glycerophospholipids resulting in the production of a free fatty acid and a lysophospholipid [86]. Free fatty acids and their metabolites are biologically active in such processes as inflammation, cell signaling, and cell death. Arachidonic acid, for example, is metabolized to prostaglandins, prostacyclins, thromboxanes and leukotrienes, all of which play a role in inflammatory responses and cell signaling [87]. The resulting lysophospholipids serve as substrates for the re-esterification of free fatty acids by CoA-dependent acyltransferases and are also cell signaling molecules [82]. The deacylation and reacylation of phospholipids is termed "The Lands Cycle" and may be involved in membrane remodeling and the maintenance of membrane homeostasis under physiological and pathological conditions. However, there are limited studies investigating this phenomenon in cellular systems [88].

Calcium-independent phospholipase $A_2\gamma$ (iPLA$_2\gamma$ is one of seven $Ca^{2+}$-independent $PLA_2$ enzymes [81]. Our studies in renal cells showed that iPLA$_2\gamma$ has a unique subcellular localization in that its expression and activity were found in both the endoplasmic reticulum (ER) and the mitochondria, while iPLA$_2\gamma$ activity was not present [68, 97-98]. We also determined that iPLA$_2\gamma$ has divergent roles in cell injury and death, which may

be explained by unique roles and functions within subcellular compartments [81]. Pharmacological inhibition of iPLA$_2\gamma$ with the selective inhibitor bromoenol lactone (BEL) reduced cisplatin-induced apoptotic renal proximal tubule cell (RPTC) death and prevented $Ca^{2+}$-induced mitochondrial permeability transition by preventing arachidonic acid release in isolated mitochondria [112-113]. In contrast, iPLA$_2\gamma$ inhibition potentiated oxidant-induced lipid peroxidation and necrotic RPTC death [68, 98]. These data implicate iPLA$_2\gamma$ as a mediator of apoptotic cell death and as a protectant in oxidant-induced necrotic cell death.

Recent studies in our laboratory using iPLA$_2\gamma$ -specific shRNA to decrease iPLA$_2\gamma$ activity and expression in RPTC confirmed its role in preventing lipid peroxidation, maintaining phospholipid homeostasis, and preserving mitochondrial function and viability under basal conditions [116]. While the loss of mitochondrial iPLA$_2\gamma$ was correlated with decreased mitochondrial uncoupled respiration, these studies pointed to ER- iPLA$_2\gamma$ in the lipid peroxidation repair/prevention pathway because knockdown of ER- iPLA$_2\gamma$ was correlated with increased lipid peroxidation. However, no studies have elucidated the role of iPLA$_2\gamma$ in the ER nor has the mechanism by which iPLA$_2\gamma$ preserves phospholipid homeostasis been determined. The goals of the present study were to understand the role of ER-iPLA$_2\gamma$ in oxidant-induced ER lipid peroxidation, fatty acid release, $Ca^{2+}$ release and necrotic cell death.

**Materials and Methods**

Female New Zealand White rabbits (1.5-2.0 kg) were purchased from Myrtle's Rabbitry (Thompson Station, TN). Fluo-4 pentapotassium salt and Fluo-5F-AM (Fluo5F) were

purchased from Molecular Probes Invitrogen (Eugene, OR). All other chemicals and materials were obtained from Sigma Chemical (St. Louis, MO) or reported previously [68, 97-98, 112, 116, 153].

**Isolation of Microsomes.** Microsomes were isolated by differential centrifugation from homogenized rabbit kidney cortex in ice-cold isolation buffer 1 (270 mM sucrose, 5 mM Tris-HCL, 1 mM EGTA, pH 7.4) for lipid peroxidation studies as described by Kinsey et al. or isolation buffer 2 (210 mM mannitol, 70 mM sucrose, 2 mM HEPES, pH 7.4) for $Ca^{2+}$ uptake studies as described by Schieppati et al. [98, 154]. Microsomes were resuspended for immediate use in lipid peroxidation buffer (150 mM KCL, 30 mM Tris-HCL, pH 7.4) at 2 mg/ml, loaded with cis-parinaric acid (12.8 μM) on ice for 10 min, pelleted by centrifugation, washed, and resuspended at 10 mg/ml in lipid peroxidation buffer. Microsomes were resuspended in isolation buffer 2 at 10 mg/ml for $Ca^{2+}$ uptake studies. Aliquots of microsomes were resuspended in 250 mM sucrose, 10 mM KCL, 10 mM imidazole, 5 mM EDTA, 2 mM DTT, 10% glycerol at 10 mg/ml and stored at -80° C, under nitrogen, until mass spectrometry analysis.

**Measurement of Microsomal Lipid Peroxidation**. A fluorescent lipid, cis-parinaric acid, was used to measure ER lipid peroxidation as described previously [98]. Briefly, microsomes (400 μg) were added to a 96-well plate and incubated with diluent, inhibitors, or antioxidants at room temperature for 20 min and then treated with 200 μM TBHP (final volume 0.2 ml in lipid peroxidation buffer). Membrane peroxidation was measured at 37° C as the loss of cis-parinaric acid fluorescence (excitation 320 nm,

emission 405 nm) over time using a Fluoroskan Ascent fluorescent plate reader (Thermo Labsystems, Franklin, MA).

**Isolation and Identification of Released Microsomal Fatty Acids.**

Thirty minutes following treatment with 200 μM TBHP or diluent, 5 wells of each group were pooled and the reaction was stopped by the addition of 50 μM butylated hydroxyanisole (BHA) and 0.5 ml methanol. To separate microsomes from released fatty acids, the reaction mixture was centrifuged at 12,000g for 20 min and supernatant removed. Lipids were extracted from the supernatant by the Bligh and Dyer method as modified by Zhang et al., evaporated under a stream of nitrogen gas to near dryness, re-suspended in 100 μL 2:1 chloroform:methanol, and subjected to electrospray ionization-mass spectrometry [155-156].

**Electrospray Ionization-Mass Spectrometry (ESI-MS)**. ESI-MS analysis was performed as described previously using a Trap XCT ion-trap mass spectrometer (Agilent Technologies, Santa Clara, CA) with a nitrogen drying gas flow-rate of 30 psi at 350°C and a nebulizer pressure of 8 L/min [116, 156]. The scanning range was from 100-2200 *m/z* in the negative ion detection mode on 5 μL of the sample scanned for 1.4 min with a mobile phase of acetonitrile:methanol:water (2:3:1) in 0.1% ammonium formate. Fatty acid species were identified according to their *m/z* values and confirmed using MS/MS analysis based on previous studies by Kerwin et al., and Zhang et al., [156-158]. The *m/z* values 303, 319, 335, and 351 represent arachidonic acid species 20:4, 20:4-OH, 20:4-OOH, and 20:4-$(OH)_3$, respectively. *M/z* values 279, 295, and 311 represent linoleic acid species 18:2, 18:2-OH, and 18:2-OOH, respectively. For statistical analysis, *m/z* values

and peak intensities were collected in Microsoft Excel format. The m/z values were truncated to the integer and data were aligned using Microsoft Access. The peak intensity of each species for each treatment group was compared with that of the control for that experiment and displayed as % control.

**Measurement of Microsomal $Ca^{2+}$ Uptake and Release**. The membrane impermeant $Ca^{2+}$ sensitive probe, fluo-4 free acid, was used to measure extramicrosomal $Ca^{2+}$. Briefly, microsomes (200 μg) were added to a 96 well-plate in $Ca^{2+}$ uptake buffer (100 mM KCL, 30 mM imidazole-HCl buffer, 5 mM $NaN_3$, 20 mM ammonium oxalate, pH 7.0, ~6 μM $Ca^{2+}$) and incubated with diluent, inhibitors, or antioxidant at room temperature for 10 min [154]. Sarcoplasmic/endoplasmic reticulum $Ca^{2+}$ ATPase (SERCA) dependent $Ca^{2+}$ uptake was initiated by the addition of 2.5 mM MgATP, microsomes were allowed to load 20-30 min at 37°C, and further loading was inhibited with thapsigargin (250 nM), a SERCA pump inhibitor. Microsomes were then treated with 2 mM TBHP and Fluo-4 free acid (200 nM) was added immediately prior to fluorescence measurements at designated timepoints (excitation 480 nm, emission 520 nm) using a Fluoroskan Ascent fluorescent plate reader (Thermo Labsystems, Franklin, MA).

**Isolation of Rabbit Renal Proximal Tubule Cell (RPTC) and culture conditions.** RPTC were isolated using the iron oxide perfusion method and grown in 35 mm tissue culture dishes under improved conditions as described previously [146-147]. The culture medium was a 1:1 mixture of Dulbecco's modified Eagle's medium/Ham's F-12 medium

(without glucose, phenol red, or sodium pyruvate) supplemented with 15 mM HEPES buffer, 2.5 mM L-glutamine, 1 μM pyridoxine HCl, 15 mM sodium bicarbonate, and 6 mM lactate. Hydrocortisone (50 nM), selenium (5 ng/ml), human transferrin (5 μg/ml), bovine insulin (10 nM), and L-ascorbic acid-2-phosphate (50 μM) were added daily to fresh culture medium. Confluent monolayers were subjected to treatments as described below.

**RPTC Loading and Treatment.** RPTC were loaded, as previously described[159]. In brief, RPTC were co-loaded with 2 μM Fluo5F and 100 nM TMRM, washed, then incubated with 1 μM Fluo5F and 40 nM TMRM in the extracellular medium. After loading, RPTC were pretreated with BEL, *(S)*-BEL, or diluent control (DMSO) and incubated for 30 minutes.

**Microscopic Imaging and Analysis.** RPTC were imaged, as previously described, on a Leica Microsystems,TCS SP2 AOBS laser scanning confocal microscope (LSCM) in an upright microscope configuration[159]. RPTC were treated with TBHP (500 μM) or diluent control at the start of the experiment and monitored for 1 hour. Images were acquired in 5-min intervals during the course of experiments. To quantify data, images were analyzed using Adobe Photoshop. Mean intensities of images in the green and red channel after background subtraction were interpreted as a quantitative measure of ER $Ca^{2+}$ and mitochondrial membrane potential, respectively. Values are graphed as the percent mean intensity of each subsequent image vs. mean intensity of the image taken at time zero. Images comprise of 7–10 cells.

**Necrotic Cell Death.** Necrotic cell death was monitored by measuring propidium iodide (PI) staining using flow cytometry as previously described [68, 113]. Briefly, RPTC were exposed to 200 μM TBHP or diluent (control) for 4 hrs after pretreatment with BEL

and/or thapsigargin for 30 min. Media was removed, cells washed, incubated in binding buffer (10 mM HEPES, 140 mM NaCl, 5 mM KCl, 1 mM $MgCl_2$, 1.8 mM $CaCl_2$, pH 7.4) containing PI (25 μg/ml), and washed again in binding buffer without PI. Cells were then removed from the monolayer using a rubber policeman and subjected to flow cytometry (Becton Dickinson Facscalibur).

**Statistical Analysis.** Microsomes/RPTC isolated from one rabbit represents one experiment (n = 1). The appropriate analysis of variance (ANOVA) was performed for each data set and individual means were compared using Fisher's protected least significant difference test with $P \leq 0.05$ being considered indicative of a statistically significant difference between mean values.

## Results

The fluorescent lipid cis-parinaric acid was used to monitor oxidant-induced lipid peroxidation in microsomes. *cis*-Parinaric acid incorporates into the membrane and loses fluorescence when oxidized [160]. Treatment of microsomes with *tert*-butyl hydroperoxide (TBHP) caused an increased rate of lipid peroxidation compared with controls, and this increased rate was prevented by the addition of an antioxidant, butylated hydroxyanisole (BHA) (Figure 1). $iPLA_2\gamma$ is selectively sensitive to pharmacological inhibition by racemic BEL and enantiomer *(R)*-BEL but is less sensitive to enantiomer *(S)*-BEL [97, 124]. In these studies we used *(S)*-BEL as a negative control for $iPLA_2\gamma$ inhibition. Microsomes pretreated with (*R*)-BEL exhibited a greater rate of lipid peroxidation than TBHP alone while pretreatment with (*S*)-BEL (negative control)

had no effect (Figure 3-1). In summary, iPLA$_2\gamma$ diminished TBHP-induced ER lipid peroxidation.

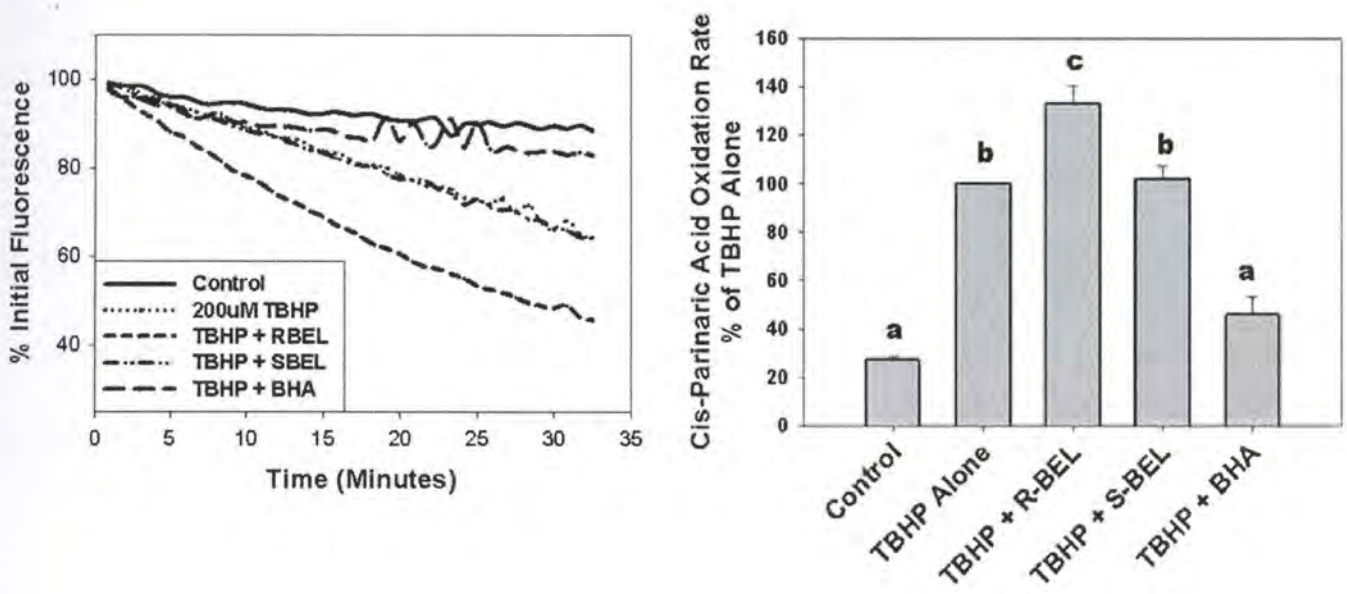


**Figure 3-1 (A) Effect of iPLA$_2\gamma$ inhibition on TBHP-induced ER membrane peroxidation (representative).** Freshly isolated rabbit kidney cortex microsomes (ER) were incubated with the fluorescent lipid cis-parinaric acid, washed, pretreated with diluent control, 16 μM (*R*)-BEL, 16 μM (*S*)-BEL, or the antioxidant BHA (50 μM), and then treated with 200 μM TBHP. The loss of cis-parinaric acid fluorescence (indicative of lipid peroxidation) was monitored over time (minutes). Results are displayed as percent initial fluorescence. (B) Effect of iPLA$_2\gamma$ inhibition on TBHP-induced ER membrane peroxidation. To determine the rate of lipid peroxidation, data was plotted as percent initial fluorescence for each treatment group and linear regression analysis was performed. Oxidation rates are displayed as percent TBHP alone. Means with different superscripts are significantly different from each other ($P < 0.05$) n=5. Values are means ± SE.

To determine the lipids released from microsomes during oxidative stress, we employed electrospray ionization-mass spectrometry (ESI-MS). The resulting ESI-Mass Spectra revealed that microsomes release several lipid species previously identified in the literature [156-158] and these species were sufficiently ionized and resolved for further mass spectrometric analysis (Figure 3-2A). Because we were interested in the

mechanism by which iPLA$_2\gamma$ prevents lipid peroxidation, we focused on linoleic (18:2) and arachidonic acid (20:4) species, products of iPLA$_2\gamma$-mediated cleavage of phospholipids. TBHP caused a 1.7-fold or greater release of arachidonic acid, linoleic acid, and their oxidized forms (18:2-OH, 18:2-OOH, 20:4-OH, 20:4-OOH, 20:4(OH)$_3$) (Figures 3-2A and 3-2B). Pretreatment of microsomes with BEL prevented TBHP-induced release of all linoleic acid species (18:2, 18:2-OH, 18:2-OOH), arachidonic acid species 20:4 and 20:4-OOH, and partially prevented the release of 20:4-OH and 20:4(OH)$_3$. These data provide evidence that iPLA$_2\gamma$ mediates oxidant-induced release of oxidized and unsaturated fatty acids.

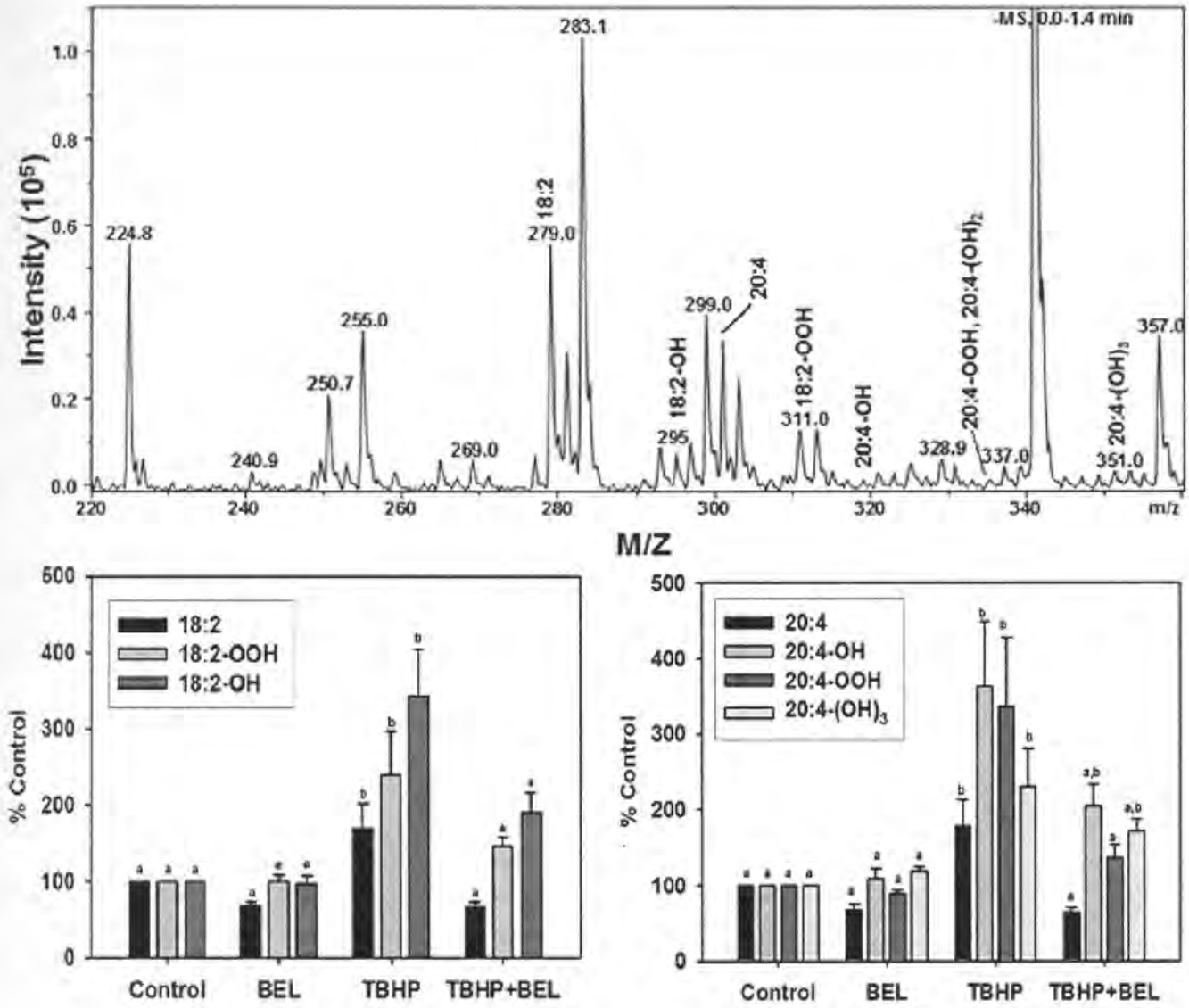


**Figure 3-2 (A). Representative Spectrum of Fatty Acids Released from Rabbit Kidney Cortex Microsomes using Electospray Ionization-Mass Spectrometry.** Released lipids were separated from microsomes using differential centrifugation, extracted by Bligh Dyer method, injected directly into ESI-Mass Spectrometer, and analyzed in negative mode. Peaks of different *m/z* values represent different lipid species. Arachidonic Acid (20:4), Linoleic Acid (18:2) and their oxidized forms were confirmed by MS/MS. (B) Effect of iPLA$_2\gamma$ inhibition on TBHP-induced Linoleic Acid (18:2) Release. Microsomes were pretreated for 20 min with BEL or diluent, treated for 30 min with 200 μM TBHP, and reaction was stopped and analyzed by ESI-MS. Linoleic Acid (18:2) and its oxidized forms (18:2-OH, 18:2-OOH) were identified according to their *m/z* values and confirmed by MS/MS analysis. Results are displayed as peak intensity of treatment group over peak intensity of control X 100 for each lipid species. Means with different superscripts are significantly different from each other ($P < 0.05$) n=4-6. Values are means ± SE. (C) Effect of iPLA$_2\gamma$ inhibition on TBHP-induced Arachidonic Acid (20:4) Release. Microsomes were pretreated for 20 min with BEL or diluent, treated for 30 min with 200 μM TBHP, and then reaction was stopped and analyzed by ESI-MS. Arachidonic Acid (20:4) and its oxidized forms (20:4-OH, 20:4-OOH, 20:4-(OH)$_3$) were identified according to their *m/z* values and confirmed by MS/MS analysis. Results are displayed as peak intensity of treatment group over peak

intensity of control X 100 for each lipid species. Means with different superscripts are significantly different from each other ($P < 0.05$) n=4-6. Values are means ± SE.

To investigate the role of $iPLA_2\gamma$ in oxidant-induced ER $Ca^{2+}$ release, we developed an assay to monitor ER $Ca^{2+}$ uptake and release in microsomes. Fluo-4 fluorescence was used to monitor extra-microsomal $Ca^{2+}$. A decrease in fluorescence corresponds to ER $Ca^{2+}$ uptake while an increase represents ER $Ca^{2+}$ release. The addition of ATP caused rapid $Ca^{2+}$ uptake (loading) as indicated by a decrease in fluorescence (Figure 3-3). Pretreatment with thapsigargin, an inhibitor of the Sarcoplasmic/Endoplasmic Reticulum ATPase (SERCA), prevented the ATP dependent $Ca^{2+}$ loading. The addition of thapsigargin at 30 min prevented further $Ca^{2+}$ loading but did not cause significant $Ca^{2+}$ release. A23187, a $Ca^{2+}$ ionophore, caused rapid release of loaded $Ca^{2+}$.

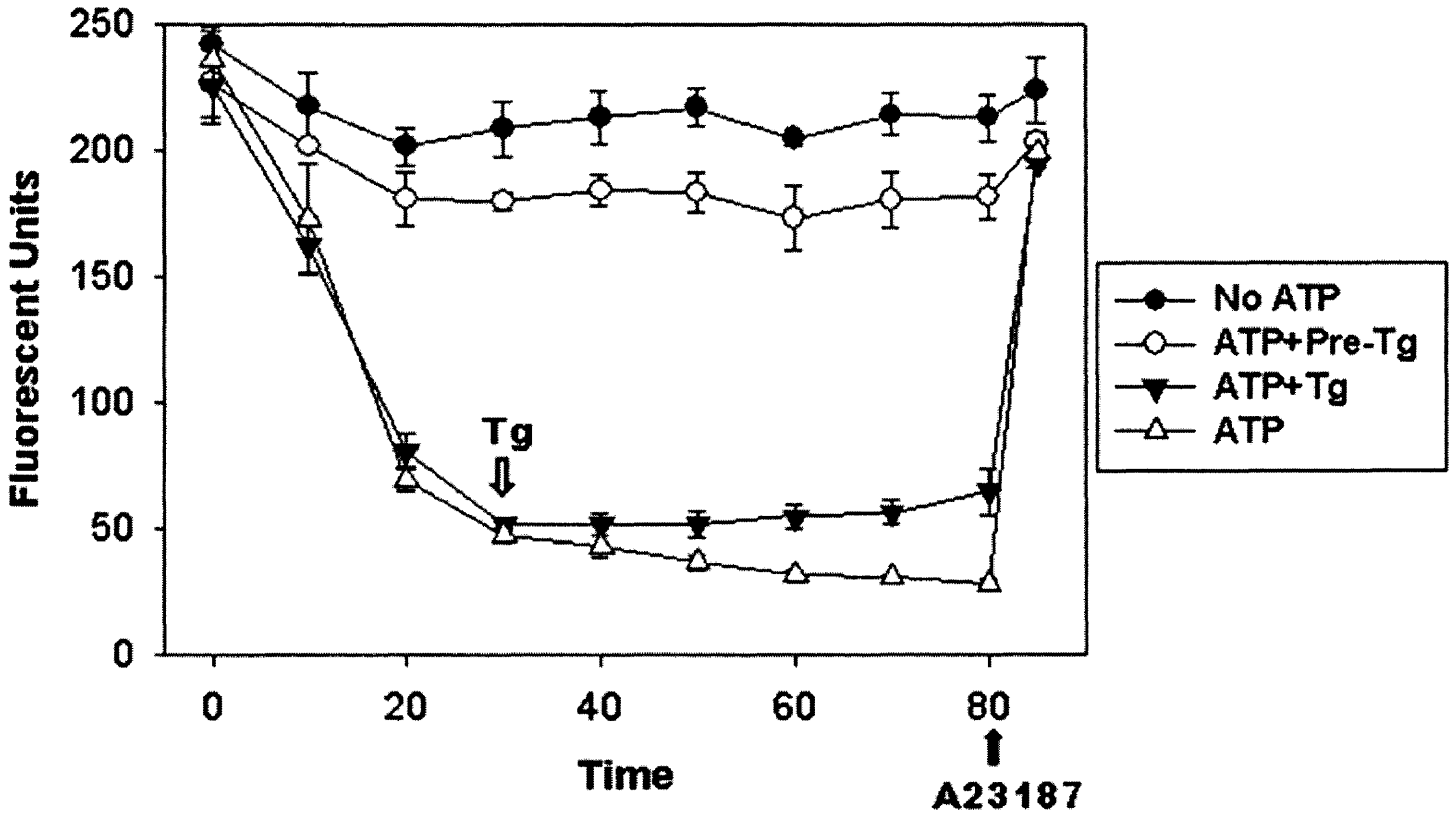


**Figure 3-3. Sarcoplasmic/Endoplasmic Reticulum $Ca^{2+}$ ATPase (SERCA) dependent calcium uptake in rabbit kidney cortex microsomes.** SERCA dependent $Ca^{2+}$ uptake was initiated by the addition of 2.5 mM ATP and microsomes were loaded with $Ca^{2+}$ (ATP). As controls, microsomes were pretreated with thapsigargin (SERCA inhibitor) prior to ATP addition (ATP+Pre-Tg), thapsigargin was added 30 min after loading was initiated (ATP+ Tg), or no ATP (diluent) was added (No ATP). 200nM Fluo-4 salt was added immediately prior to fluorescence readings at the specified time points. Means with different superscripts are significantly different from each other ($P < 0.05$) n=3. Values are means ± SE.

To test whether an oxidant causes microsomal $Ca^{2+}$ release and whether $iPLA_2\gamma$ plays a role in that release, we loaded microsomes with $Ca^{2+}$ by adding ATP for 30 min and then treated with thapsigargin to prevent further loading. Microsomes were then treated with TBHP or diluent in the presence or absence of $iPLA_2\gamma$ inhibition using BEL. $Ca^{2+}$ release occurred approximately 50 min after treatment with TBHP and pretreatment with BEL potentiated the release (Figure 3-4A). Time is plotted from the addition of TBHP.

Pretreatment with (*S*)-BEL was no different than TBHP alone and antioxidant BHA prevented oxidant-induced ER $Ca^{2+}$ release (Figure 3-4B). In summary, $iPLA_2\gamma$ diminished TBHP-induced $Ca^{2+}$ release and ER $Ca^{2+}$ release occurs after the initiation of lipid peroxidation.

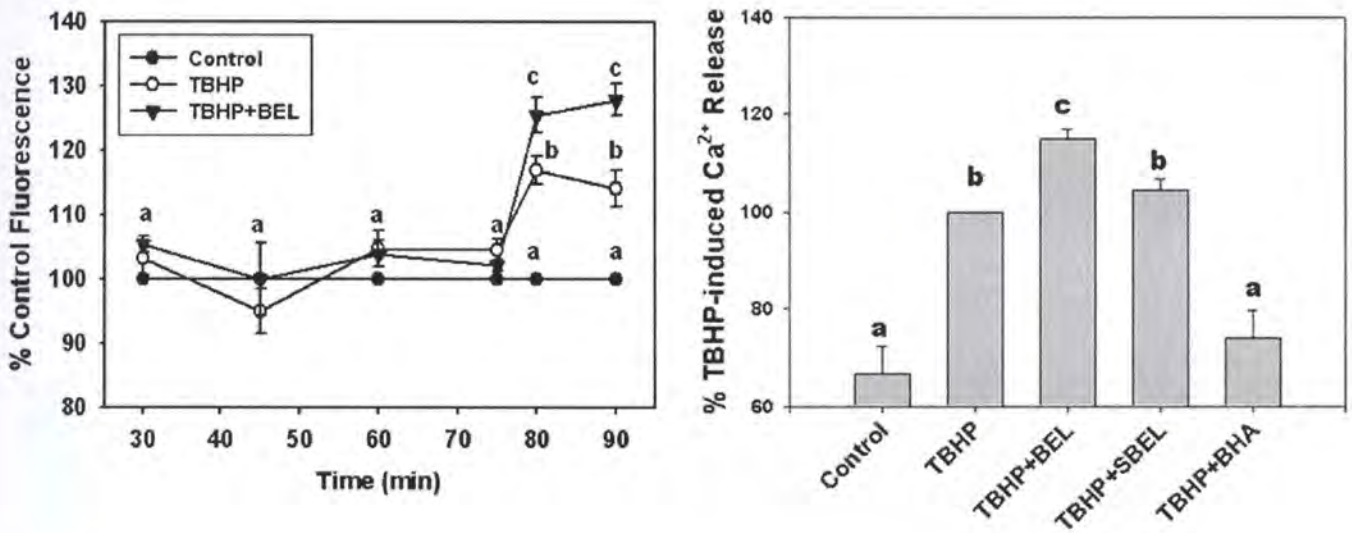


**Figure 3-4 (A) Effect of $iPLA_2\gamma$ inhibition on TBHP-induced Microsomal $Ca^{2+}$ Release**. Microsomes were pretreated at room temperature with 10 μM BEL or diluent for 10 min, loading was initiated by the addition of ATP at 37°C, and further loading was inhibited at 30 min by thapsigargin (Control). Microsomes were then treated with 2 mM TBHP in the presence (TBHP + BEL) or absence (TBHP) of BEL. Fluo-4 acid was added immediately prior to fluorescence readings at specified time points and results displayed as percent control fluorescence (microsomes loaded and treated with thapsigargin alone). Means with different superscripts are significantly different from each other ($P < 0.05$) n=4. Values are means ± SE. (B) The role of $iPLA_2\gamma$ in TBHP-induced ER $Ca^{2+}$ Release at 80 minutes (50 minutes after treatment with TBHP). Microsomes were pretreated with diluent, BEL, *(S)*-BEL (negative control), or BHA (antioxidant control) for 10 min at room temperature. Loading was initiated by the addition of 2.5 mM ATP at 37°C, microsomes were loaded for 30 min and then treated with diluent (ATP only group), 250 nM thapsigargin (Control), thapsigargin and 2 mM TBHP (TBHP), or thapsigargin and TBHP after pretreatment with 16 μM BEL (TBHP+BEL), 16 μM *(S)*-BEL (TBHP+SBEL), or 50 μM BHA (TBHP+BHA). 200 nM Fluo-4 acid was added immediately prior to fluorescence measurements 80 minutes after the initiation of loading. Results were displayed as (treatment group fluorescence-ATP only group fluorescence)/(TBHP group fluorescence-ATP only group fluorescence) X 100). Means with different superscripts are significantly different from each other ($P < 0.05$) n=5. Values are means ± SE.

To investigate the role of iPLA$_2\gamma$ in oxidant-induced ER $Ca^{2+}$ release in RPTC, cells were co-loaded with Fluo5F, a marker of ER $Ca^{2+}$, and tetramethyl rhodamine methyl ester (TMRM), a marker of polarized mitochondria. Fluorescence was monitored using laser scanning confocal microscopy (LSCM) as previously described[159]. RPTC were treated with TBHP in the presence and absence of iPLA$_2\gamma$ inhibition by BEL. Inhibition of iPLA$_2\gamma$ prior to TBHP treatment potentiated TBHP-induced ER $Ca^{2+}$ release (Fig. 5A). There was no significant loss of mitochondrial polarization in any group during this time frame (Fig. 3-5B).

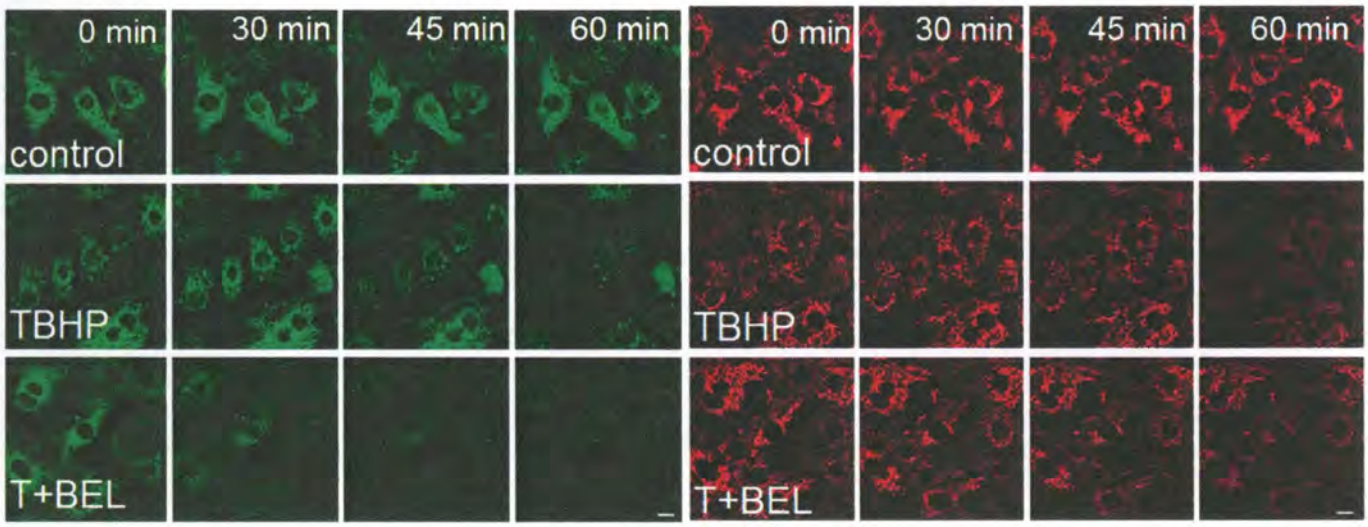


**Figure 3-5. The role of iPLA$_2\gamma$ in TBHP-induced ER $Ca^{2+}$ release and Mitochondrial Depolarization in RPTC**. RPTC were loaded, as described in materials and methods, pretreated with BEL (5 μM) or diluent control for 30 min, exposed to TBHP (500 μM) or diluent control, and then monitored for 1 hr using laser scanning confocal microscopy. Fluo5F fluorescence (green, A) and TMRM fluorescence (red, B) represents ER $Ca^{2+}$ and mitochondrial polarization, respectively. Note, TBHP alone did not induce ER $Ca^{2+}$ release at 30 minutes. In contrast, TBHP induced ER $Ca^{2+}$ release in RPTC pretreated with BEL at 30 min. There were no significant changes in mitochondrial polarization.

Quantification of TBHP-induced ER $Ca^{2+}$ release revealed 15% and 40% ER $Ca^{2+}$ release at 30 and 45 min, respectively, in RPTC pretreated with BEL and then exposed to TBHP.

In contrast, TBHP exposure alone caused no ER $Ca^{2+}$ release at 30 minutes and only 20% release at 45 min (Fig. 3-6). Pretreatment with (S)-BEL (negative control) prior to TBHP exposure was no different than TBHP alone and BEL alone nor SBEL alone caused ER $Ca^{2+}$ release. In summary, $iPLA_2\gamma$ delayed TBHP-induced ER $Ca^{2+}$ release in RPTC.

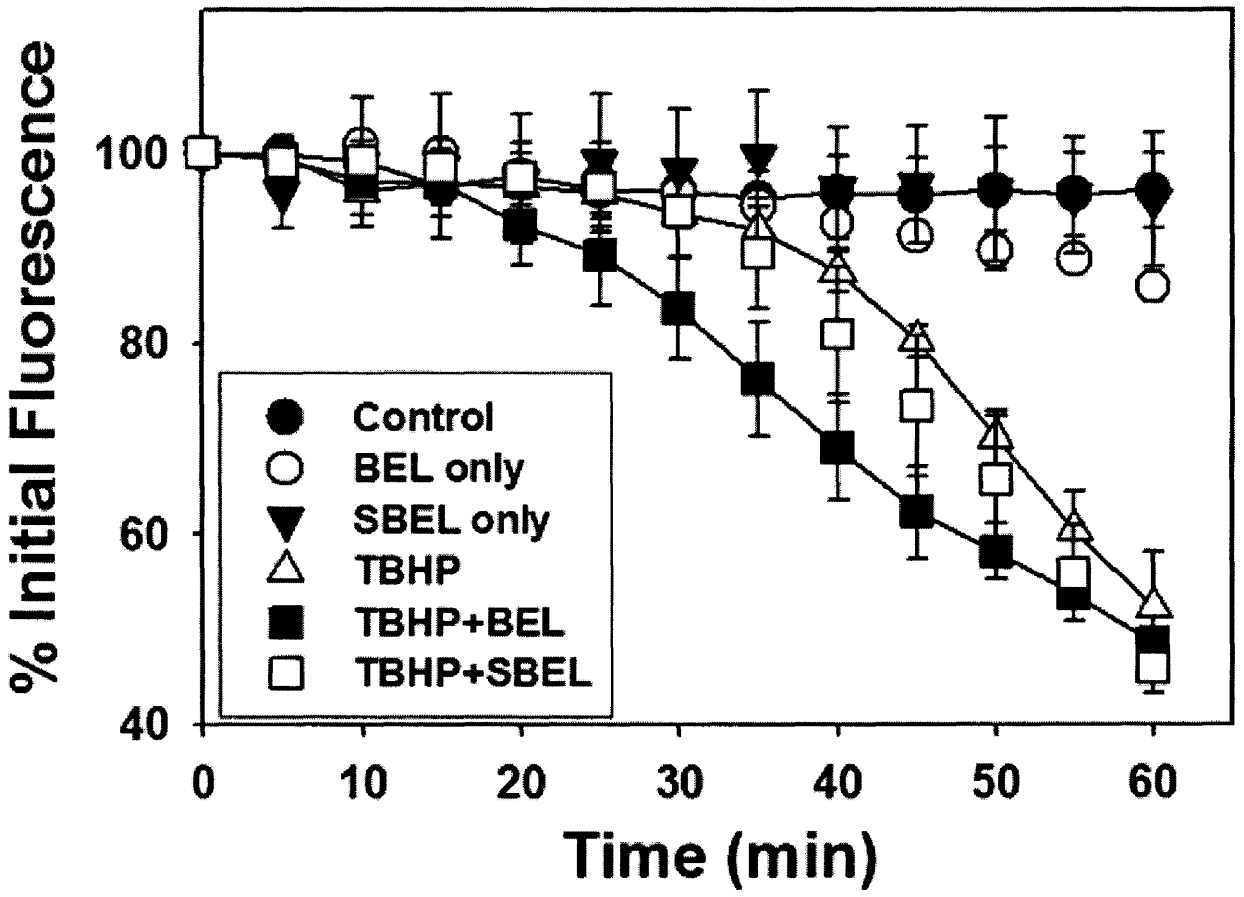


**Figure 3-6. Quantification of TBHP- induced ER $Ca^{2+}$ Release in RPTC.** RPTC were co-loaded, pretreated, exposed to TBHP, and imaged, as described in materials and methods. Values are mean intensities of images in the green channel ± SE and loss of intensity represents ER $Ca^{2+}$ release. Note earlier TBHP-induced ER $Ca^{2+}$ release under $iPLA_2\gamma$ inhibition (TBHP+BEL) compared to TBHP alone(TBHP) and negative control (TBHP+SBEL). BEL alone nor *(S)*-BEL alone caused ER $Ca^{2+}$ release.

The next experiment was designed to investigate the role of ER $Ca^{2+}$ release in oxidant-induced cell death in RPTC in the presence and absence of $iPLA_2\gamma$ inhibition. TBHP caused 30% necrotic cell death (propidium iodide (PI) staining) as compared to 2-3% in

control cells. iPLA$_2\gamma$ inhibition with BEL prior to TBHP treatment potentiated TBHP-induced necrotic cell death to 40% as previously reported [68, 98] (Figure 3-7). When ER $Ca^{2+}$ was depleted with thapsigargin prior to TBHP exposure, necrotic cell death was reduced to 17%. Equally important, the potentiation of cell death observed when iPLA$_2\gamma$ was inhibited was blocked by ER $Ca^{2+}$ depletion (Figure 3-7). BEL alone and thapsigargin alone had no effect on cell viability. In summary, ER $Ca^{2+}$ release is a major attributor to oxidant-induced necrotic cell death and the potentiation of cell death seen under iPLA$_2\gamma$ inhibition.

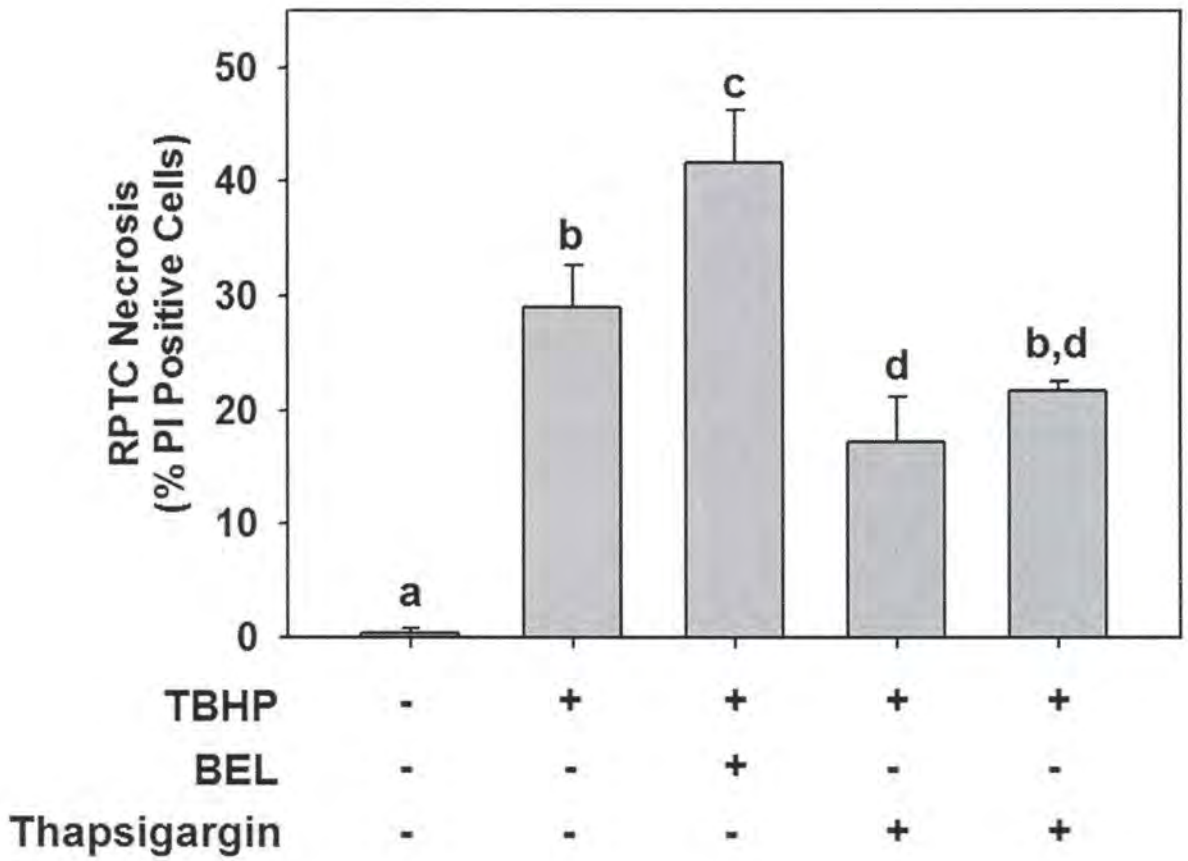


**Figure 3-7. Effect of ER $Ca^{2+}$ depletion and iPLA$_2\gamma$ inhibition on oxidant-induced RPTC necrosis.** RPTC were treated with either diluent (DMSO), BEL, and/or thapsigargin for 30 min before the addition of TBHP (200 μM). After treatment, the percent PI staining was determined by flow cytometry. Means with different superscripts are significantly different from each other ($P < 0.05$) n=5. Values are means ± SE.

Note, the potentiation of TBHP-induced necrotic cell death by BEL, but the absence of potentation by BEL when ER $Ca^{2+}$ stores are depleted with thapsigargin.

## Discussion

We previously demonstrated that $Ca^{2+}$ plays an important role in necrotic renal cell death [50, 52-53]. In 1997, we demonstrated ER $Ca^{2+}$ release was a key step in necrotic cell death and that depletion of ER $Ca^{2+}$ stores blocked death in RPTC [50]. Other studies in RPTC revealed that iPLA$_2\gamma$ inhibition potentiates oxidant induced lipid peroxidation and cell death, and knockdown of ER- iPLA$_2\gamma$ correlated with increased lipid peroxidation and loss of cell viability [68, 98] These studies demonstrated the cytoprotective role of iPLA$_2\gamma$ revealed the significance of ER $Ca^{2+}$ release during necrotic cell death, and pointed to ER- iPLA$_2\gamma$ in the putative lipid peroxidation repair/prevention pathway. However, a direct link between ER- iPLA$_2\gamma$ and oxidant-induced ER $Ca^{2+}$ release had not been established, nor had the mechanism by which ER- iPLA$_2\gamma$ is protective or is involved in the lipid peroxidation repair/prevention pathway been revealed. Thus, the goals of the present study were to understand the role of ER- iPLA$_2\gamma$ in oxidant-induced ER lipid peroxidation, fatty acid release, $Ca^{2+}$ release and necrotic cell death.

We used freshly isolated rabbit kidney cortex microsomes to further investigate the role of ER- iPLA$_2\gamma$ in oxidant stress. ER- iPLA$_2\gamma$ decreased oxidant-induced lipid peroxidation and $Ca^{2+}$ release, and mediated oxidant-induced release of oxidized and unsaturated fatty acids. These results support our hypothesis that ER- iPLA$_2\gamma$ protects

renal cells from oxidant injury by decreasing lipid peroxidation, ER $Ca^{2+}$ release and subsequent necrotic cell death. These findings are consistent with our previous work in isolated mitochondria showing that $iPLA_2\gamma$ protects mitochondria from oxidant-induced lipid peroxidation and mitochondrial swelling [98]. Also, shRNA knockdown of $iPLA_2\gamma$ in RPTC increased lipid peroxidation and sensitized RPTC to nonlethal oxidant treatment [116].

It has been proposed that phospholipases play a role in membrane remodeling and repair during oxidant stress by cleaving oxidized and/or unsaturated fatty acids from the membrane, preventing the initiation and propagation of lipid peroxidation, and allowing for the incorporation of unoxidized fatty acids [74]. ER and mitochondria are the major sites of reactive oxygen species (ROS) production and the presence of $iPLA_2\gamma$ in mitochondria and ER of rabbit RPTC makes it a likely candidate for a role in membrane repair and remodeling. The most probable mechanism by which these enzymes prevent or repair lipid peroxidation is through the cleavage and removal of oxidized fatty acids from the membrane [81]. The initiation step of lipid peroxidation involves the abstraction of a hydrogen atom from the methylene carbon of a fatty acid and therefore fatty acids with more double bonds are more vulnerable to the initiation of lipid peroxidation [75]. The resulting peroxyl radical is capable of abstracting a hydrogen atom from adjacent fatty acids, thus propagating the lipid peroxidation and potentially producing several lipid hydroperoxides [76]. This chain of events can be terminated by the removal of the reactive lipid from the site of reaction or a chain-breaking antioxidant[75-77]. In our case, the inhibition of $iPLA_2\gamma$ would result in the

accumulation of oxidized fatty acids in the membrane and contribute to the propagation of the lipid peroxidation.

Van Kujick proposed that hydroxyl or hydroperoxyl groups introduced into fatty acyl chains via lipid peroxidation creates a more hydrophilic acyl chain that would move towards the head group of a phospholipid to become more thermodynamically stable [88]. This molecular rearrangement could make the ester linkage at the *sn*-2 position more accessible to $PLA_2$ cleavage. Interestingly, both oxidized arachidonic acid and linoleic acid were released following exposure of ER to TBHP. While it may be true that oxidized fatty acids become more accessible to phospholipase cleavage, it is clear that $iPLA_2\gamma$ is readily capable of removing non-oxidized fatty acids under oxidative conditions. The release of non-oxidized fatty acids, such as arachidonic acid, during oxidant stress raises the possibility that the non-oxidized arachidonic acid may initiate an inflammatory signal through one of its metabolites. This possibility requires further exploration.

We developed an assay of microsomal $Ca^{2+}$ release using Fluo-4, a fluorescent dye with a high affinity for $Ca^{2+}$ ($K_m$~ 300 nM). ATP dependent loading was consistent with Sheippatti et al., in that it took approximately 20 min to reach maximal $Ca^{2+}$ uptake [77, 154]. There was little passive $Ca^{2+}$ loading, as depicted in microsomes incubated without ATP or pretreated with thapsigargin prior to the addition of ATP. Treatment with thapsigargin after loading did not cause release of $Ca^{2+}$ as observed in intact cells [50]. We used this to our advantage because we were interested in ER $Ca^{2+}$ release and

treated microsomes with thapsigargin after loading to ensure that any $Ca^{2+}$ released may not be re-sequestered by SERCA activity. There was not a gradual release of ER $Ca^{2+}$ but a critical point reached approximately 50 min after treatment with TBHP. We did not observe ER $Ca^{2+}$ release earlier under conditions of $iPLA_2\gamma$ inhibition, but instead we observed the potentiation of ER $Ca^{2+}$ release 50 min after TBHP treatment. These data provide evidence that $iPLA_2\gamma$ is protective by preventing the propagation of lipid peroxidation.

To investigate the role of $iPLA_2\gamma$ in oxidant-induced RPTC ER $Ca^{2+}$ release, we utilized a method developed in our laboratory of monitoring ER $Ca^{2+}$ directly using low affinity $Ca^{2+}$ indicator, Fluo5F, and laser scanning confocal microscopy. These data revealed that $iPLA_2\gamma$ inhibition resulted in oxidant-induced ER $Ca^{2+}$ release at an earlier time point than TBHP alone. Collectively, these data support our hypothesis that ER- $iPLA_2\gamma$ protects renal cells from oxidant-induced necrotic cell death by preventing ER lipid peroxidation, preserving ER membrane integrity, and blocking ER $Ca^{2+}$ release and loss of $Ca^{2+}$ homeostasis.

Interestingly, $iPLA_2\gamma$ inhibition alone was not sufficient to cause ER $Ca^{2+}$ release within the course of the experiment. These data suggest that $iPLA_2\gamma$ is most important under conditions of elevated oxidant stress such as would be experienced during ischemia/reperfusion or toxicant injury. Additionally, our studies in RPTC reveal that oxidant-induced ER $Ca^{2+}$ release occurs prior to loss of mitochondrial membrane potential and cell death.

To confirm ER $Ca^{2+}$ release is a mediator of oxidant-induced cell death and that $iPLA_2\gamma$ plays a pivotal role in this process, we depleted the ER of $Ca^{2+}$ prior to oxidant injury and monitored necrotic cell death in the presence and absence of $iPLA_2\gamma$ inhibition. Depletion of ER $Ca^{2+}$ prior to oxidant injury greatly reduced necrotic cell death and blocked the potentiation of cell death seen under $iPLA_2\gamma$ inhibition. These data reveal that the protection from necrotic cell death by $iPLA_2\gamma$ during oxidant injury is closely tied with ER $Ca^{2+}$ release. This compilation of evidence supports our hypothesis that ER-$iPLA_2\gamma$ is protective during oxidant injury and reveals the mechanisms by which ER $iPLA_2\gamma$ protects the ER from oxidant-induced lipid peroxidation and $Ca^{2+}$ release.

# Chapter 4

## Genetic Ablation of $Ca^{2+}$–Independent Phospholipase $A_2\gamma$ Induces Lipid Peroxidation, Oxidative DNA Damage and Loss of Phospholipid Homeostasis in Mouse Kidney


### Abstract

Calcium-independent phospholipase $A_2\gamma$ (iPLA$_2\gamma$) protects primary renal cells from oxidant injury by preventing or repairing oxidant-induced lipid peroxidation. We tested this hypothesis *in vivo* using mice genetically ablated of iPLA$_2\gamma$ (KO mice) and investigated its role in age-related renal oxidant injury. Urinary 8-isoprostanes and 8-hydroxy-2'-deoxyguanosine (8-OHdG), biomarkers of lipid peroxidation and oxidative DNA damage, respectively, increased in 13 month KO mice compared to WT mice. Urinary lipidomic analysis demonstrated decreases in phospholipid species 38:6, 38:5 and 37:5 phosphatidylcholine and increases in 6-10 carbon fatty acids, with methyl or keto additions. Thirteen month KO mouse kidney cortex exhibited higher lipid peroxidation and 8-OHdG staining compared to WT mice. No differences in kidney function were detected between KO and WT mice at 2 or 13 months of age. Renal mitochondrial respiratory proteins NDUFB8 and COX-1, and mitochondrial DNA copy number increased in KO mice. KO mice exhibited increased mRNA levels of GPx4, an antioxidant enzyme that contains lipid hydroperoxidase activity. Collectively, these

studies reveal that genetic ablation of iPLA$_2\gamma$ results in 1) increased renal oxidative lipid and DNA damage, 2) disruption of mitochondrial homeostasis with increased respiratory proteins and mtDNA, and 3) a compensatory increase in GPx4. These data provide evidence that iPLA$_2\gamma$ is critical for the prevention or repair of lipid peroxidation in oxidative kidney injury.

## Introduction

Phospholipase $A_2$ ($PLA_2$) enzymes hydrolyze the *sn-2* ester bond of glycerophospholipids, producing a free fatty acid and a lysophospholipid [86]. Free fatty acids serve as signaling molecules and/or can be further metabolized to produce mediators of inflammation, cell signaling and death. For example, arachidonic acid is metabolized to prostaglandins, prostacyclins, thromboxanes and leukotrienes; all of which are major components of inflammatory and signaling pathways [87]. Lysophospholipids can serve as substrates for the re-esterification of free fatty acids by CoA-dependent acyltransferases [82]. The ability of $PLA_2$ to release fatty acids from phospholipid membranes and, in turn, allow for the re-esterification of free fatty acids from cellular pools is the basis for its putative involvement in membrane remodeling/repair pathways; however, their role in these pathways have not been fully elucidated [88].

iPLA$_2\gamma$ is one of seven $Ca^{2+}$-independent $PLA_2$ and belongs to the Group VIB family. Our previous studies detected high levels of iPLA$_2\gamma$ expression and activity in rabbit renal cells that were localized to the endoplasmic reticulum (ER) and mitochondria, the

major sites of reactive oxygen species (ROS) production and targets of oxidant injury [68, 97-98, 112]. Pharmacological inhibition of iPLA$_2\gamma$ potentiated oxidant-induced lipid peroxidation in isolated mitochondria and ER, and potentiated oxidant-induced mitochondrial permeability transition (MPT) and ER $Ca^{2+}$ release, respectively [98, 161]. Pharmacological inhibition of iPLA$_2\gamma$ also potentiated lipid peroxidation and necrotic cell death in renal proximal tubule cells (RPTC) [68]. Recently, we showed that knockdown of iPLA$_2\gamma$ using shRNA increased several species of phosphatidylcholine, phosphatidylethanolamine, and phosphatidylglycerol phospholipid classes [116]. Additionally, we demonstrated iPLA$_2\gamma$ mediated release of oxidized and non-oxidized fatty acids from the ER during oxidative stress [161]. These data provide strong evidence that iPLA$_2\gamma$ is a major component of the membrane remodeling/repair pathway and is thereby protective during oxidant stress in renal cells.

Mancuso et al. generated mice null for iPLA$_2\gamma$ by genetically ablating the enzyme's active site [136]. These mice were more vulnerable to cardiac stress (transverse aortic constriction), were resistant to high fat diet-induced weight gain, exhibited cognitive dysfunction and exhibited multiple dysfunctional bio-energetic phenotypes, such as cold intolerance and reduced exercise endurance, compared to their wild type liter mates [134-136]. Interestingly, Yoda et al. also generated mice null of iPLA$_2\gamma$ and reported increased lipid peroxidation in skeletal muscle, and, similarly to the work of Mancuso et al., alterations in cardiolipin content and mitochondrial dysfunction [141]. Together, these data support our previous findings that impairment of iPLA$_2\gamma$ increases oxidative

stress, alters lipid homeostasis, and increases mitochondrial dysfunction *in vitro*. The effects of knocking out iPLA$_2\gamma$ in the kidney have not been studied.

The goal of these studies was to examine the consequences of iPLA$_2\gamma$ loss in the kidney, particularly with respect to age. Because oxidant stress is a major component of age-related deterioration of kidney function and iPLA$_2\gamma$ protects RPTC from oxidative stress, we hypothesized that mice genetically ablated of iPLA$_2\gamma$ will have increased levels of oxidative stress and display altered lipid homeostasis, and that these changes will be more apparent as mice age.

## Experimental Procedures

### Mouse Husbandry

Mice of a mixed genetic background of C57BL/6 x 129/Sv with the region encoding the active site of the iPLA$_2\gamma$ removed [136] were a gift from Dr. Richard Gross at Washington University School of Medicine, St. Louis, MO. Mice were housed in standard animal rooms under normal conditions: 12 hr dark (18.00–06.00 hr)–12 hr artificial light (06.00–18.00 hr) cycle; temperature maintained at 21 ± 1°C; and relative humidity varied between 30 and 60% and received food and water *ad libitum*. Heterozygous mice were bred under pathogen-free conditions and the resulting WT and KO male mice were used for these studies. PCR analysis was performed for genotyping, as previously described [136]. All studies were reviewed and approved by the institutional animal care and use committee of the Medical University of South Carolina

and were in accordance with the National Institutes of Health guidelines for humane treatment of animals.

**Urine and Tissue Collection**

For 24 hr urine collection, mice were weighed, and then housed individually in metabolic cages. Urine samples were centrifuged at 800 g for 5 min, supernatant volume measured and antioxidant (BHT, 0.05%) added. Samples were either analyzed immediately or aliquoted and frozen at -80°C for further analysis. Mice were then euthanized by intraperitoneal injection of pentobarbital, blood taken via cardiac puncture, and kidneys collected for tissue analysis. A portion of the kidney was fixed in 10% buffered formalin for greater than 24 hr and subsequently processed for histology or immunohistochemistry. The remaining kidney tissue was stored at -80°C. Serum was separated from whole blood by standard methods, BHT added, and was either used immediately or stored at -80°C.

**Urine and Serum Assays**

Urine and serum creatinine were measured using a QuantiChrom Creatinine Assay Kit according to the manufacturer's protocol (Hayward, CA). Each sample was tested in duplicate and values expressed in mg/dl. 8-isoprostane and 8-OHdG were measured in urine using ELISA assay kits as markers of lipid peroxidation and oxidative DNA damage, respectively (Cayman Chemicals, Ann Arbor, MI). Generally, samples were diluted 1:20 and 1:1000 for 8-isoprostane and 8-OHdG, respectively.

**Histology**

Renal tissues were fixed in 10% buffered formalin, dehydrated, and embedded in paraffin. For general histology, sections were stained with hematoxylin/eosin or PAS and were scored in a blinded fashion by a renal pathologist, Dr. Judit Megyesi, University of Arkansas for Medical Sciences. Briefly, morphologic damage (tubular necrosis, loss of brush border, casts, inflammatory cells, tubular dilatation, distal damage, degeneration, red blood cell extravazation, interstitial edema, glomerular changes, and interstitial fibrotic foci) of the entire kidney section was scored semi quantitatively using the following scale: none= 0; <10%= 1; 11-25%= 2; 26-75%= 3; and 75%= 4.

**Immunohistochemistry**

Slides were emersed twice in xylene for 5 min and were dehydrated by emersion in 100%, 95% and 70% histological grade ethanol, consecutively, for 6 min each. Slides were rinsed in PBS, incubated in 30% $H_20_2$ for 30 min, and then incubated in 2% normal horse serum for 20 min to block non-specific binding. Slides were washed twice with PBS and incubated with primary antibodies against 8-OHdG (9.75 μg/ml) for 18 hours. Slides were washed three times in PBS for 5 min, incubated for 30 min in PBS containing a universal secondary antibody and Elite Reagent (Vector labs; Burlingame, CA, USA), and then incubated for 30 min with DAB reagent and Gills Hematoxylin, as a counter stain. Slides were bathed in ammonium hydroxide (10% v/v), dehydrated, and fluoromount and cover slips were applied. Images were taken using a Nikon AZ100 fluorescence microscope and positively stained nuclei per field were counted from three

random images (25X) in a double blinded fashion. 8-OHdG antibody was purchased from Rockland Immunochemicals (Gilbertsville, PA, USA).

**Tissue Lipid Peroxidation Assay**

To measure thiobarbituric acid reacting substances (TBARS), mouse kidney cortex (~25 mg) was placed in 500 µl RIPA Buffer (50 mM Tris-HCL, 150 mM NaCl, 1 % Triton X-100, 1% Sodium Deoxycholate, 0.1 % SDS, 1 mM EDTA) containing protease inhibitors and BHT (0.05%) and sonicated on ice for 15 sec at 1400 V. An aliquot (50 µl) was taken for protein quantification. Samples were centrifuged at 1600 g for 10 min at 4°C and supernatant used for the assay. Color reagent containing 200 µl 8.1% SDS, 1.5 ml 20% acetic acid (pH=3.5), 1.5 ml 0.8% thiobarbituric acid, and 700 µl water was added vigorously to 100 µl sample (supernatant) in a glass vial and boiled for 1 hr at 95°C. To stop the reaction, the mixture was placed on ice for 10 min, then centrifuged at 3000 g for 10 min. A 200 ul aliquot of supernatant was taken and absorbance measured at 650 nm. 1, 1, 3, 3-Tetraethoxy-propane was used as a standard. Methods were modified from Ohkawa *et al.* [162].

**Bligh-Dyer lipid extraction**

Urine lipids were extracted using chloroform and methanol according to the method of Bligh and Dyer [155]. Urine (1 mL) was mixed with 2 mL methanol: water (2.0:0.8 v/v), transferred to a glass test tube, 1.25 ml chloroform was added, and tubes were vortexed for 30 sec and allowed to sit for 10 min on ice. Tubes were centrifuged at 213 g for 1

min and the bottom chloroform layer was transferred to a new test tube. The extraction steps were repeated and the chloroform layers combined. The collected chloroform layers were dried under argon, reconstituted with 50 μL of methanol:chloroform (2:1 v/v), and stored at -20°C.

**Lipid phosphorus assay**

Lipid phosphorus was quantified using a modified Bartlett inorganic phosphorous assay [163]. Lipid extract (10 μL) was mixed with 400 μL of 10N sulfuric acid and heated at 180-200°C for 1 hr in a glass test tube. After this time, 100 μL of 30% hydrogen peroxide was added while vortexing and the tube was heated for an additional 1.5 hr. The tube was removed from heat and 4.6 mL of molybdate reagent and 100 μL of 15% ascorbic acid were added consecutively while vortexing. Samples were then placed in a boiling water bath for 10 min before absorbance was read at 825 nm.

**Characterization and quantitation of urinary lipids using electrospray ionization-mass spectrometry (ESI/MS).**

Lipid extract samples (20 pmol/μl) were prepared by reconstituting in chloroform: methanol (2:1, v/v). Samples were analyzed using an Agilent Trap XCT ion-trap mass spectrometer equipped with an electrospray ion source (Agilent, Santa Clara, CA). Samples (5 μL) were introduced by means of a flow injector into the ESI chamber at a rate of 0.2 mL/min. The elution solvent was acetonitrile:methanol:water (2:3:1, v/v/v) containing 0.1% (w/v) ammonium formate (pH 6.4). The mass spectrometer was

operated in both positive and negative scanning mode. The flow rate of nitrogen drying gas was 8 L/min at 350°C. The capillary and cone voltages were set at 2.5 kV and 30 V respectively. Qualitative identification of individual phospholipid and fatty acid species was based on their calculated theoretical monoisotopic mass values, followed by a subsequent round of MS to identify fragmentation products (MS/MS). Relative abundance was determined by comparison to the total ion count in each sample.

**Immunoblot Analysis**

Approximately 25 mg of frozen kidney tissues were homogenized and disrupted by sonication for 30 sec using homogenization buffer supplemented with protease inhibitors. Equal amounts of tissue homogenates were separated by SDS-PAGE and electrophoretically transferred to nitrocellulose membranes. After treatment with 5% skim milk for 1 hr at room temperature, membranes were incubated with various antibodies NDUFB8 & COX I (Invitrogen, Carlsbad, CA ), ATP Synthase β (Abcam, Cambridge, MA) and GAPDH (Fitzgerald, Concord, MA) overnight at 4°C and then incubated with an appropriate horseradish peroxidase-conjugated secondary antibody (Santa Cruz Biotechnology, Santa Cruz, CA) for 1 hr at room temperature. Bound antibodies were visualized after chemiluminescence detection on an AlphaEase FC stand-alone imaging system (San Leandro, CA).

**Mitochondrial DNA Copy Number**

Real-time PCR was used to determine relative quantities of mitochondrial DNA content in WT and KO animal kidney tissues. Total genomic DNA was extracted using a DNeasy

Blood and Tissue kit (QIAGEN, Valencia, CA). DNA was quantified by measuring *A*260 values and 50 ng of total DNA was used for PCR, as previously described [164]. Primers specific to the mitochondrial-encoded ND6 gene were used to assess mitochondrial DNA copy numbers. Primers designed against the nuclear-encoded tubulin gene were used for normalization and are listed in Table 4-1.

| *Gene* | *Sequence* |
|---|---|
| *GPx4* | FW: TGT GCA TCCC GCG ATG ATT |
| | REV: CCC TGT ACT TAT CCA GGC AGA |
| *GR-1* | FW: GAC ACC TCT TCC TTC GAC TAC C |
| | REV: CCC AGC TTG TGA CTC TCC AC |
| *ND6* | FW: AGG GCT TGG GTT GAT TGT TAG |
| | REV: TGC CAT CGC AGT AGT ATA CCC |
| *Prdx6* | FW: CAT CCG CTT CCA CGA TTT CCT |
| | REV: CTC TGC CAA GTT CTG TGG TG |
| *Tubulin* | FW: CTC TCT GTC GAT TAC GGC AAG |
| | REV: TGG TGA GGA TGG AGT TGT AGG |

**Table 4-1. Primers used for qRT-PCR experiments**

## Quantitative Real-Time PCR

Total RNA was isolated from kidney tissues with TRIzol reagent (Invitrogen). cDNA was synthesized from 1 μg of RNA template using a RevertAid™ First Strand cDNA Synthesis Kit (Fermentas Inc., Glen Bernie, MD). PCR was carried out, as previously described [19], using 3 μl of 1:3 diluted cDNA template combined with Maxima® SYBR Green qPCR Master Mix (2X) at a final concentration of 1X (Fermentas Inc.), ROX (Fermentas Inc.) and primers (Invitrogen, Carlsbad, CA) at a concentration of 10 nM and

400 nM respectively. Sequences of primers used for real-time PCRs are listed in Table 4-1.

**Statistical Analysis**

Tissues isolated from one mouse represents N = 1. The appropriate analysis of variance (ANOVA) was performed for each data set and individual means were compared using Fisher's protected least significant difference test with $P \leq 0.05$ being considered indicative of a statistically significant difference between mean values.

**Results**

Male KO mice appeared normal at birth and exhibited normal ambulatory activity as previously described [136]. To assess general phenotypic features of KO mice, we measured age-related differences in weight (Table 4-2). There were no significant differences in weight between male KO and WT mice at 2 months; however, KO mice did not gain weight after 2 months of age. KO mice were ~55% the weight of WT mice at 13 months. KO mice at 13 months of age began to show kyphosis and reduced ambulatory activity. These findings are consistent with previous reports [136, 141].

| | 2 months | | 13 months | |
|---|---|---|---|---|
| | WT | KO | WT | KO |
| Weight (g) | 21 ± 1 | 20 ± 1 | 47 ± 1 | 23 ± 1* |
| Serum Creatinine (mg/dl) | 0.32 ± 0.1 | 0.36 ± 0.1 | 0.33 ± 0.1 | 0.37 ± 0.1 |
| Urine Volume (ml/24 hr)/kg | 90 ± 25 | 78 ± 11 | 20 ± 1 | 21 ± 1 |
| Urine Creatinine (mg/ml)/kg | 675 ± 112 | 595 ± 85 | 815 ± 145 | 940 ± 151 |
| Creatinine Clearance (ml/min)/kg | 2.8 ± 0.8 | 2.0 ± 0.6 | 2.0 ± 0.6 | 1.7 ± 0.5 |

**Table 4-2. General age-related phenotypic features and kidney function of iPLA2γ -/- mice** Weight and serum creatinine were measured. Mice were placed in metabolic cages for 24 hrs and urine volume and urinary creatinine were measured and corrected for weight. Creatinine clearance was calculated. Values are means ± SE in the units designated. Means highlighted with an asterisk denotes mean of KO animals is significantly different from mean of WT animals within the age group (N=4-8) $p<0.05$.

To assess the effects of genetic ablation of $iPLA_2\gamma$ on kidney function, we measured serum and urine creatinine, urine volume and calculated creatinine clearance. There were no significant differences in these parameters between WT and KO animals at 2 or 13 months when standardized to body weight (Table 4-2). In summary, KO mice did not display overt changes in renal function.

Kidney histology was evaluated for tubular necrosis, loss of brush border, casts, inflammatory cells, tubular dilatation, distal tubule damage, degeneration, red blood cell extravasation, interstitial edema, glomerular changes, and interstitial fibrotic foci. Kidney cortex from 2 month old KO mice exhibited tubular degeneration and loss of

brush border compared to 2 month WT controls (Fig. 4-1, Table 4-3). Kidney tissues from 13 month WT controls exhibited increased markers of the aging kidney (i.e. loss of brush border, tubular dilatation and degeneration, glomerular changes, and interstitial fibrotic foci). KO mice exhibited similar age-related histological changes except tubular dilatation was decreased in 13 month iPLA$_2\gamma$ KO animals compared to 13 month WT controls. In summary, while genetic ablation of iPLA$_2\gamma$ resulted in some changes of kidney morphology at 2 months of age compared to WT mice, kidney morphology at 13 months of age was not markedly different between KO and WT mice.

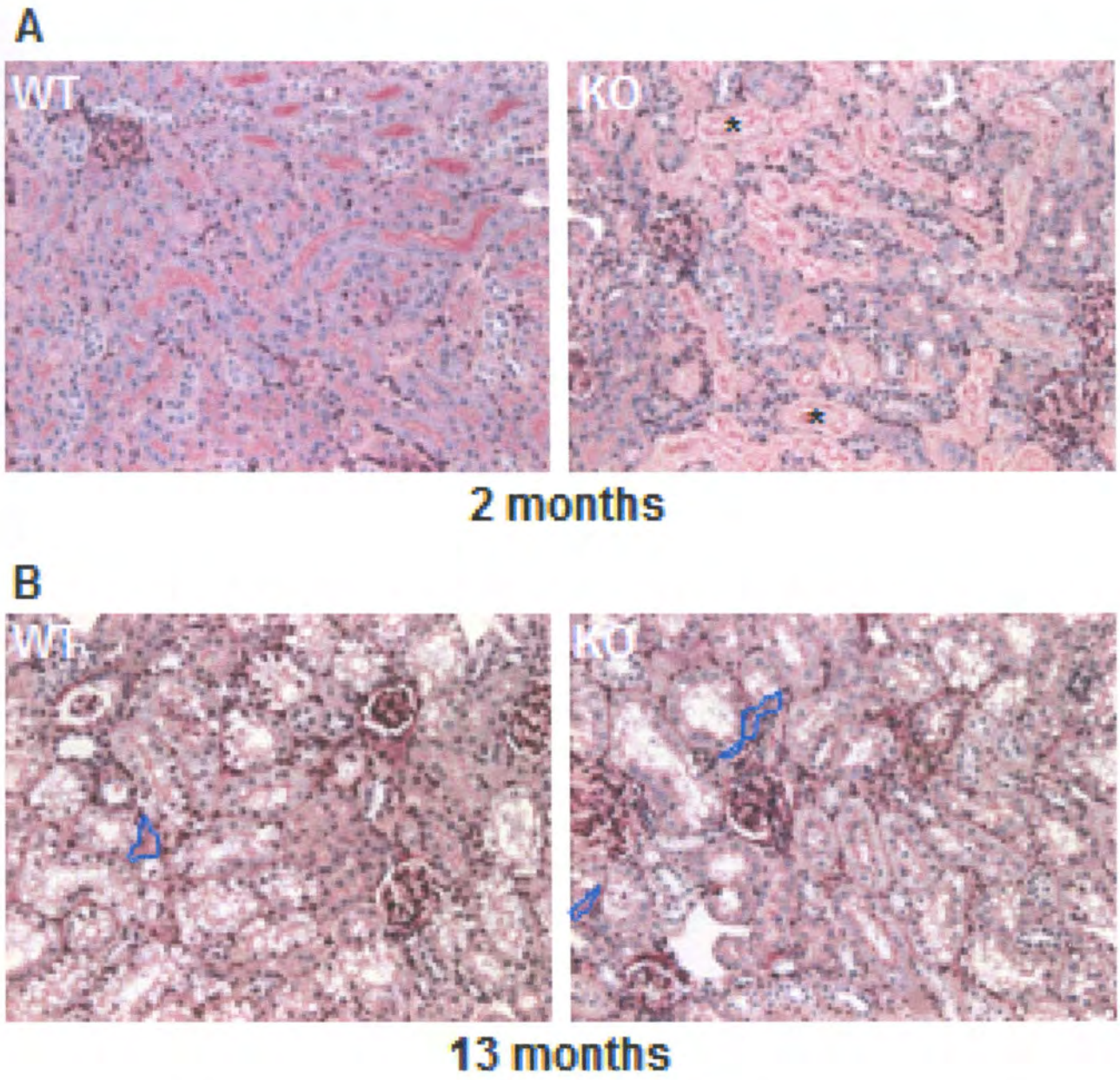


**Figure 4-1. Effects of iPLA$_2\gamma$ -/- ablation and aging on mice kidney histology.** Periodic Acid/Schiff reagent (PAS) stained sections of 2 and 13 month old iPLA$_2\gamma$ KO and WT mouse kidney at 40X magnification. Tubules highlighted with an asterisk exhibit loss of brush border and tubular degeneration. Regions outlined in blue exhibit interstitial fibrotic foci.

| | 2 months | | 13 months | |
|---|---|---|---|---|
| | WT | KO | WT | KO |
| Tubular Necrosis | 0 ± 0 | 1.3 ± 0.8 | 0 ± 0 | 0 ± 0 |
| Loss of Brush Border | 0.2 ± 0.2 | 2.5 ± 0.5* | 3.3 ± 0.2 | 3.0 ± 0.4 |
| Casts | 0 ± 0 | 1.3 ± 0.8 | 1.5 ± 0.2 | 0.8 ± 0.2 |
| Inflammatory Cells | 1.0 ± 0.5 | 2.2 ± 0.5 | 2.5 ± 0.2 | 2.5 ± 0.3 |
| Tubular Dilatation | 0 ± 0 | 0.7 ± 0.5 | 2.0 ± 0.3 | 0.6 ± 0.4* |
| Distal Damage | 0 ± 0 | 1.1 ± 0.7 | 0.2 ± 0.2 | 0.4 ± 0.2 |
| Degeneration | 0.5 ± 0.5 | 2.3 ± 0.6* | 3.5 ± 0.2 | 3.0 ± 0.2 |
| Red Blood Cell Extravazation | 1.0 ± 0.4 | 2.5 ± 0.4 | 1.5 ± 0.2 | 1.8 ± 0.5 |
| Interstitial Edema | 0 ± 0 | 0.2 ± 0.2 | 0 ± 0 | 0 ± 0 |
| Glomerular Changes | 0 ± 0 | 0 ± 0 | 2.3 ± 0.2 | 2.4 ± 0.2 |
| Interstitial Fibrotic Foci | 0 ± 0 | 0 ± 0 | 1.9 ± 0.2 | 1.6 ± 0.2 |

**Table 4-3. iPLA2γ -/- mice kidney histology and aging.** Histological sections of 2 and 13 month $iPLA_2\gamma$ KO and WT mouse kidney sections were stained with hematoxylin/eosin or PAS and scored in a blinded fashion by a renal pathologist. Morphological damage in 10-12 fields per section were quantified using the following scale: none= 0; <10%= 1; 11-25%= 2; 26-75%= 3; and 75%= 4. Values are mean scores ± SE. Means highlighted with an asterisk denotes mean of KO animals is significantly different from mean of WT animals within the age group.

To investigate the effects of genetic ablation of $iPLA_2\gamma$ on oxidant injury *in vivo*, we measured urinary 8-isoprostanes and 8-hydroxy-2'-deoxyguanosine (8-OHdG), biomarkers of lipid peroxidation and oxidative DNA damage, respectively. Because there was no change in serum creatinine, and as creatinine excretion correlated with weight, we normalized the data to urinary creatinine concentration within each sample. There were no differences in urinary 8-isoprostanes or 8-OHdG concentrations in KO and WT mice at 2 months of age (Fig. 4-2). However, 13 month KO mice excreted 9-fold higher 8-isoprostane and 2-fold higher 8-OHdG compared to 13 month WT mice. In

summary, genetic ablation of iPLA$_2\gamma$ increased markers of lipid peroxidation and oxidative DNA damage in the urine.

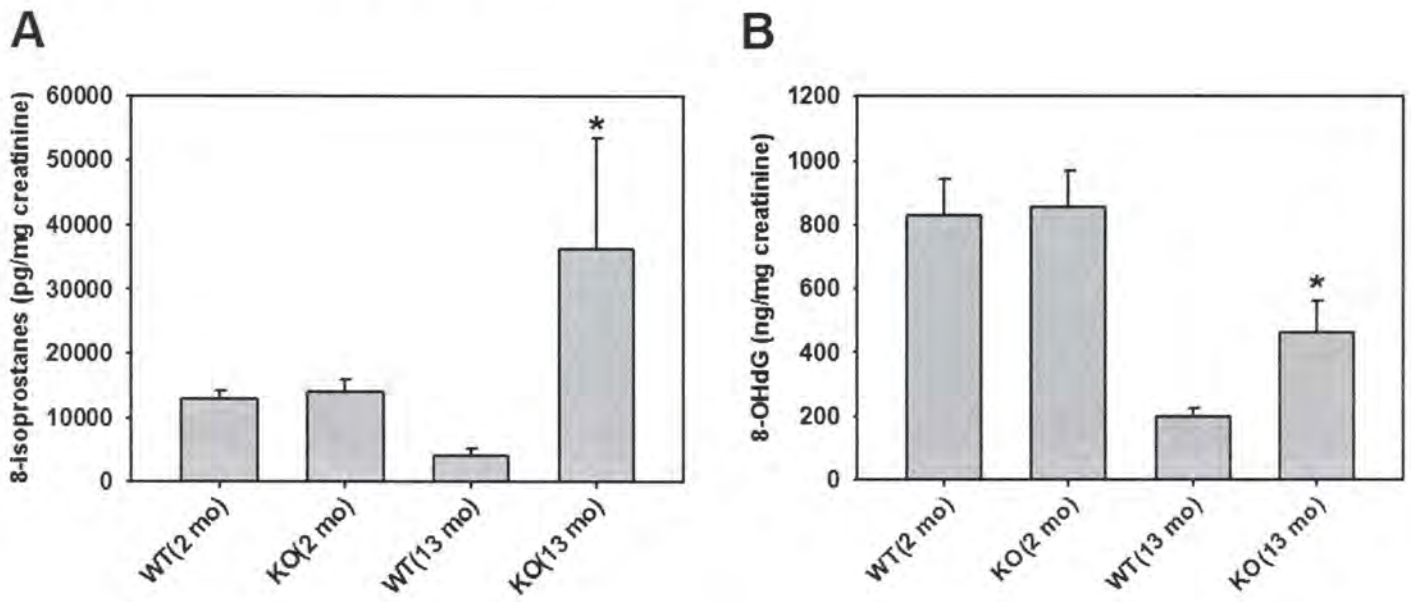


**Figure 4-2. Increased urinary markers of oxidative stress and oxidative DNA damage in aged iPLA$_2\gamma$ -/- mice.** Urine was collected for 24 hr from 2 and 13 month old male iPLA$_2\gamma$ KO and WT mice. Urinary 8-isoprostanes **(A)** and 8-OHdG **(B)**, markers of oxidative stress and oxidative DNA damage respectively, were quantified using an ELISA assay kit and normalized to urine creatinine. Values are mean (pg/mg creatinine) ± SE for 8-isoprostanes and mean (ng/mg creatinine) ± SE for 8-OHdG. Means highlighted with an asterisk denotes that the mean of KO animals is significantly different from the mean of WT animals within the age group (N=3-7, $p< 0.05$).

To assess kidney specific oxidative DNA damage, we stained the kidney tissue for 8-OHdG using immunohistochemistry. There was a 2-fold increase in 8-OHdG staining in KO mice at 2 and 13 months compared to WT age-matched control animals (Fig. 4-3A and B, and Fig. 4-4). Interestingly, 8-OHdG staining was more pronounced in the cortex and proximal tubules with little evidence of 8-OHdG staining in glomeruli.

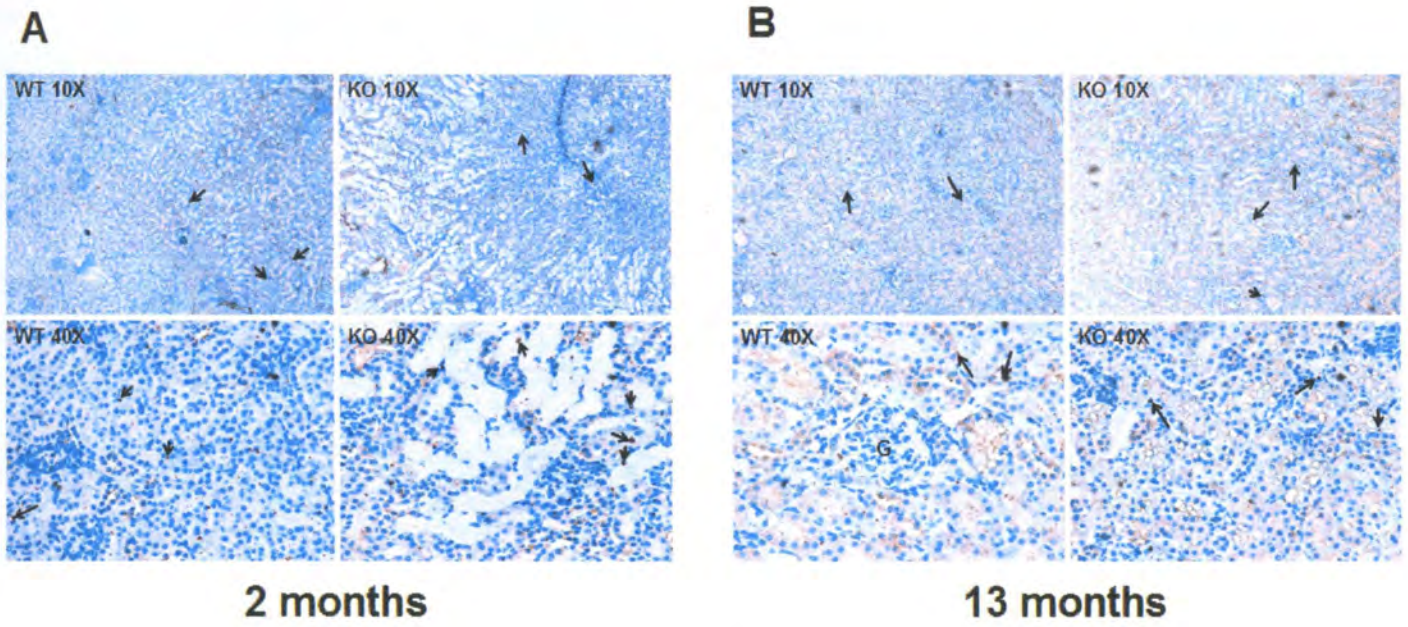


**Figure 4-3. Kidney specific oxidant injury in iPLA$_2\gamma$ -/- mouse kidney cortex.** *Increased oxidative DNA damage.* Immunohistochemistry using an antibody specific to 8-hydroxy-2'-deoxyguanosine (8-OHdG) was performed on sections of 2 month old **(A)** and 13 month old **(B)** iPLA$_2\gamma$ WT and KO mouse kidney cortex. "G" denotes glomeruli and arrows point to 8-OHdG stained nuclei. Note: nuclei stained for 8-OHdG are present mostly in proximal tubule segments and not in glomeruli.

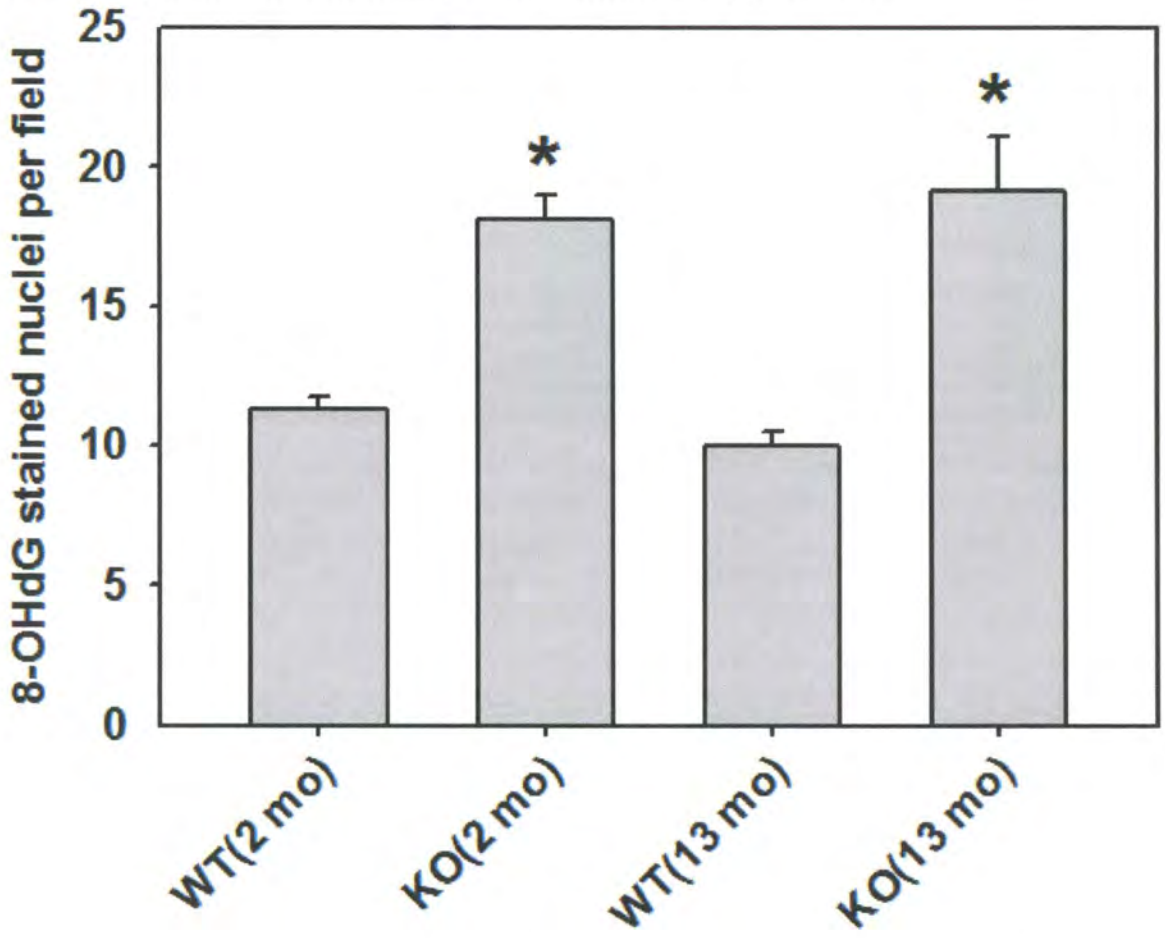


**Figure 4-4. Quantification of nuclei stained for 8-OHdG**. Darkly stained nuclei were counted per field in a double-blinded fashion on sections of 2 and 13 month iPLA$_2\gamma$ WT

and KO mouse kidney cortex. Data are expressed as stained nuclei per field (25X) and are presented as means ± SEM.

We measured thiobarbituric acid reacting species (TBARS), a marker of lipid peroxidation, in mouse kidney cortex. There were no differences in TBARS formation in KO and WT kidney cortex at 2 months of age. However, kidney cortex of 13 month iPLA$_2\gamma$ KO mice exhibited 1.7-fold higher TBARS content than 13 month WT controls (Fig. 4-5).

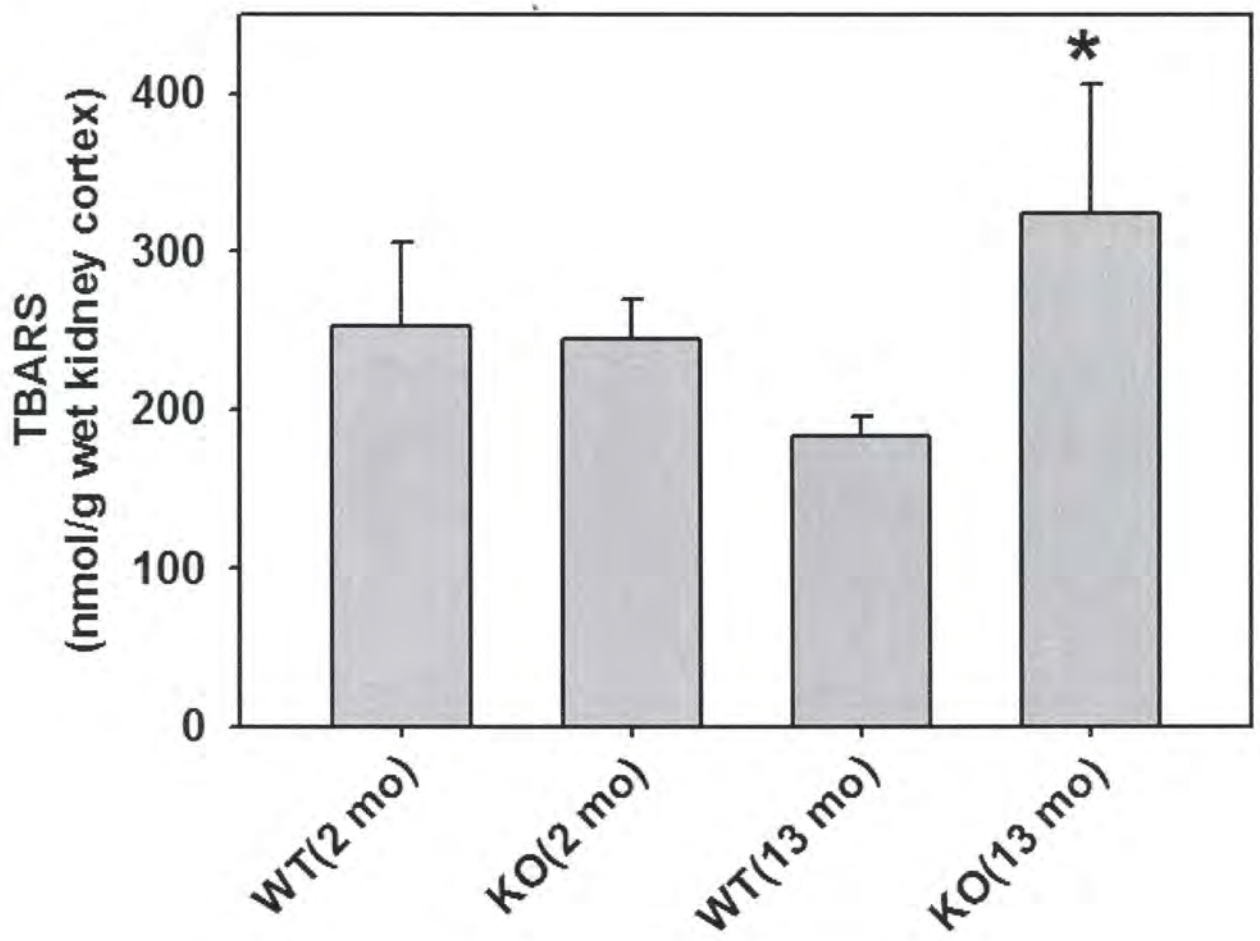


**Figure 4-5. Increased lipid peroxidation (TBARS).** Kidney cortex of 2 and 13 month male iPLA$_2\gamma$ WT and KO mice were isolated and thiobarbituric acid reacting species (TBARS) were measured as described in Materials and Methods section. Data (nmol/g wet kidney cortex) are presented as mean ± SEM. Means highlighted with an asterisk denotes that the mean of KO animals is significantly different from the mean of WT animals within the age group.

To assess the effects of genetic ablation of iPLA$_2\gamma$ on lipid homeostasis, we performed lipidomic analysis of urine from 13 month old WT and KO mice using ESI-MS/MS. The intensities of phospholipid species with *m/z* values of 790.6, 792.5 and 794.4 were decreased in KO mice compared to WT controls and were identified as 38:6, 38:5 and 37:5 phosphatidylcholine, respectively (Fig. 4-6). Analysis of urine fatty acid using ESI-MS revealed no changes in palmitic, linoleic, stearic or arachidonic acid between 13 month WT and KO mice urine (data not shown). However, there were significant increases in intensities at *m/z* values of 128.7, 143.7 and 178.4 in KO mice urine compared to WT controls (Fig. 4-6). Analysis using Lipid Maps (www.lipidmaps.org) and subsequent MS (ESI-MS/MS) suggested that these species are fatty acids contain 6-10 carbons with methyl or keto additions. In summary, genetic ablation of iPLA$_2\gamma$ decreased phosphatidylcholine species and increased fatty acids with methyl or keto additions in mouse urine.

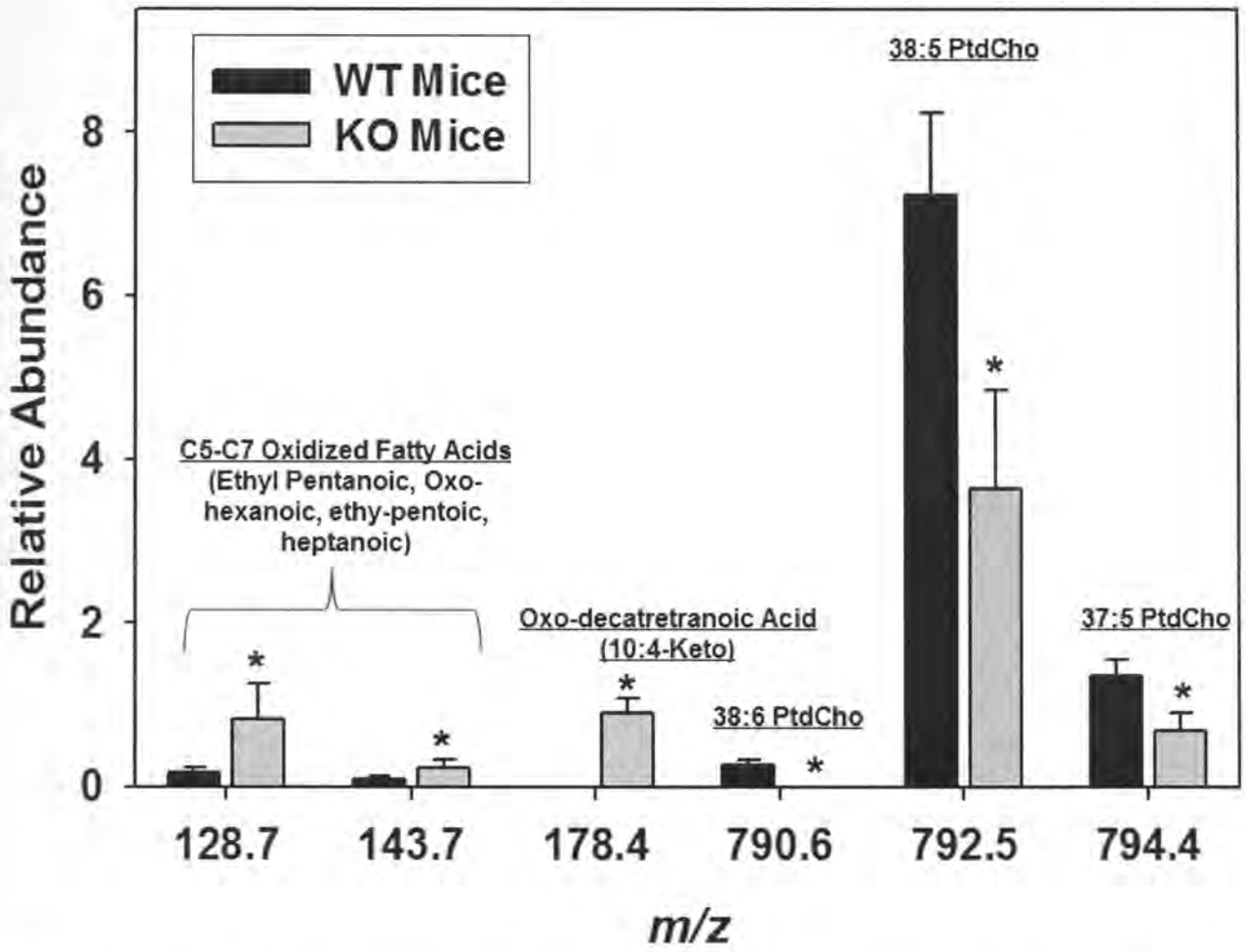


**Figure 4-6. Effect of genetic ablation of iPLA$_2\gamma$ on phospholipid and fatty acid homeostasis in mice urine.** Urine was collected for 24 hr from 13 month old male iPLA$_2\gamma$ KO and WT mice and analyzed for phospholipids and fatty acids using ESI-MS. Data are normalized to total ion count and *m/z* are those identified in the negative (128.7, 147.7 and 178.4) and positive (790.6, 792.5 and 794.4) modes. The identities for these lipids are indicated in the graph and are based on theoretical m/z value in Lipid Maps (www.lipidmaps.org) and subsequent MS/MS analysis. Data are presented as the means ± SD of 3-6 separate mice and means highlighted with an asterisk denotes a significant difference from WT animals.

To assess the effect of genetic ablation of iPLA$_2\gamma$ on mitochondrial respiratory enzymes, we measured protein levels of NDUFB8 (Complex I), COX-1 (Complex IV), and ATP synthase β (Complex V) of the electron transport chain (ETC). ATP Synthase β and NDUFB8 are nuclear encoded, while COX-1 is mitochondrial encoded. There was a 1.5-fold increase in NDUFB8 protein expression in KO mice kidney cortex in 2 and 13 month animals compared to 2 month WT controls (Fig. 4-7A and B). COX-1 protein

expression increased by 50% in KO mice kidney cortex at 2 months compared to controls and trended to increase at 13 months. In contrast, ATP synthase β protein expression decreased by ~50% in 2 month KO animals compared to 2 month controls, but returned to control levels at 13 months. In summary, genetic ablation of $iPLA_2\gamma$ increased the expression of NDUFB8 (Complex I) and COX-1 (Complex IV), but not ATP synthase β (Complex V).

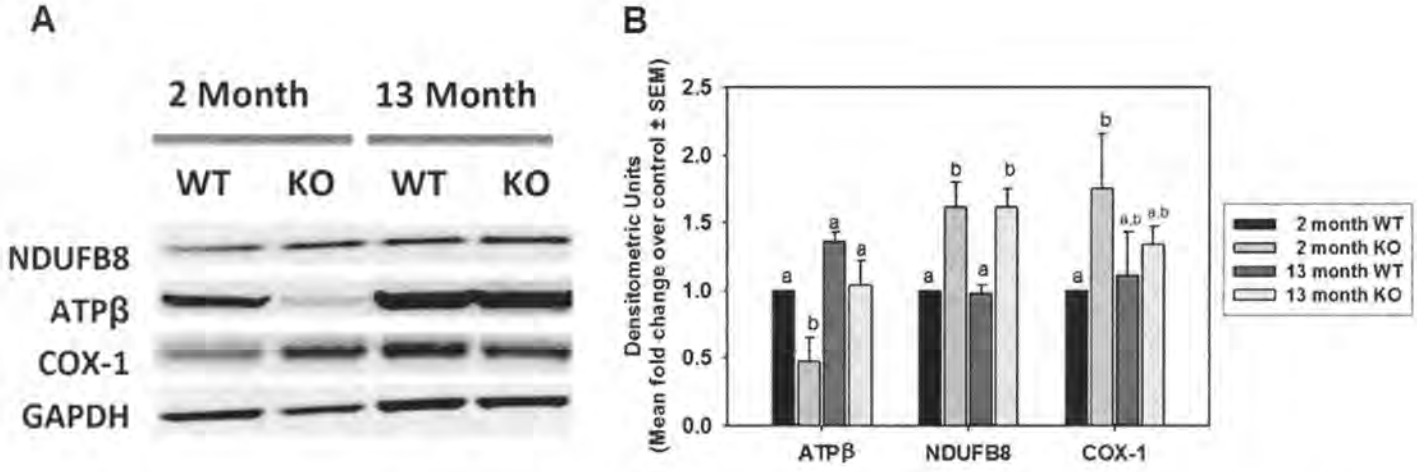


**Figure 4-7. Effect of genetic ablation of $iPLA_2\gamma$ on mitochondrial respiratory proteins in 2 and 13 month old mice kidneys. (A)** Expression of mitochondrial respiratory proteins (NDUFB8, COX-1, and ATP Synthase β) in kidney cortex of 2 and 13 months old male $iPLA_2\gamma$ KO and WT mice was examined by immunoblot analysis (representative). **(B)** Data were normalized by GAPDH protein expression (internal control) and presented as mean ± SEM fold change over control (2 month WT animals). Bars with different superscripts are significantly different from each other (N = 3-7, $p<0.05$).

Oxidative stress and subsequent loss of mitochondrial function, reduced mitochondrial efficiency, and increased mitochondrial DNA (mtDNA) damage and mutation are believed to be major components of aging [165]. We used real-time PCR to assess the effect of genetic ablation of $iPLA_2\gamma$ and aging on kidney cortex mtDNA copy number. Mitochondrial copy number increased with age and KO mice exhibited greater

mitochondrial copy numbers than WT mice at 2 month; this trend was sustained at 13 months (Fig. 4-8).

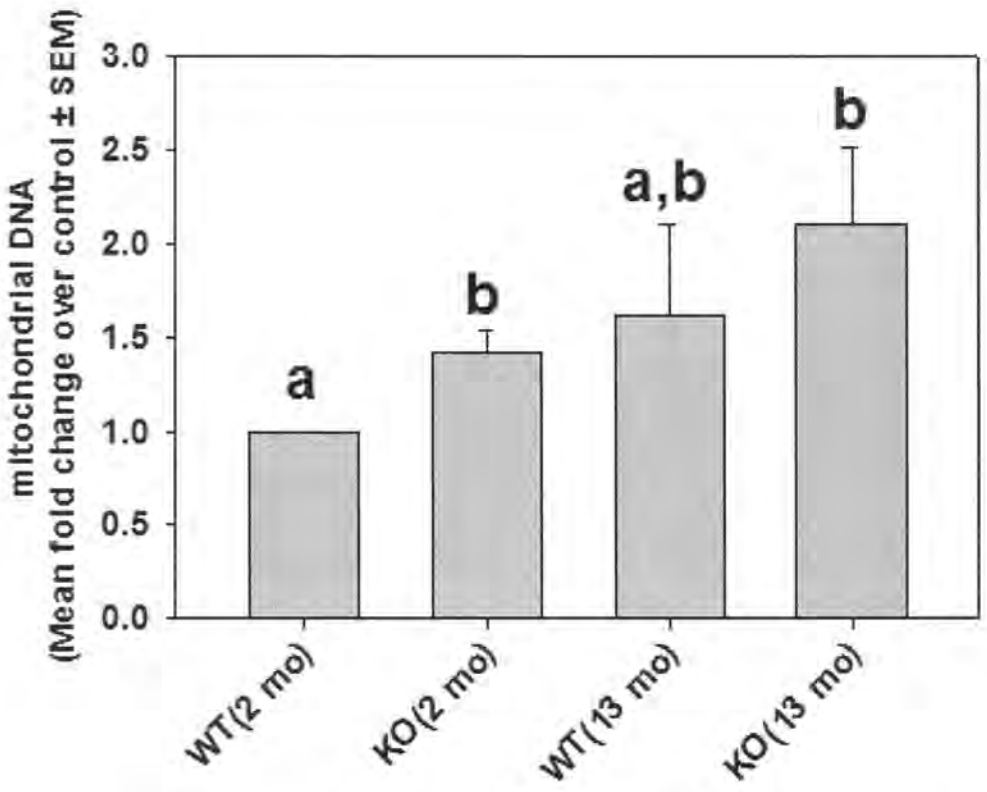


**Figure 4-8. Increased mitochondrial copy number in aged iPLA$_2\gamma$ -/- mice kidney cortex.** DNA was isolated from kidney cortex of 2 and 13 month old male iPLA$_2\gamma$ KO and WT mice and analyzed by real-time PCR for relative quantities of mitochondrial-encoded ND6 gene and normalized to nuclear-encoded tubulin gene. Data are presented as the means ± SEM fold change over control (2 month WT animals). Bars with different superscripts are significantly different from each other (N = 3-7, $p<0.05$).

Upregulation of antioxidant enzyme stress response pathways are believed to be a compensatory mechanism by which cellular systems maintain function and viability during aging and increased oxidant stress, and mRNA levels of antioxidant enzymes are markers of oxidant stress response in the kidney [166-168]. Glutathione peroxidase 4 (GPx4), a phospholipid hydroperoxidase, and peroxiredoxin 6 (Prdx6), a member of thiol-specific antioxidant enzyme family with both glutathione peroxidase and

phospholipase $A_2$ activity, are antioxidant enzymes that reduce lipid hydroperoxides and are thought to play a role in lipid peroxidation-induced oxidant stress response and regulation of phospholipid turnover [169-171]. Glutathione reductase 1 (GR1) converts oxidized glutathione to glutathione but does not have lipid hydroperoxidase activity [172]. To assess the antioxidant enzyme stress response following iPLA$_2\gamma$ ablation, we measured mRNA expression of these enzymes in WT and KO animals at 2 and 13 months of age using real-time PCR (Fig. 4-9). There was a 3-fold increase in GPx4 mRNA expression in 2 month iPLA$_2\gamma$ KO mice compared to 2 month control animals (Fig. 4-9A). At 13 months, there was a 2-fold increase in both KO and WT mice GPx4 mRNA expression compared to 2 month WT controls. Conversely, Prdx6 mRNA expression decreased by 60% in 2 month KO mice compared to 2 month controls (Fig. 4-9B). There were no differences in Prdx6 mRNA levels between 13 month KO and control mice, and these levels were similar to those observed in 2 month controls. There were no differences in GR1 mRNA levels between KO and WT mice at either age (Fig. 4-9C). In summary, genetic ablation of iPLA$_2\gamma$ resulted in a compensatory increase in GPx-4 and a decrease in Prdx6 at 2 months of age, but no changes in GR1 mRNA expression.

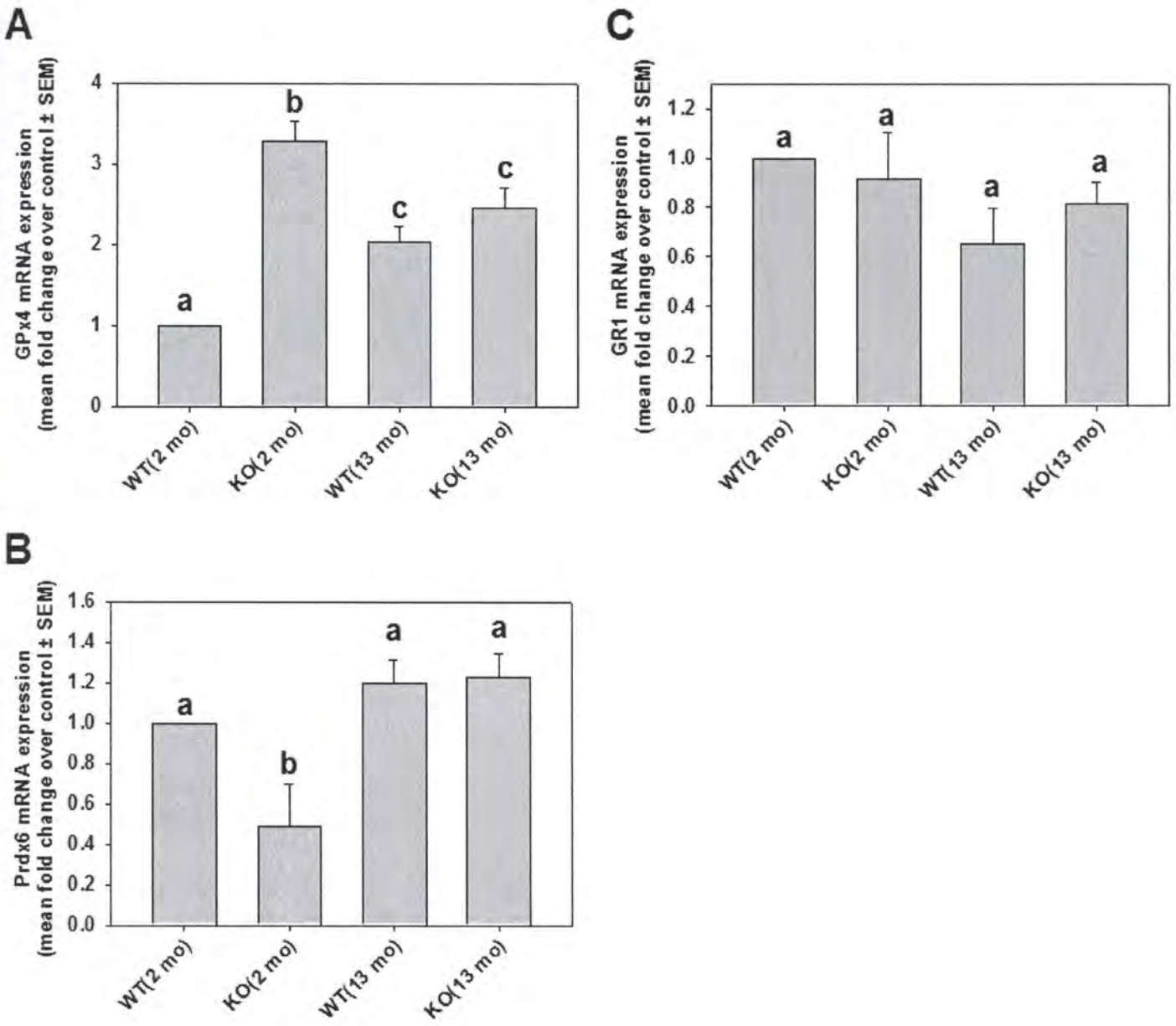


**Figure 4-9. Effect of genetic ablation of iPLA$_2\gamma$ on antioxidant stress response proteins mRNA expression in 2 and 13 month old mice kidney cortex.** mRNA was isolated from 2 and 13 month old male iPLA$_2\gamma$ KO and WT mice kidney cortex and analyzed by real-time PCR for relative quantities of **(A)** Glutathione Peroxidase 4 (GPx4), **(B)** Peroxiredoxin 6 (Prdx6) and **(C)** Glutathione Reduction 1 (GR1). Data were normalized to tubulin mRNA expression (internal control) and presented as mean ± SEM fold change over control (2 month WT animals). Bars with different superscripts are significantly different from each other (N = 3-7, $p<0.05$).

## Discussion

We previously demonstrated in primary cultures of renal cells that pharmacological inhibition of iPLA$_2\gamma$ potentiated oxidant-induced lipid peroxidation, ER $Ca^{2+}$ release,

mitochondrial permeability transition, and renal cell death [68, 97-98, 161]. Genetic ablation of iPLA$_2\gamma$ using shRNA resulted in increased lipid peroxidation, loss of cell viability, and increased vulnerability to oxidant stress in renal cells [116]. These studies revealed the protective role of iPLA$_2\gamma$ in renal cells and implicated the enzyme in putative membrane remodeling/repair pathways.

Mancuso et al. showed increased susceptibility to cardiac stress, cognitive dysfunction, mitochondrial dysfunction (heart, brain, and skeletal muscle) and loss of lipid homeostasis in mice null for iPLA$_2\gamma$, and Yoda et al. showed increased lipid peroxidation, loss of lipid homeostasis, mitochondrial dysfunction, and induction of oxidant-stress related proteins in skeletal muscle [134-136, 141]. Together, these findings support our previous data revealing iPLA$_2\gamma$ as a protective enzyme of oxidative stress, and provide evidence that impairment of iPLA$_2\gamma$ *in vivo* results in increased oxidant stress, mitochondrial dysfunction, and organ dysfunction. Because oxidant injury is a major component of age-related loss of kidney function, the goal of the present study was to elucidate the role of iPLA$_2\gamma$ in age-related renal oxidant injury.

To determine if genetic ablation of iPLA$_2\gamma$ resulted in age-related loss of kidney function, several parameters of kidney function were monitored, including serum creatinine concentration and urinary creatinine clearance. Genetic ablation of iPLA$_2\gamma$ was not sufficient to decrease these clinical markers of kidney function. However, creatinine measurements have inherent limitations in measuring kidney function and more sensitive

measures of kidney function have long-been sought [173]. Urinary NGAL, although a more sensitive measurement of acute kidney injury [174], is not an effective marker of chronic kidney injury or impairment [175], and there were no age or phenotype related changes in urinary NGAL excretion (data not shown). However, the absence of increased NGAL excretion should be interpreted cautiously [176].

Despite no changes in clinical markers of kidney function in young and aged mice, kidney histology in 2 month old mice exhibited loss of brush border and tubular degeneration. These findings are suggestive of tubular dysfunction in 2 month old iPLA$_2\gamma$ ablated mice that is not sufficient to overcome the reserve capacity of the kidney. Similarly, greater than a 50% loss of function of kidney cortical tissue is often necessary to lead to clinical markers of kidney dysfunction in humans, such as increased serum creatinine [173]. Interestingly, there were no remarkable differences in gross histology between KO and WT animals at 13 months, which suggests a compensatory response and recovery of tubular structure. Similarly, genetic ablation of iPLA$_2\gamma$ in the brain also showed no differences between KO and WT animals in H&E staining in aged animals, but immunohistochemistry revealed small ubiquitin-positive inclusions suggesting pathology.

Our *in vitro* studies using renal cells revealed that iPLA$_2\gamma$ loss results in oxidant injury (5-10). Here, we show that genetic ablation of iPLA$_2\gamma$ results in kidney oxidant stress *in vivo*. Lipid metabolites in the blood and urine, such as 8-isoprostanes, are markers of oxidative stress [177] and excretion of 8-isoprostanes was increased in aged iPLA$_2\gamma$ KO

animals. 8-isoprostane is a prostaglandin-$F_2$-like compound produced by free radical-catalyzed peroxidation of arachidonic acid *in vivo.* Additionally, iPLA$_2\gamma$ KO animals exhibited increased kidney cortex lipid peroxidation as measured by TBARS assay, revealing kidney specific oxidant injury. To our knowledge, these data are the first to reveal genetic ablation of iPLA$_2\gamma$ results in kidney lipid peroxidation *in vivo.*

To further characterize iPLA$_2\gamma$-induced oxidant injury in the kidney, we stained for 8-OHdG. 8-OHdG is a marker of oxidative DNA damage and oxidative stress and can be measured in serum, urine, and tissue [112, 178]. Unbound 8-OH dG is freely filtered by the kidney and accumulates in the urine. Organs with limited cell turnover, such as kidney, heart, brain, and liver, accumulate 8-OHdG with oxidant injury, and 8-OHdG in the urine is proportional to 8-OHdG levels in the tissues and reflects multi-organ oxidative DNA damage. The increase in 8-OHdG excretion in aged iPLA$_2\gamma$ KO animals suggests increased oxidant injury. This hypothesis is supported by the increase in 8-OHdG staining in the kidney cortex of aged iPLA$_2\gamma$ KO animals. These data reveal that genetic ablation of iPLA$_2\gamma$ results in both lipid peroxidation and oxidative DNA damage in mouse kidney cortex.

Our *in vitro* studies in renal cells revealed that iPLA$_2\gamma$ mediates fatty acid release and maintenance of phospholipid homeostasis during oxidative stress [113, 116, 161]. In this study, we measured urinary levels of phospholipids and fatty acids. While few phospholipid species were identified in mouse urine, phospholipid species (38:6, 38:5

and 37:5 phosphatidylcholine) were decreased in iPLA$_2\gamma$ KO animals compared to controls. These data provide evidence that these phospholipids may be the downstream targets of iPLA$_2\gamma$ ablation-induced oxidative stress, substrates of iPLA$_2\gamma$ activity, and/or are the result of iPLA$_2\gamma$-mediated phospholipid repair. Similarly, our previous studies revealed that iPLA$_2\gamma$ knockdown increased only a few phospholipids (one phosphatidylcholine) in renal cells out of the 267 *m/z* values studied [116], and inhibition of iPLA$_2\gamma$ in isolated mitochondrial and ER prevented the release of plasmenylcholine and phosphatidylcholine substrates [98].

The 6-10 carbon fatty acids with methyl or keto additions, increased in iPLA$_2\gamma$ KO animals, likely represent lipid peroxides or oxidized fatty acids. This finding agrees with our previous studies in microsomes, which showed that oxidant stress increased the release of unsaturated and/or oxidized fatty acids and iPLA$_2\gamma$ mediated their release [161]. These findings provide strong evidence that genetic ablation of iPLA$_2\gamma$ leads to alterations in fatty acid and phospholipid homeostasis. Together, these findings, along with increased urinary 8-isoprostanes and increased TBARS content in kidney cortex of iPLA$_2\gamma$ KO animals, provide evidence that genetic ablation of iPLA$_2\gamma$ results in lipid peroxidation *in vivo* in the kidney.

Mitochondria are both producers and targets of oxidative stress. Protein analysis revealed that iPLA$_2\gamma$ ablation induced changes in renal mitochondrial respiratory proteins (ATP synthase β, NDUFB8, and COX1). These changes likely reflect a compensatory

response to oxidative stress to maintain cell and tissue viability. NDUFB8 and COX-1 are components of Complex I and IV, respectively, and oxidant-induced dysfunction of these enzymes can result in electron leak leading to the formation of superoxide radicals and further ROS production [179-180]. In contrast, ATP synthase β (Complex V) couples $O_2$ consumption by the electron transport chain with ADP phosphorylation [179]. Interestingly, both NDUFB8 and COX-1 proteins and mtDNA copy number are increased, or trend to increase, in iPLA$_2$γ KO mice compared to control animals. Increased NDUFB8, COX-1, and mtDNA copy number, may reflect a compensatory increase in mitochondrial number and/or recovery of function necessary to maintain cell and tissue viability[165].

In contrast to NDUFB8 and COX-1, ATP synthase β protein expression decreased in 2 month KO mice, but recovered at 13 months in KO animals. The reason for this decrease at 2 months is not clear. It may be the result of direct damage, or a compensatory response to reduce ATP production in the presence of increased NDUFB8, COX-1 and mtDNA. Mancuso et al. demonstrated inefficient Complex IV $O_2$ reduction suggesting mitochondrial dysfunction in cardiac mitochondria of 4-6 month old KO animals, supporting this hypothesis. Return of ATP synthase β protein levels and sustained increases in Complex I and IV enzymes in 13 month KO animals is suggestive of an adequate compensatory response to maintain ATP production capacity and therefore tissue viability. Regardless, these findings provide strong evidence that iPLA$_2$γ ablation-induced oxidant injury disrupts electron transport chain complexes and results in a compensatory response.

Several other compensatory pathways are required to maintain cellular viability under oxidant stress such as the upregulation of antioxidant enzyme stress response pathways [166]. The increase in GPx4 mRNA in iPLA$_2\gamma$ KO mice supports the conclusion that genetic ablation of iPLA$_2\gamma$ induces a compensatory response in antioxidant enzymes. GPx4 is responsible for the majority of lipid hydroperoxidase activity in mammalian cells at physiological pH [166]. It is interesting that mRNA for this gene increased in correlation with increases in 8-isoprostanes and oxidized lipids.

In contrast to GPx4, level of Prdx6 decreased in KO mice at 2 months. Prdx6, has both lipid hydroperoxidase activity and phospholipase $A_2$ activity, but the hydroperoxidase activity is 40-fold greater than its phospholipase activity at physiological pH [169-171]. Other studies revealed that Prdx6 is regulated by ERK and p38 pathways and these pathways are also implicated in iPLA$_2$ regulation as demonstrated by an upregulation of both iPLA$_2$ and Prdx6 with PMA treatment and, conversely, knockdown of iPLA$_2$ increased MAPK activation [181-182]. Our data suggests that common signaling pathways may exist between Prdx6 and iPLA$_2\gamma$ and these findings should be further explored.

These data showing genetic ablation of iPLA$_2\gamma$ does not effect GR1 mRNA expression but alters the expression of GPx4 and Prdx6, supports the hypothesis that iPLA$_2\gamma$ ablation induced lipid peroxidation and not an overall increase in redox cycling under these

conditions. Similarly, Yoda et al. reported increased MDA content and the induction of antioxidant enzymes in the skeletal muscle of mice genetically ablated of iPLA$_2\gamma$.

These data reveal that genetic ablation of iPLA$_2\gamma$ results in oxidant injury (lipid peroxidation, oxidative DNA damage) that coincides with a disruption of mitochondrial respiratory protein expression and loss of lipid homeostasis in the kidney. Additionally, these studies reveal that genetic ablation of iPLA$_2\gamma$ induces compensatory responses to oxidative stress, such as increased mtDNA, modulation of mitochondrial respiratory proteins, and upregulation of oxidant stress response pathways. Despite the increase in oxidative stress in the kidney, iPLA$_2\gamma$ ablation-associated oxidant injury does not appear to be great enough to overcome kidney reserve and regenerative capacity as iPLA$_2\gamma$ ablated mice do not exhibit greater loss of kidney function at 13 months of age. It should be pointed out that further studies are needed in older mice to fully assess the effect of iPLA$_2\gamma$ ablation on aging and oxidative stress. Interestingly, Mancuso *et al.* showed that ablation of iPLA$_2\gamma$ alone was not sufficient to cause cardiac dysfunction, but a subsequent insult, transverse aortic constriction, revealed cardiac dysfunction in iPLA$_2\gamma$ KO mice [136]. Similarly, age-associated changes in kidney structure and function are not always sufficient to cause kidney dysfunction, but it is believed that these changes make the kidney more vulnerable to subsequent insults (ie. ischemia/reperfusion-, drug-, and toxicant injury) [183-184]. A subsequent kidney insult, such as ischemia/reperfusion or toxicant injury, may reveal kidney dysfunction in KO mice.

# Chapter 5

# Conclusions and Future Directions

## Conclusions

In conclusion, acute kidney injury and chronic kidney disease are becoming more prevalent and have high morbidity and mortality that have been unchanged for many years. Current therapeutics targeted towards preventing or treating kidney injury and disease have been unsuccessful. Calcium-independent phospholipase $A_2\gamma$ ($iPLA_2\gamma$) is one of seven $Ca^{2+}$-independent $PLA_2$ enzymes and represents a potential therapeutic target in kidney disease [81]. Our studies in renal cells showed that $iPLA_2\gamma$ has a unique subcellular localization in that its expression and activity were found in both the endoplasmic reticulum (ER) and the mitochondria, while $iPLA_2\beta$ activity was not present [68, 97-98]. We also determined that $iPLA_2\gamma$ has divergent roles in cell injury and death, which may be explained by unique roles and functions within subcellular compartments [81]. Specifically, $iPLA_2\gamma$ is protective during oxidant-induced necrotic cell death, but seems to mediate apoptosis-induced cell death. Additionally, $iPLA_2\gamma$ in mitochondria plays a protective role during oxidant-induced lipid peroxidation and subsequent mitochondrial swelling, but seems to mediate $Ca^{2+}$ induced mitochondrial swelling via arachidonic acid signaling. Unfortunately, lack of organelle specific inhibitors of $iPLA_2\gamma$

limited studies to isolated organelles and studies in RPTC were not able to distinguish the respective contributions of ER- and mitochondrial- iPLA$_2\gamma$. However, recent studies in our laboratory using iPLA$_2\gamma$-specific shRNA to decrease iPLA$_2\gamma$ activity and expression in RPTC decreased ER- iPLA$_2\gamma$ prior to mitochondrial- iPLA$_2\gamma$. These studies confirmed role of iPLA$_2\gamma$ in preventing lipid peroxidation and preserving mitochondrial function and viability under basal conditions [116]. More importantly, while the loss of mitochondrial iPLA$_2\gamma$ was correlated with decreased mitochondrial uncoupled respiration, these studies pointed to ER- iPLA$_2\gamma$ in the lipid peroxidation repair/prevention pathway because knockdown of ER- iPLA$_2\gamma$, and not mitochondrial- iPLA$_2\gamma$, was correlated with increased lipid peroxidation. However, no studies have elucidated the role of iPLA$_2\gamma$ in the ER nor has the mechanism by which iPLA$_2\gamma$ preserves phospholipid homeostasis been determined. The goals of these studies were to elucidate the role of ER- iPLA$_2\gamma$ in oxidant-induced ER lipid peroxidation, loss of lipid homeostasis, $Ca^{2+}$ release and renal cell death.

Sarcoplasmic/endoplasmic reticulum (ER) $Ca^{2+}$ is the most abundant store of intracellular $Ca^{2+}$, and its release is an important trigger of physiological and pathophysiological processes, including signaling and cell death pathways. Previous work in our laboratory revealed the importance of ER $Ca^{2+}$ in toxicant-induced necrotic renal proximal tubular cell (RPTC) death. The studies presented here focus on RPTC necrotic cell death. In order to ultimately elucidate the role of iPLA$_2\gamma$ in toxicant-induced ER $Ca^{2+}$ release and necrotic RPTC death, we needed to develop an assay to visualize ER $Ca^{2+}$ release in

RPTC. Prior methods of monitoring ER $Ca^{2+}$ required extensive loading techniques, disruption of cell membranes, and/or genetic manipulation of cells to express $Ca^{2+}$ sensitive proteins. These techniques were not ideal because of our use of primary cells and employing these methods would likely further disrupt RPTC physiology. The purpose of this study (Chapter 2) was to evaluate the use of confocal microscopy and Fluo5F, a low affinity $Ca^{2+}$ indicator, to directly monitor changes in RPTC ER $Ca^{2+}$. Fluo5F staining reflected ER $Ca^{2+}$, resolved ER structure, and showed no colocalization with tetramethyl rhodamine methyl ester (TMRM), a marker of mitochondrial membrane potential. These data provide evidence that confocal microscopy and Fluo5F are useful and effective tools for directly monitoring ER $Ca^{2+}$ in intact cells. These studies furthered our understanding of RPTC ER $Ca^{2+}$ stores and $Ca^{2+}$ release-induced mitochondrial depolarization. This assay would later be used to elucidate the role of $iPLA_2\gamma$ in oxidant-induced ER $Ca^{2+}$ release in RPTC.

Oxidant-induced lipid peroxidation and cell death are major components of ischemia-reperfusion and toxicant injury. Our present studies reveal the role of ER- $iPLA_2\gamma$ in oxidant-induced ER lipid peroxidation, $Ca^{2+}$ release, and cell death in isolated ER (microsomes) and RPTC (Chapter 3). We developed assays using cis-parinaric acid, a lipid moiety that loses fluorescence with oxidation, and Fluo-4, a $Ca^{2+}$ -sensitive probe, to monitor microsomal lipid peroxidation and $Ca^{2+}$ release, respectively. Traditional methods of measuring microsomal $Ca^{2+}$ release utilized radioactive $^{45}Ca$ and isolation filters. These methods were cumbersome, required relatively large amounts of microsomes, and lacked the ability to continuously measure $Ca^{2+}$ release in real-time.

The use of cis-parinaric acid and fluo-4 allowed for the measurement of both lipid peroxidation and $Ca^{2+}$ release in real-time under similar conditions. Oxidant, *tert*-butyl hydroperoxide (TBHP), caused ER lipid peroxidation and $Ca^{2+}$ release in isolated rabbit kidney cortex microsomes. ER- iPLA$_2\gamma$ inhibition, using bromoenol lactone (BEL), potentiated both oxidant-induced ER lipid peroxidation and $Ca^{2+}$ release. These finding correlated with our studies in mitochondria showing that mitochondrial- iPLA$_2\gamma$ prevented oxidant-induced lipid peroxidation and mitochondrial swelling. Additionally, the initiation of lipid peroxidation occurred prior to microsomal $Ca^{2+}$ release and these studies excluded the role mitochondria and mitochondrial-iPLA$_2\gamma$. Together, these findings provide evidence that ER $Ca^{2+}$ release is the result of lipid peroxidation- induced membrane disruption and not signaling.

PLA$_2$ enzymes catalyze the hydrolysis of fatty acids at the *sn*-2 position of glycerophospholipids resulting in the production of a free fatty acid and a lysophospholipid. Fatty acids at the sn-2 position tend to be unsaturated and are therefore more vulnerable to oxidative stress. PLA$_2$s were hypothesized to play a role in membrane remodeling/repair by preferentially cleaving damaged (oxidized) fatty acids from the membrane and allowing the re-esterification of native (non-oxidized) fatty acids and lysophospholipid. We utilized electrospray ionization-mass spectrometry (ESI-MS) to investigate the role of ER- iPLA$_2\gamma$ in oxidant-induced ER fatty acid release. Fatty acid assessment revealed that ER- iPLA$_2\gamma$ mediates the TBHP-induced release of arachidonic acid (20:4), linoleic acid (18:2), and their oxidized forms (18:2-OH, 18:2-OOH, 20:4-

OH, 20:4-OOH, 20:4-$(OH)_3$). These findings provide evidence that ER- iPLA$_2\gamma$ prevents ER $Ca^{2+}$ release by mediating the release of unsaturated and/or oxidized fatty acids and thereby maintaining ER membrane integrity. Additionally, these findings, to our knowledge, are the first to connect $PLA_2$ activity, its role in membrane remodeling/repair, and the pathophysiological consequences of the loss of $PLA_2$ activity with respect to membrane repair.

We then demonstrated in intact cells that iPLA$_2\gamma$ inhibition also accelerated oxidant-induced ER $Ca^{2+}$ release in RPTC using the methods developed in Chapter 2. To connect oxidant-induced ER $Ca^{2+}$ release with necrotic cell death, we carried out studies using flow cytometry. Depletion of RPTC ER $Ca^{2+}$ stores with thapsigargin, an ER $Ca^{2+}$ pump inhibitor, prior to TBHP exposure reduced necrotic cell death and blocked the potentiation of TBHP-induced necrotic cell death by BEL. These data provide strong evidence that ER- iPLA$_2\gamma$ protects renal cells from oxidant-induced necrotic cell death by preventing ER $Ca^{2+}$ release. These findings, along with the studies in microsomes, provide evidence that ER- iPLA$_2\gamma$ releases unsaturated and/or oxidized fatty acids during oxidant stress to preserve ER membrane integrity and prevent ER $Ca^{2+}$ release, thereby preventing necrotic cell death. These studies, to our knowledge, are the first elucidate the mechanism by which ER- iPLA$_2\gamma$ is cytoprotective during oxidative stress.

We tested this hypothesis *in vivo* using mice genetically ablated of iPLA$_2\gamma$ (KO mice) and investigated its role in age-related renal oxidant injury. To determine oxidant injury,

we measured urinary 8-isoprostanes and 8-hydroxy-2'-deoxyguanosine (8-OHdG), biomarkers of lipid peroxidation and oxidative DNA damage, respectively. Both 8-OHdG and 8-isoprostanes increased in aged KO mice. These date provide evidence that genetic ablation of iPLA$_2\gamma$ results in increased oxidative stress in KO animals. However, because these markers in urine reflect global changes in oxidant status, further studies were required to elucidate the role iPLA$_2\gamma$ in the kidney, specifically.

Interestingly, urinary lipidomic analysis in KO animals using ESI-MS demonstrated decreases in phospholipid species 38:6, 38:5 and 37:5 phosphatidylcholine and increases in 6-10 carbon fatty acids, with methyl or keto additions. These findings correlated with our studies in microsomes (Chapter 3) demonstrating iPLA$_2\gamma$ is cytoprotective by preventing lipid peroxidation and preserving membrane homeostasis. Previous studies using shRNA to knockdown iPLA$_2\gamma$ in RPTC demonstrated a similar build-up of phosphatidylcholine containing phospholipids. These findings provide strong evidence that the mechanism by which iPLA$_2\gamma$ is protective *in vitro* is physiologically relevant *in vivo*.

To further investigate the role of iPLA$_2\gamma$ in kidney oxidant stress *in vivo*, we measured kidney specific oxidant injury. Our findings that 13 month KO mouse kidney cortex exhibited higher lipid peroxidation and 8-OHdG staining confirmed kidney specific oxidant injury. These findings were correlated with changes in renal mitochondrial respiratory proteins ATP Synthase β, NDUFB8, and COX-1, increases in mitochondrial DNA copy number, and increases in GPx4 mRNA expression in KO mice. Increased

mitochondrial DNA copy number is thought to be a compensatory response to oxidative stress to maintain mitochondrial number and function and GPx4 is an antioxidant enzyme that contains lipid hydroperoxidase activity and is believed to be a component of the membrane remodeling/repair pathway. Interestingly, genetic ablation of iPLA$_2\gamma$ did not result in loss of kidney function. It is likely that iPLA$_2\gamma$ ablation, as expected, induced oxidant injury, but resulted in a compensatory response to maintain tissue viability as evidenced by mitochondrial changes and increases in oxidant stress response pathways. Collectively, these data support our hypothesis that ER- iPLA$_2\gamma$ protects renal cells from oxidant-induced necrotic cell death by preventing ER lipid peroxidation, preserving ER membrane integrity, and blocking ER $Ca^{2+}$ release and loss of $Ca^{2+}$ homeostasis. These studies revealed ER- iPLA$_2\gamma$ preferentially cleaves unsaturated and/or oxidized fatty acids under oxidant stress and provides the mechanism by which it is protective. We also confirmed iPLA$_2\gamma$ plays a similar and crucial role in oxidative stress *in vivo*. Together, these studies have elucidated the role of iPLA$_2\gamma$ in oxidant-induced renal cell death, revealed the mechanism by which ER- iPLA$_2\gamma$ is cytoprotective, and has furthered our understanding of kidney physiology and pathophysiology in the setting of aging and oxidant injury. iPLA$_2\gamma$ represents a potential therapeutic target to prevent acute kidney injury in patients at high risk or hasten recovery of kidney function following AKI. Further understanding of the role of iPLA$_2\gamma$ in chronic kidney disease may elucidate therapeutics that would prevent the progression of CKD to end-stage renal disease and failure.

**Future Directions**

The studies presented here focus on the role of iPLA$_2\gamma$ in oxidant-induced necrotic cell death and have uncovered several questions that require further investigation. Additionally, the role of iPLA$_2\gamma$ in apoptosis-induced renal cell death or its role in cell signaling was not investigated within the scope of these studies. Potential investigations will be presented here.

Our previous studies demonstrated iPLA$_2\gamma$ mediates cisplatin-induced renal apoptotic cell death and studies in mitochondria demonstrated iPLA$_2\gamma$ mediates $Ca^{2+}$- induced mitochondrial swelling through an arachidonic acid-dependent initiation of mitochondrial pore transition. Because apoptosis is thought to be a major component of age-related loss of kidney function and thought to play a role in the progression of chronic kidney disease to end-stage renal failure, elucidating the role of iPLA$_2\gamma$ in apoptosis-induced cell death may uncover potential therapeutics in renal injury. The assays developed and experimental methods utilized during the course of these experiments may be used to further investigate the role of iPLA$_2\gamma$ in apoptosis. Specifically, renal cell imaging using confocal microscopy to monitor mitochondrial membrane potential and $Ca^{2+}$ dynamics may help to elucidate the role of iPLA$_2\gamma$ in cisplatin-induced renal cell apoptosis.

iPLA$_2\gamma$ regulation was not investigated during the course of these experiments. Our previous studies demonstrate phorbol 12-myristate 13-acetate (PMA), a protein kinase C (PKC) activator, increased ER-iPLA$_2\gamma$ activity and potentiated cisplatin-induced

apoptosis [112]. Interestingly, RPTC exposed to PMA activates only ER-iPLA$_2\gamma$ and not mitochondrial iPLA$_2\gamma$ (Figure 5-1). These findings suggest that ER-iPLA$_2\gamma$ activity may be more closely regulated by phosphorylation status. Furthermore, exposure of RPTC to PKCε V1-2 specifically decreased ER-iPLA$_2\gamma$ activity and prevented PMA-induced activation of ER-iPLA$_2\gamma$. Together these findings suggest that ER-iPLA$_2\gamma$, and not mitochondrial iPLA$_2\gamma$, is regulated by PKCε-induced phosphorylation and ER-iPLA$_2\gamma$ activity may be specifically manipulated while mitochondrial- iPLA$_2\gamma$ remains unchanged.

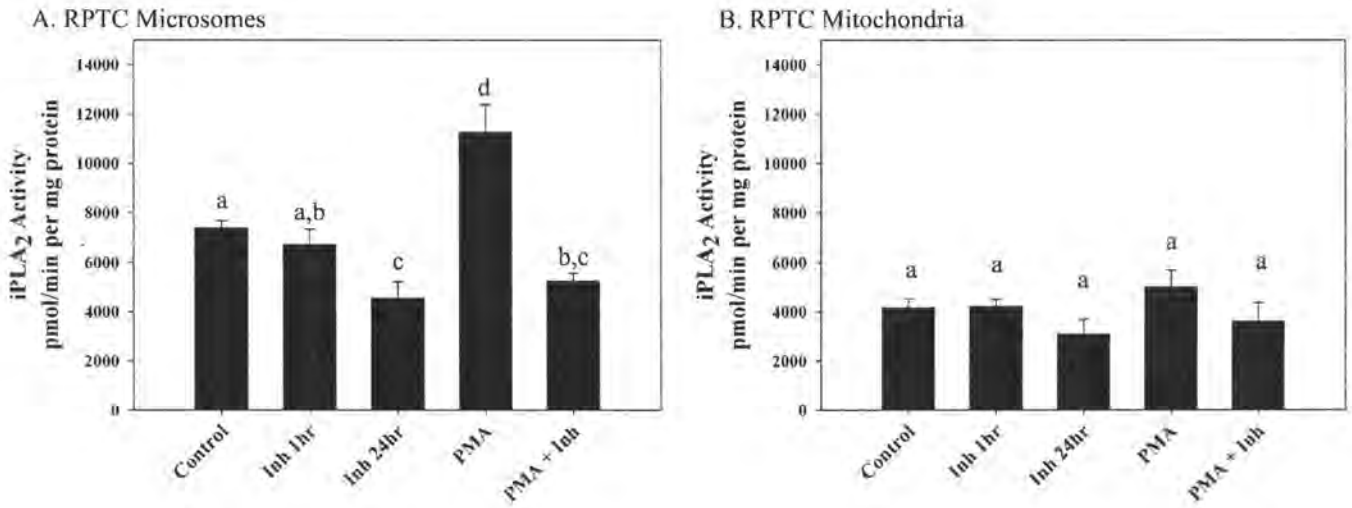


**Figure 5-1. Effect of PMA and PKCε inhibitor on ER and mitochondrial iPLA$_2\gamma$ activity in RPTC.** RPTC were exposed to the PKCε V1-2 inhibitor (Inh, 20 μM) for 1 hr and 24 hr or PMA (100 nM for 30 minutes) in the presence and absence of the PKCε V1-2 inhibitor (1 hour pretreatment). ER and mitochondrial fractions were isolated from RPTC and iPLA$_2$ activity measured using synthetic plasmenylcholine (16:0, [$^3$H]18:1). Data are presented as the mean + SEM. Means with different superscripts are significantly different from each other, $p < 0.05$, n=4.

It has been proposed that iPLA$_2\gamma$ activity and function is regulated by phophorylation and differential expression of splice variants. Analysis of the amino acid sequence of iPLA$_2\gamma$

showed that there are many potential serine, threonine and tyrosine phosphorylation sites [96, 185]. However, the phosphorylation of specific amino acids on iPLA$_2\gamma$ has not been has not been investigated and little is known of the kinases and phosphatases involved. Experiments directed at elucidating the mechanism by which iPLA$_2\gamma$ is regulated by phosphorylaton need to be addressed.

Our studies in microsomes presented in Chapter 3 revealed several interesting findings using ESI-MS. The goal of these studies were to elucidate the mechanism by which ER-iPLA$_2\gamma$ prevents lipid peroxidation, and these studies demonstrated ER-iPLA$_2\gamma$ mediates the release of unsaturated and/or oxidized fatty acids during oxidative stress. However, these studies also revealed that inhibition of ER-iPLA$_2\gamma$ by BEL increased the release of a lipid species at M/z 345. This species may represent 1) a signaling molecule involved in the initiation of ER $Ca^{2+}$ release, 2) the build-up of a lipid substrate specifically acted upon by ER-iPLA$_2\gamma$ and/or 3) the byproduct of ER membrane disruption. Further investigation of this lipid moiety may reveal the long sought after iPLA$_2\gamma$ substrate/signaling molecule (Figure 5-2).

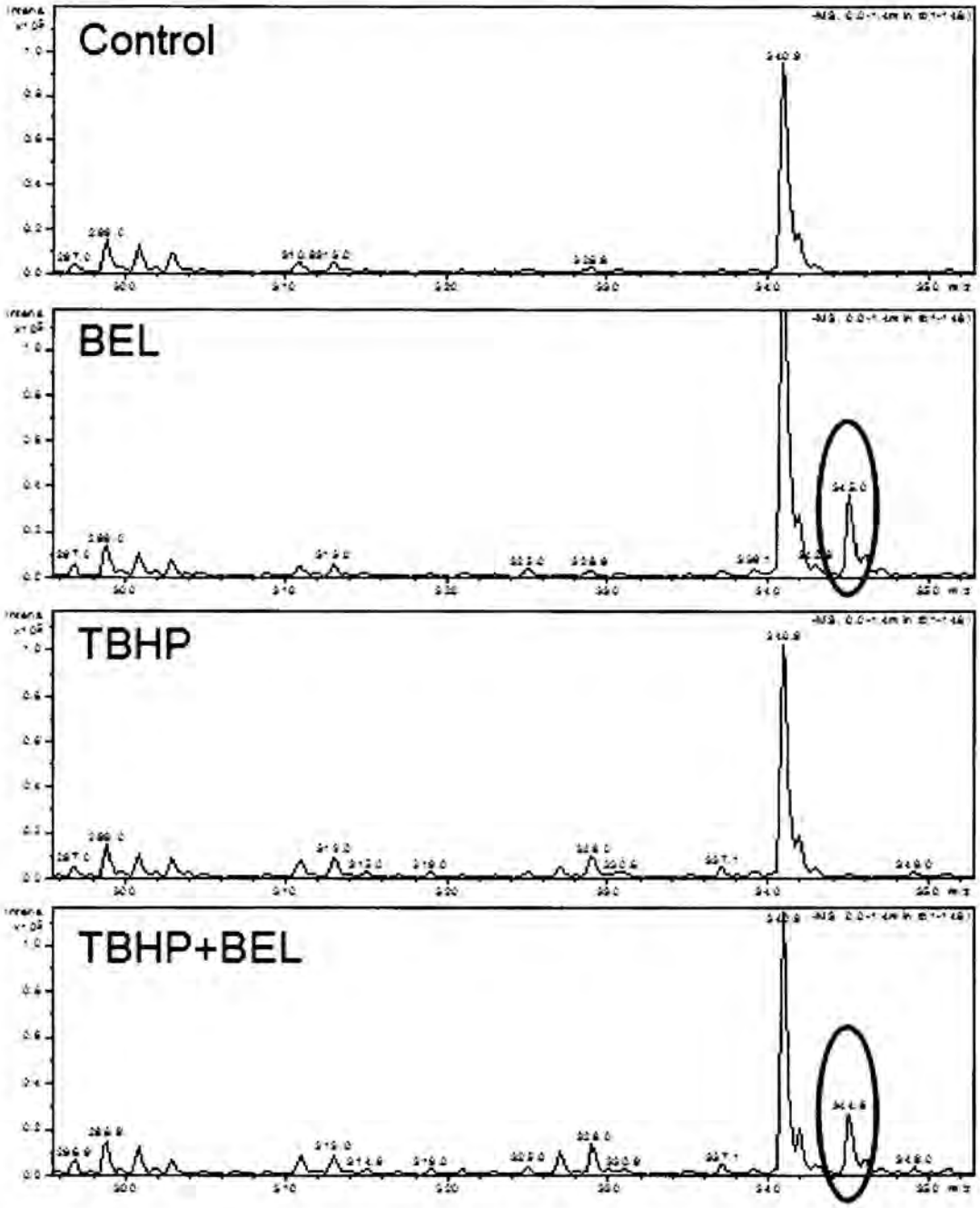


**Figure 5-2. Inhibition of iPLA$_2\gamma$ induces the release of lipid (m/z 345) from microsomes.** Released lipids were separated from microsomes using differential centrifugation, extracted by Bligh Dyer method, injected directly into ESI-Mass Spectrometer, and analyzed in negative mode. Microsomes were pretreated for 20 min with BEL or diluent, treated for 30 min with 200 μM TBHP, and reaction was stopped and analyzed by ESI-MS.

Our studies in mice genetically ablated of iPLA$_2\gamma$ (Chapter 4) suggest ablation-associated oxidant injury is not great enough to overcome kidney reserve and regenerative capacity and iPLA$_2\gamma$ ablated mice do not exhibit greater loss of kidney function at 13 months of age. Interestingly, Mancuso *et al.* showed that ablation of iPLA$_2\gamma$ alone was not sufficient

to cause cardiac dysfunction, but a subsequent insult, transverse aortic constriction, revealed cardiac dysfunction in iPLA$_2\gamma$ KO mice [136]. Similarly, age-associated changes in kidney structure and function are not always sufficient to cause kidney dysfunction, but it is believed that these changes make the kidney more vulnerable to subsequent insults (ie. ischemia/reperfusion-, drug-, and toxicant injury) [183-184]. A subsequent kidney insult, such as ischemia/reperfusion or toxicant injury, may reveal kidney dysfunction in KO mice. We have developed a model of ischemia/reperfusion (Figure 5-3) and toxicant injury (Figure 5-4) that may be used to reveal kidney dysfunction in mice genetically ablate of iPLA$_2\gamma$.

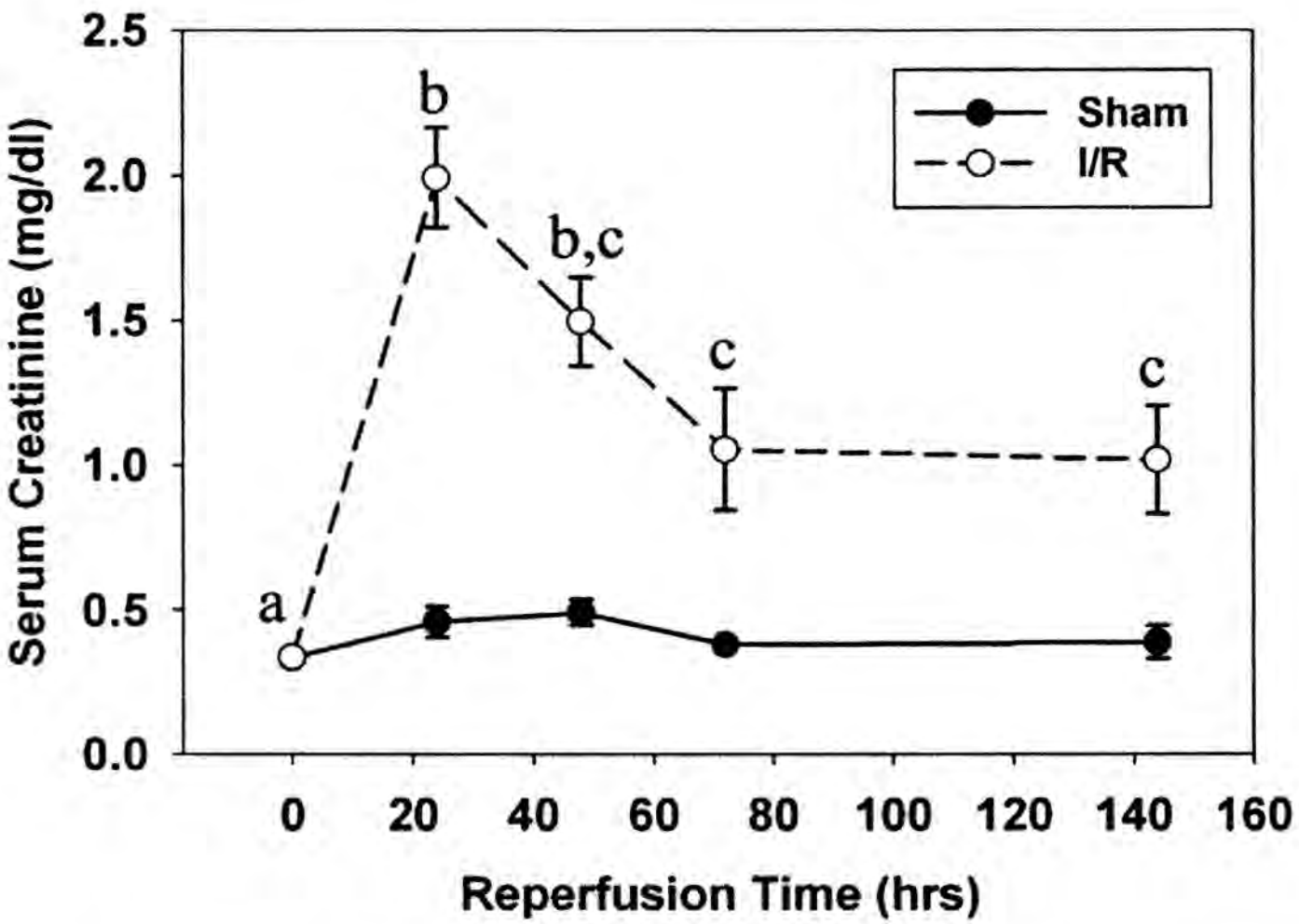


**Figure 5-3. Kidney dysfunction after ischemia-reperfusion injury.** Serum creatinine levels were significantly elevated 24 h after reperfusion, and then slowly decreased

between 24 h and 144 h without returning to normal levels. Different superscripts above data points are significantly different from one another ($P < 0.05$). From Funk and Schnellmann, 2011 [19].

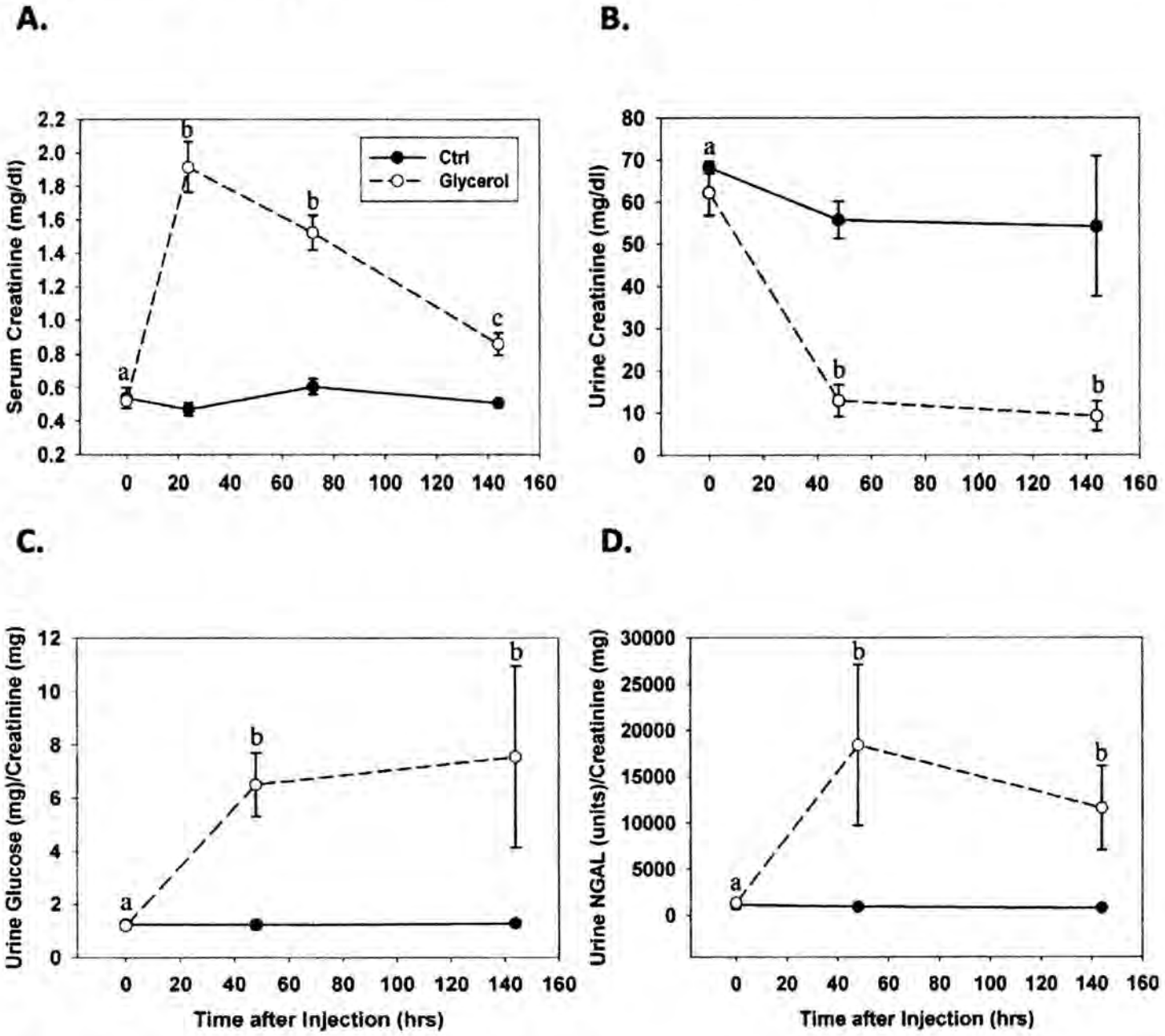


**Figure 5-4. Renal dysfunction after glycerol-induced myoglobinuria.** (A) Serum creatinine was maximal 24 h after injection, and partially recovered between 24 h and 144 h after injury without returning to normal levels. (B) Urine creatinine was reduced 48 h after injury and remained decreased at 144 h. Urine glucose (C) and NGAL (D) were elevated 48 h after glycerol injection and remained elevated at 144 h. Different superscripts above data points are significantly different from one another ($P < 0.05$). From Funk and Schnellmann, 2011 [19].

Additional studies are need in KO mice to further elucidate the role of $iPLA_2\gamma$ in oxidant injury and loss of renal function *in vivo*. Studies in animals older than 13 months may

reveal an earlier onset of age-associated loss of kidney function in iPLA$_2\gamma$ ablated mice. Additionally, older KO animals should be subjected to our model of ischemia/reperfusion-induced kidney injury and may reveal iPLA$_2\gamma$ ablated animals are more vulnerable to a subsequent injury. There are several studies of iPLA$_2\gamma$ that require further investigation and may further our understanding of the role iPLA$_2\gamma$ in renal physiology and pathophysiology, responses of renal cells to oxidant injury, and the molecular and physiological changes within the aging kidney.

## References


1. Eaton, D.C., et al., *Vander's renal physiology.* 6th ed. 2004, New York: Lange Medical Books/McGraw Hill, Medical Pub. Division. vii, 214 p.

2. Needham, E., *Management of acute renal failure.* Am Fam Physician, 2005. **72**(9): p. 1739-46.

3. Bellomo, R., et al., *Acute renal failure - definition, outcome measures, animal models, fluid therapy and information technology needs: the Second International Consensus Conference of the Acute Dialysis Quality Initiative (ADQI) Group.* Crit Care, 2004. **8**(4): p. R204-12.

4. Ricci, Z., D. Cruz, and C. Ronco, *The RIFLE criteria and mortality in acute kidney injury: A systematic review.* Kidney Int, 2008. **73**(5): p. 538-46.

5. Joannidis, M. and P.G. Metnitz, *Epidemiology and natural history of acute renal failure in the ICU.* Crit Care Clin, 2005. **21**(2): p. 239-49.

6. Silva Junior, G.B., et al., *Risk factors for death among critically ill patients with acute renal failure.* Sao Paulo Med J, 2006. **124**(5): p. 257-63.

7. Chertow, G.M., et al., *Independent association between acute renal failure and mortality following cardiac surgery.* Am J Med, 1998. **104**(4): p. 343-8.

8. Coca, S.G., et al., *Long-term risk of mortality and other adverse outcomes after acute kidney injury: a systematic review and meta-analysis.* Am J Kidney Dis, 2009. **53**(6): p. 961-73.

9. Ronco, C. and P. Honore, *Renal support in critically ill patients with acute kidney injury.* N Engl J Med, 2008. **359**(18): p. 1959; author reply 1961-2.

10. Thakar, C.V., et al., *Incidence and outcomes of acute kidney injury in intensive care units: a Veterans Administration study.* Crit Care Med, 2009. **37**(9): p. 2552-8.

11. Chertow, G.M., et al., *Acute kidney injury, mortality, length of stay, and costs in hospitalized patients.* J Am Soc Nephrol, 2005. **16**(11): p. 3365-70.

12. Coresh, J., et al., *Prevalence of chronic kidney disease in the United States.* JAMA, 2007. **298**(17): p. 2038-47.

13. Manns, B., et al., *Cost of acute renal failure requiring dialysis in the intensive care unit: clinical and resource implications of renal recovery.* Crit Care Med, 2003. **31**(2): p. 449-55.

14. Kinsey, G.R. and M.D. Okusa, *Pathogenesis of acute kidney injury: foundation for clinical practice.* Am J Kidney Dis, 2011. **58**(2): p. 291-301.

15. Schoolwerth, A.C., et al., *Renal considerations in angiotensin converting enzyme inhibitor therapy: a statement for healthcare professionals from the Council on the Kidney in Cardiovascular Disease and the Council for High Blood Pressure Research of the American Heart Association.* Circulation, 2001. **104**(16): p. 1985-91.

16. Abuelo, J.G., *Normotensive ischemic acute renal failure.* N Engl J Med, 2007. **357**(8): p. 797-805.

17. Patel, T.V., S. Kumar, and A.K. Singh, *Post-renal acute renal failure.* Kidney Int, 2007. **72**(7): p. 890-4.

18. Lameire, N., *The pathophysiology of acute renal failure.* Crit Care Clin, 2005. **21**(2): p. 197-210.

19. Funk, J.A. and R.G. Schnellmann, *Persistent Disruption of Mitochondrial Homeostasis after Acute Kidney Injury.* Am J Physiol Renal Physiol, 2011.

20. Cummings, B.S. and R.G. Schnellmann, *Pathophysiology of Nephrotoxic Cell Injury*, in *Diseases of the Kidney and Urinary Tract*, R.W. Schrier, Editor. 2001, Lippinkot, Williams and Wilkins: Philadelphia, PA. p. 1071-1091.

21. Edelstein, C.L. and R.W. Schrier, *Pathophysiology of Ischemic Acute Renal Failure*, in *Diseases of the Kidney and Urinary Tract*, R.W. Schrier, Editor. 2001, Lippinkot, Williams and Wilkins: Philadelphia, PA. p. 1041-1069.

22. Guder, W.G. and B.D. Ross, *Enzyme distribution along the nephron.* Kidney Int, 1984. **26**(2): p. 101-11.

23. Barbier, O., et al., *Effect of heavy metals on, and handling by, the kidney.* Nephron Physiol, 2005. **99**(4): p. p105-10.

24. Bonventre, J.V. and J.M. Weinberg, *Recent advances in the pathophysiology of ischemic acute renal failure.* J Am Soc Nephrol, 2003. **14**(8): p. 2199-210.

25. Lieberthal, W., S.A. Menza, and J.S. Levine, *Graded ATP depletion can cause necrosis or apoptosis of cultured mouse proximal tubular cells.* Am J Physiol, 1998. **274**(2 Pt 2): p. F315-27.

26. Lemasters, J.J., *V. Necrapoptosis and the mitochondrial permeability transition: shared pathways to necrosis and apoptosis.* Am J Physiol, 1999. **276**(1 Pt 1): p. G1-6.

27. McHugh, P. and M. Turina, *Apoptosis and necrosis: a review for surgeons.* Surg Infect (Larchmt), 2006. 7(1): p. 53-68.

28. Barros, L.F., J. Castro, and C.X. Bittner, *Ion movements in cell death: from protection to execution.* Biol Res, 2002. **35**(2): p. 209-14.

29. Liu, X. and R.G. Schnellmann, *Calpain mediates progressive plasma membrane permeability and proteolysis of cytoskeleton-associated paxillin, talin, and vinculin during renal cell death.* J Pharmacol Exp Ther, 2003. **304**(1): p. 63-70.

30. Lemasters, J.J., et al., *Role of mitochondrial inner membrane permeabilization in necrotic cell death, apoptosis, and autophagy.* Antioxid Redox Signal, 2002. **4**(5): p. 769-81.

31. Dong, Z., et al., *Development of porous defects in plasma membranes of adenosine triphosphate-depleted Madin-Darby canine kidney cells and its inhibition by glycine.* Lab Invest, 1998. **78**(6): p. 657-68.

32. Nishimura, Y. and J.J. Lemasters, *Glycine blocks opening of a death channel in cultured hepatic sinusoidal endothelial cells during chemical hypoxia.* Cell Death Differ, 2001. **8**(8): p. 850-8.

33. Dagher, P.C., *Apoptosis in ischemic renal injury: roles of GTP depletion and p53.* Kidney Int, 2004. **66**(2): p. 506-9.

34. Lorz, C., et al., *Proapoptotic Fas Ligand Is Expressed by Normal Kidney Tubular Epithelium and Injured Glomeruli.* 2000. p. 1266-1277.

35. Gogvadze, V., S. Orrenius, and B. Zhivotovsky, *Multiple pathways of cytochrome c release from mitochondria in apoptosis.* Biochimica et Biophysica Acta (BBA) - Bioenergetics, 2006. **1757**(5-6): p. 639-647.

36. van Loo, G., et al., *The role of mitochondrial factors in apoptosis: a Russian roulette with more than one bullet.* Cell Death Differ, 2002. **9**(10): p. 1031-42.

37. Turrens, J.F., *Mitochondrial formation of reactive oxygen species.* J Physiol, 2003. **552**(Pt 2): p. 335-44.

38. Erdogan, H., et al., *Protein oxidation and lipid peroxidation after renal ischemia-reperfusion injury: protective effects of erdosteine and N-acetylcysteine.* Urol Res, 2006. **34**(1): p. 41-6.

39. Kadkhodaee, M., et al., *Detection of hydroxyl and carbon-centred radicals by EPR spectroscopy after ischaemia and reperfusion of the rat kidney.* Free Radic Res, 1996. **25**(1): p. 31-42.

40. Kadkhodaee, M., et al., *Hydroxyl radical generation following ischaemia-reperfusion in cell-free perfused rat kidney.* Biochim Biophys Acta, 1995. **1243**(2): p. 169-74.

41. Noiri, E., et al., *Oxidative and nitrosative stress in acute renal ischemia.* Am J Physiol Renal Physiol, 2001. **281**(5): p. F948-57.

42. Petrosillo, G., et al., *Decreased complex III activity in mitochondria isolated from rat heart subjected to ischemia and reperfusion: role of reactive oxygen species and cardiolipin.* Faseb J, 2003. **17**(6): p. 714-6.

43. Raess, B.U., C.E. Keenan, and E.J. McConnell, *Effects of 4-OH-2,3-trans-Nonenal on Human Erythrocyte Plasma Membrane Ca2+Pump and Passive Ca2+Permeability,.* Biochemical and Biophysical Research Communications, 1997. **235**(3): p. 451-454.

44. Berridge, M.J., *Inositol trisphosphate and calcium signaling.* Ann N Y Acad Sci, 1995. **766**: p. 31-43.

45. Cummings, B.S., et al., *Identification of caspase-independent apoptosis in epithelial and cancer cells.* J Pharmacol Exp Ther, 2004. **310**(1): p. 126-34.

46. Lemasters, J.J., et al., *The mitochondrial permeability transition in cell death: a common mechanism in necrosis, apoptosis and autophagy.* Biochim Biophys Acta, 1998. **1366**(1-2): p. 177-96.

47. Lemasters, J.J., et al., *Confocal microscopy of the mitochondrial permeability transition in necrotic cell killing, apoptosis and autophagy.* Biofactors, 1998. **8**(3-4): p. 283-5.

48. Schnellmann, R.G., *Intracellular calcium chelators and oxidant-induced renal proximal tubule cell death.* J Biochem Toxicol, 1991. **6**(4): p. 299-303.

49. Waters, S.L., et al., *Calpains mediate calcium and chloride influx during the late phase of cell injury.* J Pharmacol Exp Ther, 1997. **283**(3): p. 1177-84.

50. Waters, S.L., J.K. Wong, and R.G. Schnellmann, *Depletion of endoplasmic reticulum calcium stores protects against hypoxia- and mitochondrial inhibitor-induced cellular injury and death.* Biochem Biophys Res Commun, 1997. **240**(1): p. 57-60.

51. Pozzan, T., et al., *Molecular and cellular physiology of intracellular calcium stores.* Physiol Rev, 1994. **74**(3): p. 595-636.

52. Liu, X., T. Van Vleet, and R.G. Schnellmann, *The role of calpain in oncotic cell death.* Annu Rev Pharmacol Toxicol, 2004. **44**: p. 349-70.

53. Harriman, J.F., et al., *Endoplasmic reticulum Ca(2+) signaling and calpains mediate renal cell death.* Cell Death Differ, 2002. **9**(7): p. 734-41.

54. Muruganandan, S. and A.E. Cribb, *Calpain-induced endoplasmic reticulum stress and cell death following cytotoxic damage to renal cells.* Toxicol Sci, 2006. **94**(1): p. 118-28.

55. Bernardi, P., *Mitochondrial transport of cations: channels, exchangers, and permeability transition.* Physiol Rev, 1999. **79**(4): p. 1127-55.

56. Weinberg, J.M., *The cell biology of ischemic renal injury.* Kidney Int, 1991. **39**(3): p. 476-500.

57. Schwerzmann, K. and P.L. Pedersen, *Regulation of the mitochondrial ATP synthase/ATPase complex.* Arch Biochem Biophys, 1986. **250**(1): p. 1-18.

58. Zager, R.A., K.M. Burkhart, and D.S. Conrad, *Isoflurane alters proximal tubular cell susceptibility to toxic and hypoxic forms of attack.* Kidney Int, 1999. **55**(1): p. 148-59.

59. Zager, R.A., et al., *Plasma membrane phospholipid integrity and orientation during hypoxic and toxic proximal tubular attack.* Kidney Int, 1999. **56**(1): p. 104-17.

60. Zager, R.A., *Pathogenetic mechanisms in nephrotoxic acute renal failure.* Semin Nephrol, 1997. **17**(1): p. 3-14.

61. Bonventre, J.V. and W.J. Koroshetz, *Phospholipase A2 (PLA2) activity in gerbil brain: characterization of cytosolic and membrane-associated forms and effects of ischemia and reperfusion on enzymatic activity.* J Lipid Mediat, 1993. **6**(1-3): p. 457-71.

62. Chiariello, M., et al., *Inhibition of ischemia-induced phospholipase activation by quinacrine protects jeopardized myocardium in rats with coronary artery occlusion.* J Pharmacol Exp Ther, 1987. **241**(2): p. 560-8.

63. Clemens, J.A., P.P. Ho, and J.A. Panetta, *LY178002 reduces rat brain damage after transient global forebrain ischemia.* Stroke, 1991. **22**(8): p. 1048-52.

64. Nguyen, V.D., D.A. Cieslinski, and H.D. Humes, *Importance of adenosine triphosphate in phospholipase A2-induced rabbit renal proximal tubule cell injury.* J Clin Invest, 1988. **82**(3): p. 1098-105.

65. Portilla, D., et al., *Role of cytosolic calcium-independent plasmalogen-selective phospholipase A2 in hypoxic injury to rabbit proximal tubules.* J Clin Invest, 1994. **93**(4): p. 1609-15.

66. Zager, R.A., et al., *Phospholipase A2 activity can protect renal tubules from oxygen deprivation injury.* Proc Natl Acad Sci U S A, 1993. **90**(17): p. 8297-301.

67. Zager, R.A., et al., *Phospholipase A2-induced cytoprotection of proximal tubules: potential determinants and specificity for ATP depletion-mediated injury.* J Am Soc Nephrol, 1996. **7**(1): p. 64-72.

68. Cummings, B.S., J. McHowat, and R.G. Schnellmann, *Role of an endoplasmic reticulum Ca(2+)-independent phospholipase A(2) in oxidant-induced renal cell death.* Am J Physiol Renal Physiol, 2002. **283**(3): p. F492-8.

69. Sud, M., et al., *LMSD: LIPID MAPS structure database.* Nucleic Acids Res, 2007. **35**(Database issue): p. D527-32.

70. Montrucchio, G., G. Alloatti, and G. Camussi, *Role of platelet-activating factor in cardiovascular pathophysiology.* Physiol Rev, 2000. **80**(4): p. 1669-99.

71. Subbanagounder, G., et al., *Evidence that phospholipid oxidation products and/or platelet-activating factor play an important role in early atherogenesis : in vitro and In vivo inhibition by WEB 2086.* Circ Res, 1999. **85**(4): p. 311-8.

72. Cook, J.A., et al., *Prostaglandins, thromboxanes, leukotrienes, and cytochrome P-450 metabolites of arachidonic acid.* New Horiz, 1993. **1**(1): p. 60-9.

73. Rule, D.C., J.R. Busboom, and C.J. Kercher, *Effect of dietary canola on fatty acid composition of bovine adipose tissue, muscle, kidney, and liver.* J Anim Sci, 1994. **72**(10): p. 2735-44.

74. Kagan, V.E., *Lipid Peroxidation in Biomembranes.* 1988, Boca Raton, FL: CRC Press.

75. Halliwell, B. and S. Chirico, *Lipid peroxidation: its mechanism, measurement, and significance.* Am J Clin Nutr, 1993. **57**(5 Suppl): p. 715S-724S; discussion 724S-725S.

76. Gutteridge, J.M., *Lipid peroxidation and antioxidants as biomarkers of tissue damage.* Clin Chem, 1995. **41**(12 Pt 2): p. 1819-28.

77. Okabe, E., et al., *The effect of oxygen free radicals on calcium permeability and calcium loading at steady state in cardiac sarcoplasmic reticulum.* Mol Pharmacol, 1988. **34**(3): p. 388-94.

78. Buettner, G.R., *The pecking order of free radicals and antioxidants: lipid peroxidation, alpha-tocopherol, and ascorbate.* Arch Biochem Biophys, 1993. **300**(2): p. 535-43.

79. Leray, C. *http://www.cyberlipid.org/perox/oxid0002.htm#1.* 2007.

80. Wood, R. and R.D. Harlow, *Structural analyses of rat liver phosphoglycerides.* Arch Biochem Biophys, 1969. **135**(1): p. 272-81.

81. Schaloske, R.H. and E.A. Dennis, *The phospholipase A2 superfamily and its group numbering system.* Biochim Biophys Acta, 2006. **1761**(11): p. 1246-59.

82. Lands, W.E., *Lipid Metabolism.* Annu Rev Biochem, 1965. **34**: p. 313-46.

83. Salgo, M.G., F.P. Corongiu, and A. Sevanian, *Peroxidation and phospholipase A2 hydrolytic susceptibility of liposomes consisting of mixed species of phosphatidylcholine and phosphatidylethanolamine.* Biochim Biophys Acta, 1992. **1127**(2): p. 131-40.

84. Sevanian, A., S.F. Muakkassah-Kelly, and S. Montestruque, *The influence of phospholipase A2 and glutathione peroxidase on the elimination of membrane lipid peroxides.* Arch Biochem Biophys, 1983. **223**(2): p. 441-52.

85. Sevanian, A. and E. Kim, *Phospholipase A2 dependent release of fatty acids from peroxidized membranes.* J Free Radic Biol Med, 1985. **1**(4): p. 263-71.

86. Six, D.A. and E.A. Dennis, *The expanding superfamily of phospholipase A(2) enzymes: classification and characterization.* Biochim Biophys Acta, 2000. **1488**(1-2): p. 1-19.

87. Glaser, K.B., *Regulation of phospholipase A2 enzymes: selective inhibitors and their pharmacological potential.* Adv Pharmacol, 1995. **32**: p. 31-66.

88. F Van Kuijk, A.S., G J Handelman, E A Dratz, *A new role for phospholipase A2: protection of membranes from lipid peroxidation damage.* Trends Biochemical Science, 1987: p. 31-34.

89. Dufton, M.J. and R.C. Hider, *Classification of phospholipases A2 according to sequence. Evolutionary and pharmacological implications.* Eur J Biochem, 1983. **137**(3): p. 545-51.

90. Jenkins, C.M., et al., *Identification, cloning, expression, and purification of three novel human calcium-independent phospholipase A2 family members possessing triacylglycerol lipase and acylglycerol transacylase activities.* J Biol Chem, 2004. **279**(47): p. 48968-75.

91. Hazen, S.L., R.J. Stuppy, and R.W. Gross, *Purification and characterization of canine myocardial cytosolic phospholipase A2. A calcium-independent phospholipase with absolute fl-2 regiospecificity for diradyl glycerophospholipids.* J Biol Chem, 1990. **265**(18): p. 10622-30.

92. Balsinde, J. and M.A. Balboa, *Cellular regulation and proposed biological functions of group VIA calcium-independent phospholipase A2 in activated cells.* Cell Signal, 2005. **17**(9): p. 1052-62.

93. van Tienhoven, M., et al., *Human neuropathy target esterase catalyzes hydrolysis of membrane lipids.* J Biol Chem, 2002. **277**(23): p. 20942-8.

94. Jenkins, C.M., et al., *Identification, Cloning, Expression, and Purification of Three Novel Human Calcium-independent Phospholipase A2 Family Members Possessing Triacylglycerol Lipase and Acylglycerol Transacylase Activities.* J. Biol. Chem., 2004. **279**(47): p. 48968-48975.

95. Mancuso, D.J., C.M. Jenkins, and R.W. Gross, *The genomic organization, complete mRNA sequence, cloning, and expression of a novel human intracellular membrane-associated calcium-independent phospholipase A(2).* J Biol Chem, 2000. **275**(14): p. 9937-45.

96. Tanaka, H., R. Takeya, and H. Sumimoto, *A novel intracellular membrane-bound calcium-independent phospholipase A(2).* Biochem Biophys Res Commun, 2000. **272**(2): p. 320-6.

97. Kinsey, G.R., et al., *Identification and distribution of endoplasmic reticulum iPLA2.* Biochem Biophys Res Commun, 2005. **327**(1): p. 287-93.

98. Kinsey, G.R., et al., *Identification of calcium-independent phospholipase A2gamma in mitochondria and its role in mitochondrial oxidative stress.* Am J Physiol Renal Physiol, 2007. **292**(2): p. F853-60.

99. Tang, J., et al., *A novel cytosolic calcium-independent phospholipase A2 contains eight ankyrin motifs.* J Biol Chem, 1997. **272**(13): p. 8567-75.

100. Larsson, P.K., H.E. Claesson, and B.P. Kennedy, *Multiple splice variants of the human calcium-independent phospholipase A2 and their effect on enzyme activity.* J Biol Chem, 1998. **273**(1): p. 207-14.

101. Hazen, S.L. and R.W. Gross, *ATP-dependent regulation of rabbit myocardial cytosolic calcium-independent phospholipase A2.* J Biol Chem, 1991. **266**(22): p. 14526-34.

102. Wolf, M.J. and R.W. Gross, *The calcium-dependent association and functional coupling of calmodulin with myocardial phospholipase A2. Implications for*

*cardiac cycle-dependent alterations in phospholipolysis.* J Biol Chem, 1996. **271**(35): p. 20989-92.

103. Lauber, K., et al., *Apoptotic cells induce migration of phagocytes via caspase-3-mediated release of a lipid attraction signal.* Cell, 2003. **113**(6): p. 717-30.

104. Ramanadham, S., et al., *Pancreatic islets and insulinoma cells express a novel isoform of group VIA phospholipase A2 (iPLA2 beta) that participates in glucose-stimulated insulin secretion and is not produced by alternate splicing of the iPLA2 beta transcript.* Biochemistry, 2003. **42**(47): p. 13929-40.

105. Balsinde, J., *Roles of various phospholipases A2 in providing lysophospholipid acceptors for fatty acid phospholipid incorporation and remodelling.* Biochem J, 2002. **364**(Pt 3): p. 695-702.

106. Smani, T., et al., *Ca2+-independent phospholipase A2 is a novel determinant of store-operated Ca2+ entry.* J Biol Chem, 2003. **278**(14): p. 11909-15.

107. Mancuso, D.J., et al., *Cardiac ischemia activates calcium-independent phospholipase A2beta, precipitating ventricular tachyarrhythmias in transgenic mice: rescue of the lethal electrophysiologic phenotype by mechanism-based inhibition.* J Biol Chem, 2003. **278**(25): p. 22231-6.

108. Perez, R., et al., *Role of Group VIA Calcium-independent Phospholipase A2 in Arachidonic Acid Release, Phospholipid Fatty Acid Incorporation, and Apoptosis in U937 Cells Responding to Hydrogen Peroxide.* 2004. p. 40385-40391.

109. Mancuso, D.J., et al., *Dramatic accumulation of triglycerides and precipitation of cardiac hemodynamic dysfunction during brief caloric restriction in transgenic myocardium expressing human calcium-independent phospholipase A2gamma.* J Biol Chem, 2007. **282**(12): p. 9216-27.

110. Mancuso, D.J., et al., *Complex transcriptional and translational regulation of iPLAgamma resulting in multiple gene products containing dual competing sites for mitochondrial or peroxisomal localization.* Eur J Biochem, 2004. **271**(23-24): p. 4709-24.

111. Steer, S.A., et al., *Regulation of membrane-associated iPLA2 activity by a novel PKC isoform in ventricular myocytes.* Am J Physiol Cell Physiol, 2002. **283**(6): p. C1621-6.

112. Cummings, B.S., J. McHowat, and R.G. Schnellmann, *Role of an endoplasmic reticulum Ca2+-independent phospholipase A2 in cisplatin-induced renal cell apoptosis.* J Pharmacol Exp Ther, 2004. **308**(3): p. 921-8.

113. Kinsey, G.R., et al., *Role of Ca2+-independent phospholipase A2gamma in Ca2+-induced mitochondrial permeability transition.* J Pharmacol Exp Ther, 2007. **321**(2): p. 707-15.

114. Cummings, B.S., et al., *Inactivation of Endoplasmic Reticulum Bound Ca2+-Independent Phospholipase A2 in Renal Cells during Oxidative Stress.* J Am Soc Nephrol, 2004. **15**(6): p. 1441-1451.

115. McHowat, J., L.M. Swift, and N. Sarvazyan, *Oxidant-induced inhibition of myocardial calcium-independent phospholipase A2.* Cardiovasc Toxicol, 2001. **1**(4): p. 309-16.

116. Kinsey, G.R., et al., *Decreased iPLA2gamma expression induces lipid peroxidation and cell death and sensitizes cells to oxidant-induced apoptosis.* J Lipid Res, 2008. **49**(7): p. 1477-87.

117. Murakami, M., et al., *Group VIB Ca2+-independent phospholipase A2gamma promotes cellular membrane hydrolysis and prostaglandin production in a manner distinct from other intracellular phospholipases A2.* J Biol Chem, 2005. **280**(14): p. 14028-41.

118. Liu, S.J. and J. McHowat, *Stimulation of different phospholipase A2 isoforms by TNF-alpha and IL-1beta in adult rat ventricular myocytes.* Am J Physiol, 1998. **275**(4 Pt 2): p. H1462-72.

119. McHowat, J. and M.H. Creer, *Thrombin activates a membrane-associated calcium-independent PLA2 in ventricular myocytes.* Am J Physiol, 1998. **274**(2 Pt 1): p. C447-54.

120. Hazen, S.L., et al., *Suicide inhibition of canine myocardial cytosolic calcium-independent phospholipase A2. Mechanism-based discrimination between calcium-dependent and -independent phospholipases A2.* J Biol Chem, 1991. **266**(11): p. 7227-32.

121. Lio, Y.C., et al., *Irreversible inhibition of Ca(2+)-independent phospholipase A2 by methyl arachidonyl fluorophosphonate.* Biochim Biophys Acta, 1996. **1302**(1): p. 55-60.

122. Ackermann, E.J., K. Conde-Frieboes, and E.A. Dennis, *Inhibition of macrophage Ca(2+)-independent phospholipase A2 by bromoenol lactone and trifluoromethyl ketones.* J Biol Chem, 1995. **270**(1): p. 445-50.

123. McHowat, J. and M.H. Creer, *Calcium-independent phospholipase A2 in isolated rabbit ventricular myocytes.* Lipids, 1998. **33**(12): p. 1203-12.

124. Jenkins, C.M., et al., *Identification of calcium-independent phospholipase A2 (iPLA2) beta, and not iPLA2gamma, as the mediator of arginine vasopressin-*

*induced arachidonic acid release in A-10 smooth muscle cells. Enantioselective mechanism-based discrimination of mammalian iPLA2s.* J Biol Chem, 2002. **277**(36): p. 32807-14.

125. Sarang, S.S., et al., *Identification of the gamma-aminobutyric acid receptor beta(2) and beta(3) subunits in rat, rabbit, and human kidneys.* J Am Soc Nephrol, 2001. **12**(6): p. 1107-13.

126. Yan, W., et al., *The highly selective production of 2-arachidonoyl lysophosphatidylcholine catalyzed by purified calcium-independent phospholipase A2gamma: identification of a novel enzymatic mediator for the generation of a key branch point intermediate in eicosanoid signaling.* J Biol Chem, 2005. **280**(29): p. 26669-79.

127. Blum, J.L., et al., *Profiling of fatty acids released during calcium-induced mitochondrial permeability transition in isolated rabbit kidney cortex mitochondria.* Toxicol In Vitro, 2011. **25**(5): p. 1001-6.

128. McHowat, J. and M.H. Creer, *Selective plasmalogen substrate utilization by thrombin-stimulated Ca(2+)-independent PLA(2) in cardiomyocytes.* Am J Physiol Heart Circ Physiol, 2000. **278**(6): p. H1933-40.

129. Yang, J., X. Han, and R.W. Gross, *Identification of hepatic peroxisomal phospholipase A(2) and characterization of arachidonic acid-containing choline glycerophospholipids in hepatic peroxisomes.* FEBS Lett, 2003. **546**(2-3): p. 247-50.

130. Beckett, C.S., et al., *Phospholipase A2-catalyzed hydrolysis of plasmalogen phospholipids in thrombin-stimulated human platelets.* Thrombosis Research, 2006.

131. Broekemeier, K.M., et al., *Pore formation and uncoupling initiate a Ca2+-independent degradation of mitochondrial phospholipids.* Biochemistry, 2002. **41**(24): p. 7771-80.

132. Williams, S.D. and R.A. Gottlieb, *Inhibition of mitochondrial calcium-independent phospholipase A2 (iPLA2) attenuates mitochondrial phospholipid loss and is cardioprotective.* Biochem J, 2002. **362**(Pt 1): p. 23-32.

133. Peterson, B., et al., *Alterations in phospholipid and fatty acid lipid profiles in primary neocortical cells during oxidant-induced cell injury.* Chem Biol Interact, 2008. **174**(3): p. 163-76.

134. Mancuso, D.J., et al., *Genetic ablation of calcium-independent phospholipase A2gamma prevents obesity and insulin resistance during high fat feeding by mitochondrial uncoupling and increased adipocyte fatty acid oxidation.* J Biol Chem, 2010. **285**(47): p. 36495-510.

135. Mancuso, D.J., et al., *Genetic ablation of calcium-independent phospholipase A2{gamma} leads to alterations in hippocampal cardiolipin content and molecular species distribution, mitochondrial degeneration, autophagy, and cognitive dysfunction.* J Biol Chem, 2009. **284**(51): p. 35632-44.

136. Mancuso, D.J., et al., *Genetic ablation of calcium-independent phospholipase A2gamma leads to alterations in mitochondrial lipid metabolism and function resulting in a deficient mitochondrial bioenergetic phenotype.* J Biol Chem, 2007. **282**(48): p. 34611-22.

137. Swift, L., J. McHowat, and N. Sarvazyan, *Inhibition of membrane-associated calcium-independent phospholipase A2 as a potential culprit of anthracycline cardiotoxicity.* Cancer Res, 2003. **63**(18): p. 5992-8.

138. McHowat, J., et al., *Changes in phospholipid content and myocardial calcium-independent phospholipase A2 activity during chronic anthracycline administration.* J Pharmacol Exp Ther, 2004: p. jpet.104.069419.

139. McHowat, J., et al., *Clinical concentrations of doxorubicin inhibit activity of myocardial membrane-associated, calcium-independent phospholipase A(2).* Cancer Res, 2001. **61**(10): p. 4024-9.

140. Atsumi, G., et al., *Fas-induced arachidonic acid release is mediated by Ca2+-independent phospholipase A2 but not cytosolic phospholipase A2, which undergoes proteolytic inactivation.* J Biol Chem, 1998. **273**(22): p. 13870-7.

141. Yoda, E., et al., *Mitochondrial dysfunction and reduced prostaglandin synthesis in skeletal muscle of Group VIB Ca2+-independent phospholipase A2gamma-deficient mice.* J Lipid Res, 2010. **51**(10): p. 3003-15.

142. Su, X., et al., *Small interfering RNA knockdown of calcium-independent phospholipases A2 beta or gamma inhibits the hormone-induced differentiation of 3T3-L1 preadipocytes.* J Biol Chem, 2004. **279**(21): p. 21740-8.

143. Jiang, Y., et al., *Glucagon receptor activates extracellular signal-regulated protein kinase 1/2 via cAMP-dependent protein kinase.* Proc Natl Acad Sci U S A, 2001. **98**(18): p. 10102-7.

144. Robert, V., et al., *Direct monitoring of the calcium concentration in the sarcoplasmic and endoplasmic reticulum of skeletal muscle myotubes.* J Biol Chem, 1998. **273**(46): p. 30372-8.

145. Montero, M., et al., *Monitoring dynamic changes in free Ca2+ concentration in the endoplasmic reticulum of intact cells.* EMBO J, 1995. **14**(22): p. 5467-75.

146. Nowak, G. and R.G. Schnellmann, *Improved culture conditions stimulate gluconeogenesis in primary cultures of renal proximal tubule cells.* Am J Physiol, 1995. **268**(4 Pt 1): p. C1053-61.

147. Nowak, G. and R.G. Schnellmann, *L-ascorbic acid regulates growth and metabolism of renal cells: improvements in cell culture.* Am J Physiol, 1996. **271**(6 Pt 1): p. C2072-80.

148. Takahashi, A., et al., *Measurement of intracellular calcium.* Physiol Rev, 1999. **79**(4): p. 1089-125.

149. Lemasters, J.J. and V.K. Ramshesh, *Imaging of mitochondrial polarization and depolarization with cationic fluorophores.* Methods Cell Biol, 2007. **80**: p. 283-95.

150. Bian, J.H., et al., *Identification of intracellular calcium pools. Selective modification by thapsigargin.* J Biol Chem, 1991. **266**(14): p. 8801-6.

151. Hirose, K., et al., *Spatiotemporal dynamics of inositol 1,4,5-trisphosphate that underlies complex Ca2+ mobilization patterns.* Science, 1999. **284**(5419): p. 1527-30.

152. Lemasters, J.J., et al., *Mitochondrial calcium and the permeability transition in cell death.* Biochim Biophys Acta, 2009. **1787**(11): p. 1395-401.

153. Cummings, B.S., J. McHowat, and R.G. Schnellmann, *Phospholipase A(2)s in cell injury and death.* J Pharmacol Exp Ther, 2000. **294**(3): p. 793-9.

154. Schieppati, A., et al., *Effect of renal ischemia on cortical microsomal calcium accumulation.* Am J Physiol, 1985. **249**(5 Pt 1): p. C476-83.

155. Bligh, E.G. and W.J. Dyer, *A rapid method of total lipid extraction and purification.* Can J Biochem Physiol, 1959. **37**(8): p. 911-7.

156. Zhang, L., B.L. Peterson, and B.S. Cummings, *The effect of inhibition of Ca2+-independent phospholipase A2 on chemotherapeutic-induced death and phospholipid profiles in renal cells.* Biochem Pharmacol, 2005. **70**(11): p. 1697-706.

157. Kerwin, J.L. and J.J. Torvik, *Identification of monohydroxy fatty acids by electrospray mass spectrometry and tandem mass spectrometry.* Anal Biochem, 1996. **237**(1): p. 56-64.

158. Kerwin, J.L., A.M. Wiens, and L.H. Ericsson, *Identification of fatty acids by electrospray mass spectrometry and tandem mass spectrometry.* J Mass Spectrom, 1996. **31**(2): p. 184-92.

159. Eaddy, A.C. and R.G. Schnellmann, *Visualization and quantification of endoplasmic reticulum Ca(2+) in renal cells using confocal microscopy and Fluo5F.* Biochem Biophys Res Commun, 2010.

160. Kuypers, F.A., et al., *Parinaric acid as a sensitive fluorescent probe for the determination of lipid peroxidation.* Biochim Biophys Acta, 1987. **921**(2): p. 266-74.

161. Eaddy AC, C.B., Mchowat J, Schnellmann RG, *The Role of Endoplasmic Reticulum Ca2+–Independent Phospholipase A2gamma in Oxidant-induced Lipid Peroxidation, Ca2+ Release, and Renal Cell Death.* Journal of Toxicological Sciences, 2012. ***In Press***.

162. Ohkawa, H., N. Ohishi, and K. Yagi, *Assay for lipid peroxides in animal tissues by thiobarbituric acid reaction.* Anal Biochem, 1979. **95**(2): p. 351-8.

163. Bartlett, G.R., *Phosphorus assay in column chromatography.* J Biol Chem, 1959. **234**(3): p. 466-8.

164. Funk, J.A., S. Odejinmi, and R.G. Schnellmann, *SRT1720 induces mitochondrial biogenesis and rescues mitochondrial function after oxidant injury in renal proximal tubule cells.* J Pharmacol Exp Ther, 2010. **333**(2): p. 593-601.

165. Lee, H.C. and Y.H. Wei, *Mitochondrial biogenesis and mitochondrial DNA maintenance of mammalian cells under oxidative stress.* Int J Biochem Cell Biol, 2005. **37**(4): p. 822-34.

166. Sohal, R.S., et al., *Oxidative damage, mitochondrial oxidant generation and antioxidant defenses during aging and in response to food restriction in the mouse.* Mech Ageing Dev, 1994. **74**(1-2): p. 121-33.

167. Dobashi, K., et al., *Kidney ischemia-reperfusion: modulation of antioxidant defenses.* Mol Cell Biochem, 2000. **205**(1-2): p. 1-11.

168. Limaye, P.V., N. Raghuram, and S. Sivakami, *Oxidative stress and gene expression of antioxidant enzymes in the renal cortex of streptozotocin-induced diabetic rats.* Mol Cell Biochem, 2003. **243**(1-2): p. 147-52.

169. Manevich, Y., et al., *Binding of peroxiredoxin 6 to substrate determines differential phospholipid hydroperoxide peroxidase and phospholipase A(2) activities.* Arch Biochem Biophys, 2009. **485**(2): p. 139-49.

170. Manevich, Y., et al., *Structure and phospholipase function of peroxiredoxin 6: identification of the catalytic triad and its role in phospholipid substrate binding.* J Lipid Res, 2007. **48**(10): p. 2306-18.

171. Manevich, Y. and A.B. Fisher, *Peroxiredoxin 6, a 1-Cys peroxiredoxin, functions in antioxidant defense and lung phospholipid metabolism.* Free Radic Biol Med, 2005. **38**(11): p. 1422-32.

172. Finkel, T. and N.J. Holbrook, *Oxidants, oxidative stress and the biology of ageing.* Nature, 2000. **408**(6809): p. 239-47.

173. Dong, K. and D.J. Quan, *Appropriately assessing renal function for drug dosing.* Nephrol Nurs J, 2010. **37**(3): p. 304-8.

174. Haase, M., et al., *Accuracy of neutrophil gelatinase-associated lipocalin (NGAL) in diagnosis and prognosis in acute kidney injury: a systematic review and meta-analysis.* Am J Kidney Dis, 2009. **54**(6): p. 1012-24.

175. Nickolas, T.L., et al., *Sensitivity and specificity of a single emergency department measurement of urinary neutrophil gelatinase-associated lipocalin for diagnosing acute kidney injury.* Ann Intern Med, 2008. **148**(11): p. 810-9.

176. Devarajan, P., *Review: neutrophil gelatinase-associated lipocalin: a troponin-like biomarker for human acute kidney injury.* Nephrology (Carlton), 2010. **15**(4): p. 419-28.

177. Halliwell, B. and C.Y. Lee, *Using isoprostanes as biomarkers of oxidative stress: some rarely considered issues.* Antioxid Redox Signal, 2010. **13**(2): p. 145-56.

178. Hermanns, R.C., et al., *Urinary excretion of biomarkers of oxidative kidney damage induced by ferric nitrilotriacetate.* Toxicol Sci, 1998. **43**(2): p. 241-9.

179. Jassem, W. and N.D. Heaton, *The role of mitochondria in ischemia/reperfusion injury in organ transplantation.* Kidney Int, 2004. **66**(2): p. 514-7.

180. Lim, S., et al., *Antioxidant enzymes induced by repeated intake of excess energy in the form of high-fat, high-carbohydrate meals are not sufficient to block oxidative stress in healthy lean individuals.* Br J Nutr, 2011. **106**(10): p. 1544-51.

181. Wu, Y., et al., *Mitogen-activated protein kinase-mediated phosphorylation of peroxiredoxin 6 regulates its phospholipase A(2) activity.* Biochem J, 2009. **419**(3): p. 669-79.

182. Sun, B., et al., *Inhibition of calcium-independent phospholipase A2 activates p38 MAPK signaling pathways during cytostasis in prostate cancer cells.* Biochem Pharmacol, 2010. **79**(12): p. 1727-35.

183. Anderson, S. and B.M. Brenner, *Effects of aging on the renal glomerulus.* Am J Med, 1986. **80**(3): p. 435-42.

184. Baylis, C. and B. Corman, *The aging kidney: insights from experimental studies.* J Am Soc Nephrol, 1998. **9**(4): p. 699-709.